SMA 13701.05R003 (VOLUME II)

SEISMIC MARGIN REVIEW

MIDLAND ENERGY CENTER PROJECT

VOLUME II

REACTOR CONTAINMENT BUILDING

prepared for

CONSUMERS POWER COMPANY
Jackson, Michigan

March, 1983

STRUCTURAL MECHANICS ASSOCIATES
A Calif. Corp.
5180 Birch Street, Newport Beach, Calif. 92660 (714) 833-7552

SMA 13701.05R003 (VOLUME II)

SEISMIC MARGIN REVIEW

MIDLAND ENERGY CENTER PROJECT

VOLUME II

REACTOR CONTAINMENT BUILDING

by

D. A. Wesley
R. P. Kennedy
R. H. Kincaid
P. S. Hashimoto
H. Banon
W. H. Tong
R. D. Thrasher

Approved: R. P. Kennedy
R. P. Kennedy
President

Approved: Thomas R. Kipp
T. R. Kipp
Manager of
Quality Assurance

prepared for

CONSUMERS POWER COMPANY
Jackson, Michigan

March, 1983

STRUCTURAL MECHANICS ASSOCIATES
A Calif. Corp.
5160 Birch Street, Newport Beach, Calif. 92660 (714) 833-7552

REVISIONS

Document Number SMA 13701.05R003(VOLUME II)

Title Seismic Margin Review
Midland Energy Center Project
Volume II
Reactor Containment Building

Rev.	Description	QA	Project Manager
10/1982	Draft for Review	Thomas R. Kipp 10/7/82	RLC for D.A. Wesley 10-7-82
3/1983	Initial Issue	Thomas R. Kipp 3/2/83	RLC for D.A. Wesley 3-2-83
Rev. 1 3/1983	Revised to incorporate additional CPC comments regarding tendon capacity, ACI 349-80 axial load capacity cutoff, and editorial changes.	Thomas R. Kipp 3/22/83	RLC for D.A. Wesley 3-22-83

SEISMIC MARGIN REVIEW

MIDLAND ENERGY CENTER PROJECT

TABLE OF CONTENTS

TABLE OF CONTENTS

TABLE OF CONTENTS (Continued)

1. INTRODUCTION

A seismic margin evaluation of the Midland Nuclear Power Generating Station has been conducted. The purpose of this assessment was to provide confidence in the safety and structural integrity of critical structures and equipment required to remain operational during an earthquake in order to achieve safe shutdown. This volume presents the results of the Seismic Margin Review (SMR) conducted for the reactor containment building.

Much of the design and construction of the Midland Plant was completed by 1973. The plant was designed in accordance with criteria and codes in effect at that time (Reference 1). The plant was originally designed to withstand both an Operating Basis Earthquake (OBE) and a Safe Shutdown Earthquake (SSE). The ground response spectra used in the initial design analyses are discussed in Volume I of this report (Reference 6).

Recently, the seismic hazard at the Midland site has been reevaluated using current methodology (Reference 3, 4 and 5). Seismic input for the site were determined in terms of site specific response spectra (SSRS) at both the original ground and at the top-of-fill locations. The original ground spectra are applicable to the reactor building. In order to assure the adequacy of the reactor building and its Category I equipment to withstand the higher postulated seismic excitation, an evaluation of this structure was conducted to determine the seismic margins to current code allowables, and if necessary, the seismic margins to failure. This report presents the results of the reactor building seismic analysis. The overall methodology used to develop the seismic models and in-structure response spectra for equipment evaluation are contained in Volume I of this report (Reference 6) and will not be presented herein.

1.1 DESCRIPTION OF THE STRUCTURE

The two reactor buildings consist of post-tensioned circular cylinders with shallow domes supported on reinforced concrete base slabs as shown in Figure II-1-1. The containment buildings are founded at Elevation 578' on glacial till material. The containment structures are embedded approximately 26 feet into the till plus an additional 30 feet of fill. The base slabs of the reactor buildings vary from 9 to 13 feet in thickness. A 2- or 3-inch expansion gap is provided between the containment and adjacent structures to prevent possible contact during seismic excitation. The interior surfaces are lined with one-fourth inch carbon steel plate with a thicker liner provided around openings and discontinuities. | 1

The principal dimensions of the reactor buildings are:

Inside Diameter	116 ft
Inside Height (top of dome)	193 ft
Vertical Wall Thickness	3-1/2 ft
Dome Thickness (minimum)	3 ft
Foundation Slab Thickness	9 to 13 ft
Liner Plate Thickness	1/4 in

Three groups of tendons oriented 120 degrees to each other are used for the dome. In the cylindrical shell, there are three equally spaced vertical buttresses 120 degrees apart. The hoop tendons in the cylinder span 240 degrees. The vertical tendons are anchored at the bottom of the base slab within a tendon gallery and on top of the ring girder. The tendons were stressed to 80 percent of ultimate strength at jacking. The cylindrical wall also includes nominal reinforcing steel for crack control. Additional reinforcing steel is provided around discontinuities. The liner plate is attached to the concrete by means of an angle grid system welded to the liner and embedded in the concrete. | 1

The reinforced concrete internal structure supports the Nuclear Steam Supply System (NSSS) components including the reactor vessel, the steam generators, and the remainder of the reactor coolant loop piping and equipment. Also located with the reactor buildings are portions of the auxiliary systems as well as the core flood tanks and combustible gas control systems. A 190-ton polar crane and 25-ton auxiliary crane are located at approximately Elevation 740'.

1.2 GROUND MOTION

The reactor building is founded on the natural material (glacial till) at the Midland site. The Seismic Margin Earthquake (SME) ground response spectra appropriate for use with structures founded on the original ground was presented in Section 2 of Volume I of this report (Reference 6) and are shown in Figure II-1-2 for reference. These spectra were developed based on an envelope of the original ground surface site specific response spectra and the original Housner spectra anchored to 0.12g peak acceleration. Volume I contains a complete description of the ground response spectra development. These spectra were used in a response spectrum analysis of the reactor building to develop seismic response loads for the seismic margin earthquake.

The ground response spectra were applied to the soil impedances at the base of the reactor building dynamic model. Vertical input was taken as 2/3 of the horizontal spectra. | 1

In-structure (floor) response spectra for the equipment evaluation were developed from time history analyses of the reactor building. A site specific artificial earthquake time history consistent with the SME ground response spectra for the original ground surface was developed as discussed in Section 2.4 of Volume I to provide the seismic input to the reactor building dynamic model. In-structure response

spectra for the equipment evaluation were developed by directly integrating the coupled equations of motion for the reactor building mathematical model and generating response time histories at all locations of interest for each of the soil cases studied.

1.3 SOIL PROPERTIES

The reactor buildings are founded on glacial till deposits. These deposits consist of very stiff to hard cohesive soils, predominantly grey, silty-clay, which extends to depths ranging from Elevation 578' to 545'. Below the cohesive soils, there is a layer of uniformly hard cohesive soils, predominantly brownish-grey, silty-clay containing some sand and gravel. From the base of the cohesive soils to bedrock, very dense, sandy soils grading into very dense, sandy soils with cobbles and boulders exist. The details of the site geology are discussed in the FSAR (Reference 1).

The site geotechnical characteristics for the Midland plant are discussed in Volume I (Reference 6) of this report. Figures II-1-3 and II-1-4 present the Midland soil profiles for the soft site and stiff site soil conditions. Figure II-1-5 presents an intermediate soil profile which was developed based on approximately midrange properties of the other two profiles. The development of the intermediate profile as well as the low strain shear modulii, strain degradation effects and other engineering characteristics used in the Seismic Margin Review (SMR) are discussed in Volume I (Reference 6). Use of the resulting wide range of soil characteristics in the seismic analysis of the reactor containment building ensures conservative response results in both the structure loads and in-structure response spectra. 1

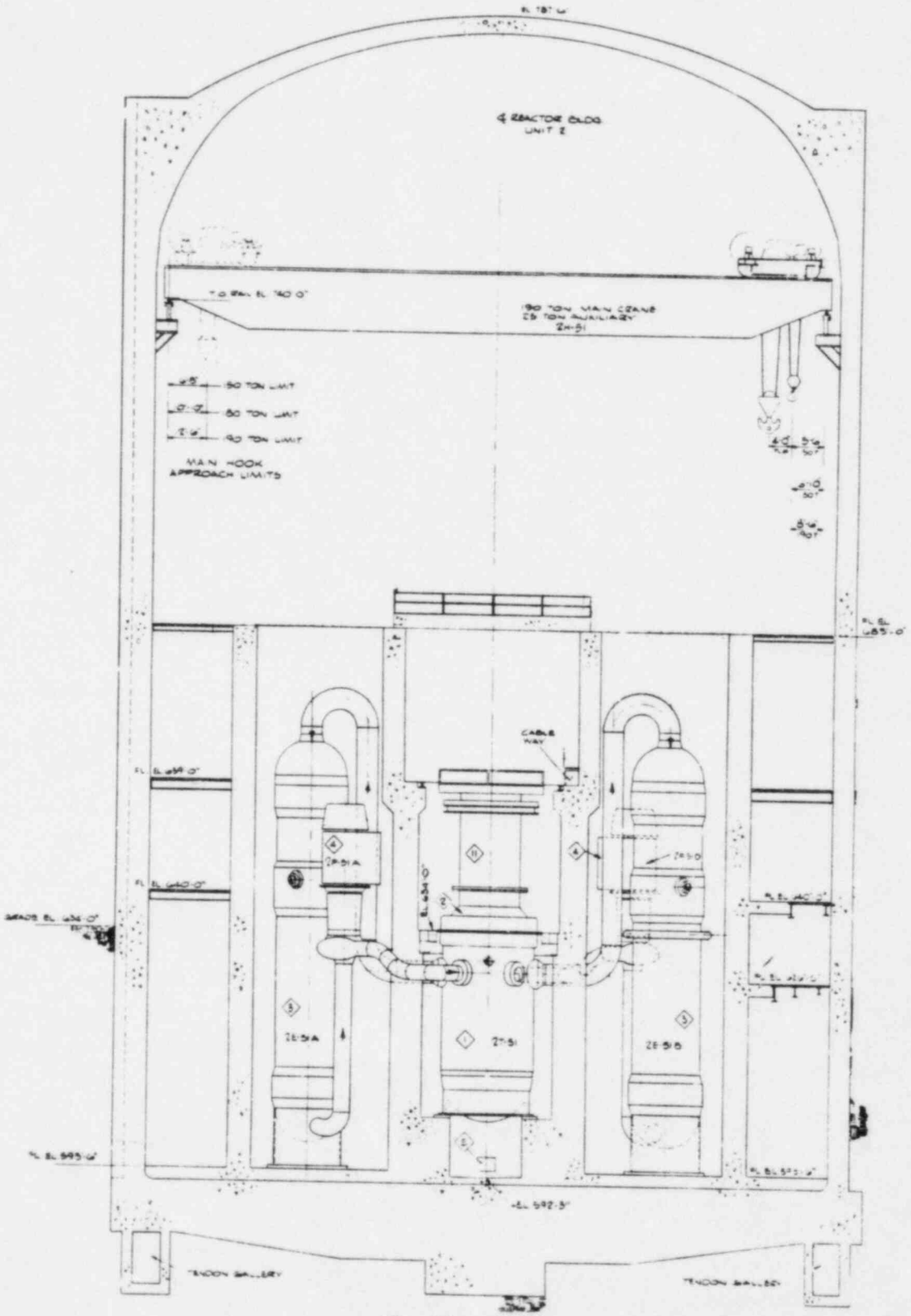

Sectional View
Looking East

FIGURE II-1-1. SECTIONAL VIEW OF REACTOR BUILDING SHOWING GENERAL STRUCTURE CONFIGURATION

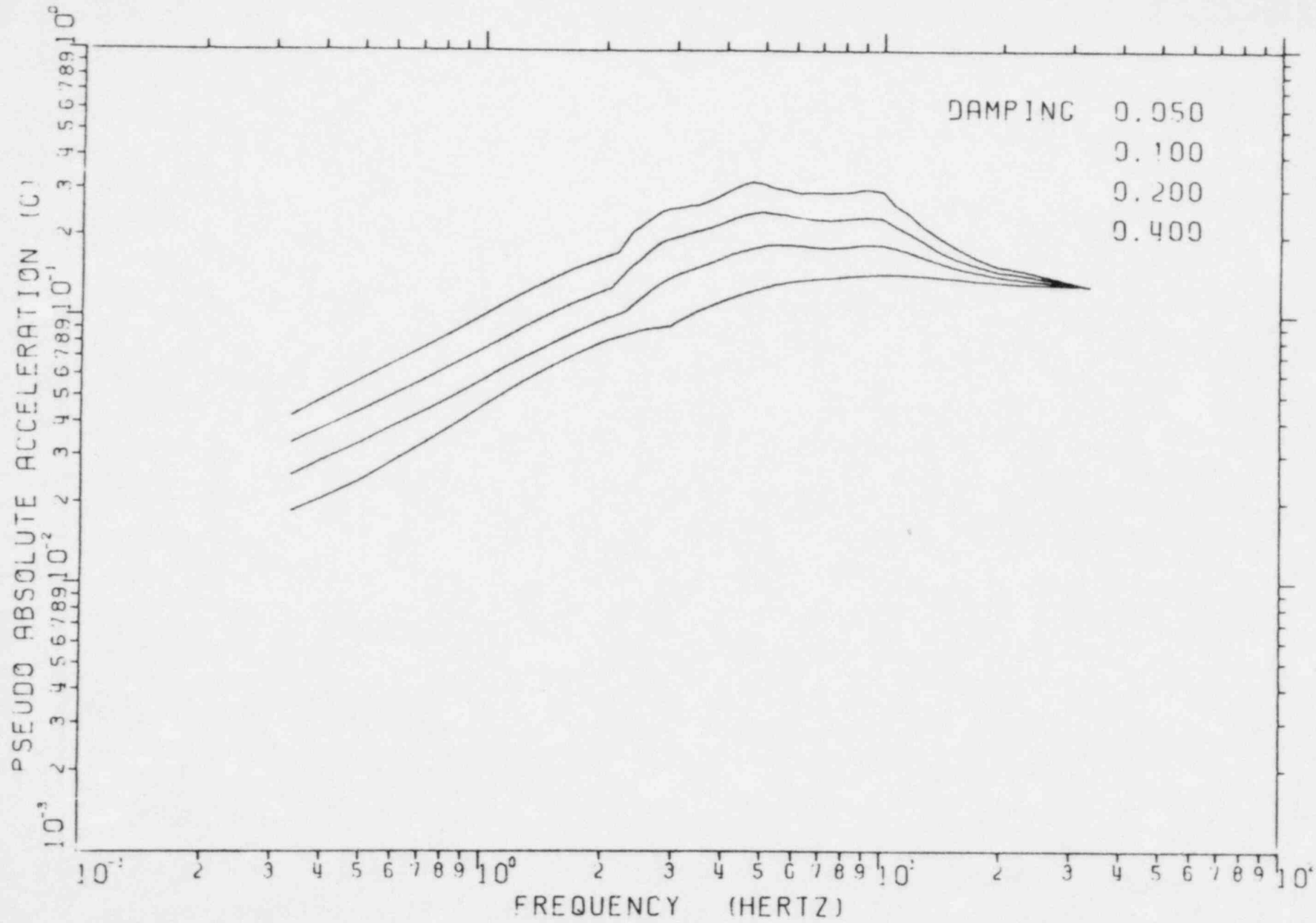

FIGURE II-1-2. SEISMIC MARGIN EARTHQUAKE ORIGINAL GROUND SURFACE ENVELOPE RESPONSE SPECTRA

Elevation

634 — Top of Grade

603 — Original Ground

Glacial Till

W_s = 135 pcf
ν = 0.47
V_s = 1290 fps

G_{max} = $7 \cdot 10^6$ psf
G_{SME} = $2 \cdot 10^6$ psf

550

Glacial Till

W_s = 135 pcf
ν = 0.47
V_s = 1690 fps

G_{max} = $12 \cdot 10^6$ psf
G_{SME} = $4.2 \cdot 10^6$ psf

410

Dense Cohesionless Material

W_s = 135 pcf
ν = 0.34
V_s = 2540 fps

G_{max} = $27 \cdot 10^6$ psf
G_{SME} = $17.8 \cdot 10^6$ psf

} Elevation 410

V_s = 2970 fps

G_{max} = $37 \cdot 10^6$ psf
G_{SME} = $25.2 \cdot 10^6$ psf

} Elevation 260

260

Bedrock

W_s = 150 pcf
ν = 0.33
V_s = 5000 fps

FIGURE II-1-3. SOIL LAYERING PROFILE REPRESENTATION OF SOFT SITE | 1

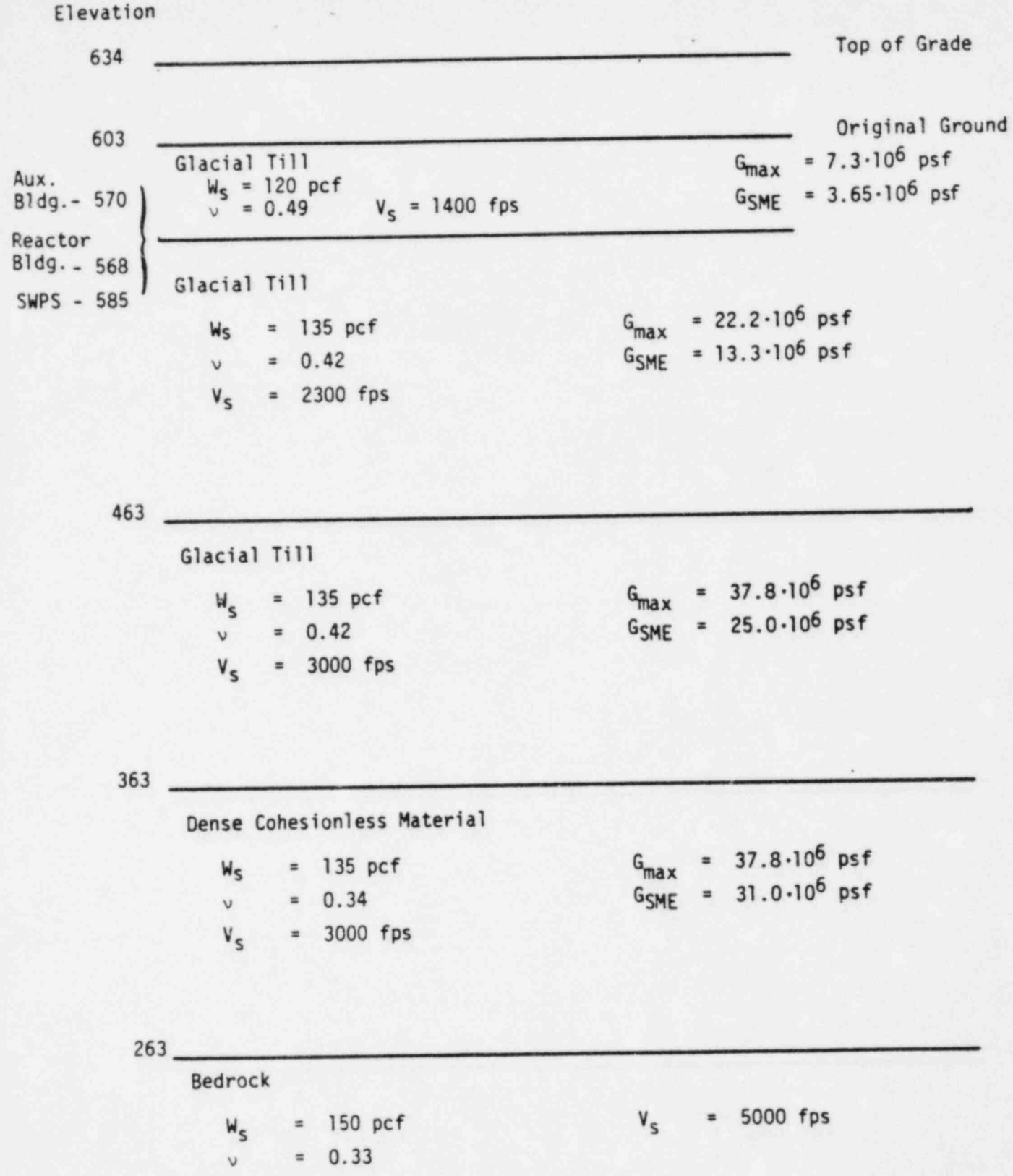

FIGURE II-1-4. SOIL LAYERING PROFILE REPRESENTATIVE OF STIFF SITE | 1

Elevation

634 — Top of Grade

603 — Original Ground

Glacial Till

W_s = 110 pcf
ν = 0.49
V_s = 1500 fps

G_{max} = $7.7 \cdot 10^6$ psf
G_{SME} = $4.08 \cdot 10^6$ psf

553

Glacial Till

W_s = 135 pcf
ν = 0.42
V_s = 1890 fps

G_{max} = $15 \cdot 10^6$ psf
G_{SME} = $7.95 \cdot 10^6$ psf

463

Dense Cohesionless Material

W_s = 135 pcf
ν = 0.34
V_s = 2468 fps

G_{max} = $25.6 \cdot 10^6$ psf
G_{SME} = $13.6 \cdot 10^6$ psf

263

Bedrock

W_s = 145 pcf
ν = 0.33

V_s = 5000 fps

FIGURE II-1-5. INTERMEDIATE SOIL PROFILE FOR MIDLAND SITE

2. SEISMIC ANALYSIS

2.1 STRUCTURE DYNAMIC MODEL

The dynamic lumped mass model for the reactor building is shown in Figure II-2-1. Since the structure is essentially symmetric with no significant torsional characteristics, a planar model is considered adequate. Different models were used for the two horizontal and vertical directions to account for minor differences in structure geometry for these degrees-of-freedom. The reactor building mathematical model was developed by Bechtel (Reference 7). As part of the SMR, this model was reviewed to ensure that overall dynamic characteristics of the structure have been adequately represented. For the SME analysis, values of rotatory inertia were calculated and included in the model. Detailed checks of the mass and stiffness properties of this model were not performed as part of the SMR. The reactor building dynamic model described herein was used to evaluate overall building response to seismic loadings as well as to generate in-structure response spectra. The overall building dynamic response developed from this model was also used to develop forces in the individual structural elements.

The reactor building dynamic model shown in Figure II-2-1 uses four lumped mass, vertical sticks to represent the containment vessel shell, the concrete internals structure, the steam generators, and the reactor vessel. The mass of the structure is lumped at major floor and equipment locations. The mass includes concrete, steel and all major equipment including the polar crane at Elevation 740'. Because the structure is considered to be symmetric, the center of mass for each floor coincided with the geometric centroid of the structure.

Beam elements define the stiffness characteristics of the structural stiffnesses between floor levels and the stiffness properties of the steam generators and reactor vessel. Additional stiffness elements are used to model vessel supports between the concrete

internals structure and reactor vessel and steam generators. All structural stiffnesses were considered to be symmetric about the reactor building centerline and coincide with center of mass locations.

The impedance functions presented in Tables II-2-4 and II-2-5 are attached to the structure portion of the reactor building model (Figure II-2-1) at Elevation 586.2 feet. The design ground motion is fed into this structure through these soil-structure interaction impedance functions to determine seismic response loads in the reactor building.

2.2 SOIL-STRUCTURE INTERACTION

2.2.1 Layered Site Analyses

The effects of the layered site characteristics on the reactor building seismic response were evaluated by developing equivalent elastic half-space soil impedances based on layered site analyses. These equivalent elastic half-space impedance functions were then modified to account for embedment effects. The layered site soil profiles presented in the previous section were used in conducting layered site analyses using the program CLASSI (Reference 8) which calculates the frequency dependent soil impedances for the structure. The reactor building foundation geometry was idealized as a 62-foot radius circular foundation. This idealized foundation is founded at Elevation 578 feet.

The results of the CLASSI analyses are presented in Figures II-2-2 to II-2-10 for the three soil profiles studied. Soil impedances were developed for vertical and horizontal translation and rocking. Torsional response was not considered since the structure was judged to be symmetric with no important torsional response. Five percent accidental torsion was included in the seismic loads for the code margin evaluations. Both the real (stiffness) and imaginary (damping) portions of the soil impedance are presented in these figures for a range of soil-structure frequencies varying from 0 to 10 hertz. Figures II-2-2

to II-2-4 present the CLASSI layered site soil impedances for the soft site soil profile while Figures II-2-5 to II-2-7 and Figures II-2-8 to II-2-10 present the corresponding CLASSI results for the intermediate soil profile and the stiff site soil profile, respectively.

The CLASSI layered site results are similar for both the soft site and intermediate soil profiles. The horizontal and vertical translation stiffness coefficients exhibit frequency dependent effects with some resonance occurring between the foundation and the underlying soil. The rocking stiffness coefficient shows substantial frequency dependence throughout the 0 to 10 hertz frequency range. Damping coefficients in all cases are relatively smooth and do not exhibit any significant resonance between the reactor building foundation and underlying soil. It should be noted that because CLASSI incorporates the five percent soil material damping in the layered site analyses, the damping coefficient terms are not zero for the static case (0 hertz) as would be expected if only geometric damping was considered in the analysis.

The stiff site soil profile stiffness and damping coefficients show little resonance due to layering effects. Some minor frequency dependence is exhibited in the impedance functions for this soil profile. The stiff site condition is normally controlling for structural loads.

2.2.2 Effective Elastic Half-Space Shear Moduli

The results of the CLASSI layered site analyses were used to develop effective elastic half-space shear moduli, G_{eff}, for all required degrees-of-freedom of the structure (horizontal and vertical translation, and rocking). The effective elastic half-space shear moduli were used to develop soil impedances which accounted for the embedment effects and soil layering. The procedure used to develop effective elastic half-space shear moduli from CLASSI layered site analysis results is presented in Section 4 of Volume I. Appendix A of the auxiliary

building SME evaluation (Reference 9) illustrates the procedure and includes a sample calculation of G_{eff}. Table II-2-1 presents the effective soil shear moduli for each of the three soil profiles studied as determined from the CLASSI layered site analyses.

The G_{eff} values tabulated in Table II-2-1 may be compared to the layered soil profiles presented in Figures II-1-3 to II-1-5 used in the CLASSI layered site analyses. For the soft site soil profile, the G_{eff} of 2,400 ksf associated with the horizontal structure translation is primarily due to the G_{SME} of 2,000 ksf associated with 28-foot thick layer beneath the structure from Elevation 550' to 578' shown in Figure II-1-3. For vertical translation and rocking, this 28-foot layer again strongly influences the effective elastic half-space shear modulus determined for these degrees-of-freedom. The effective elastic half-space shear modulus, G_{eff}, is 2,800 ksf for these degrees-of-freedom.

Results for the intermediate soil case are similar. The effective soil shear modulus, G_{eff}, of 5,300 ksf associated with horizontal structure translation again is most heavily influenced by the soft layer of glacial till immediately beneath the structure which tends to reduce the effective stiffness of the equivalent half-space. The effective soil shear modulus, G_{eff}, of 7,300 ksf determined for vertical translation and rocking of the structure is also influenced by this layer but to a lesser degree than was evident in the soft site soil profile results.

For the stiff soil profile, the G_{eff} value of 7800 ksf determined for horizontal translation shows the influence of both the 10' layer immediately beneath the structure and the stiffer material below Elevation 568'. The G_{eff} value of 11,800 ksf determined for vertical translation and rocking of the structure is primarily due to the stiffer glacial till below Elevation 568'.

Upper and lower bound soil cases were developed for the reactor building based on the effective elastic half-space shear moduli presented in Table II-2-1. The upper and lower bound soil cases represent the range of soil properties which might be possible at the Midland site. This range of soil properties is considered to adequately account for the variability from such factors as uncertainty in strain degradation effects, uncertainty in modeling soil-structure interaction, and the uncertainty in the knowledge of soil characteristics in the soil profiles studied. Based on these uncertainties, it was determined that 0.6 x G_{eff} based on the soft site soil profile represented a realistic lower bound soil case for use in the SME. Similarly, 1.3 x G_{eff} based on the stiff site soil profile was considered to be a realistic upper bound soil case for this structure. Table II-2-2 presents the G_{eff} values used for the lower, intermediate, and upper bound soil cases used in the reactor building SME analysis.

2.2.3 Energy Entrapment Due to Layering

Two types of damping may be defined for the soil. The first type, known as material or hysteretic damping, is due to energy absorption by the soil due to stressing and straining of the material. For the Midland site, this damping has been conservatively estimated to be five percent of critical damping for the SME. Material damping is not affected by layering. The second type of soil damping, known as geometric or radiation damping, involves the wave propagation of energy through the soil away from the structure. For an elastic half-space, these waves will propagate outwards to infinity. Layered soil profiles, however, tend to trap and reflect some of the energy back up towards the structure. One of the principal reasons for conducting a layered site analysis for the SME was to determine the effect of layering on the geometric damping from the structure. In effect, the geometric damping for the layered profile is reduced to some percentage of the damping which would be determined for an equivalent elastic half-space. This decrease in geometric damping may be determined through the use of a factor defined as

$$F_{Layer} = \frac{C(\text{CLASSI layered site analysis})}{C(\text{theoretical elastic half-space})}$$

where C(CLASSI layered site analysis) is the frequency dependent damping including layering effects determined by the CLASSI layered site analysis. The term C(theoretical elastic half-space) represents the geometric damping which would be calculated for the structure based on the effective elastic half-space shear moduli presented in Table II-2-1 and the reactor building foundation which has a 62-foot radius. This ratio is indicative of the amount of energy entrapped beneath the structure due to layering. The procedure for calculating F_{Layer} is presented in Reference 6. A sample calculation of a typical F_{Layer} factor is presented in Appendix A of Reference 9.

Layering factors were determined for all three soil cases for the reactor building. One set of layering factors applicable to all three soil profiles was defined. Layering factors were conservatively limited to a maximum of 75 percent of theoretical elastic half-space geometric damping for all degrees-of-freedom where F_{Layer} was determined to be greater than 0.75. This conservative cutoff on geometric damping is discussed in Reference 6. The factors defined for the reactor building are as follows:

Structure Degree-of-Freedom	Layering Factor, F_{Layer}
Horizontal Translation	0.50
Vertical Translation	0.75
Rocking	0.25

These results indicate that the impedance mismatch at the interface between the thin layers of glacial till immediately beneath the structure and the deeper layer of stiffer glacial till reduces horizontal translation geometric damping to 50 percent and rocking geometric damping to 25 percent of theoretical elastic half-space damping due to energy entrapment beneath the structure. A layering factor of 75 percent of theoretical elastic half-space geometric damping was justified for the vertical direction indicating layering was not as important for this degree-of-freedom. Increased seismic response loads and in-structure response spectra would be expected for this structure due to reduced geometric damping used for horizontal translation and rocking degrees-of-freedom compared to an elastic half-space site.

2.2.4 Development of Global Soil Stiffnesses and Dashpots

Soil springs modeling the stiffness of the soil beneath the reactor building were developed based on the effective soil shear modulus values presented in Table II-2-2 and the actual building foundation geometry. Soil stiffnesses were calculated from the frequency dependent elastic half-space equations shown in Table II-2-3. These equations and frequency dependent coefficients are presented in References 11 to 14. Unembedded soil stiffnesses for each of the three soil cases studied are shown in Table II-2-4.

Embedment effects were considered to be applied as a multiplier to the unembedded frequency dependent elastic half-space soil stiffnesses. Embedment effects considered both the soil in physical contact with the sides of the structure and stiffening of the soil due to the weight of adjacent structures. Reference 6 presents the procedure used to calculate embedment effects for the SME. Appendix A of Reference 9 presents a sample soil stiffness calculation including embedment effects for the auxiliary building. A similar procedure was used for the reactor building.

As shown by Table II-2-4, embedment effects for the reactor building soil stiffnesses are relatively small. Translational degrees-of-freedom are stiffened by about 5 percent while rotational degrees-of-freedom show an increase on the order of 13 percent. Thus, the corresponding fundamental soil-structure frequencies would be expected to increase in the range of 2 to 6 percent due embedment effects. The final global soil stiffnesses for the structure including embedment effects are presented in Table II-2-4 for each of the three soil cases studied.

Dashpots modeling soil geometric and material damping were developed using the elastic half-space equations presented in Table II-2-3. Material damping of 5 percent of critical damping was assumed for the soil. Soil dashpots were calculated accounting for layering and embedment effects as discussed in the volume on methodology and criteria (Reference 6). A sample embedded dashpot calculation for the auxiliary building demonstrating this procedure is presented in Reference 9.

Table II-2-5 presents the unembedded dashpots and embedment factors for this structure. Embedment effects for damping increased translational dashpots 7 to 15 percent above their unembedded values. Rotational dashpots were increased by about 39 percent due to the stiffening effects from the surrounding soil. The embedded dashpots including 5 percent material damping are presented in Table II-2-5.

TABLE II-2-1

Reactor Building Effective Elastic Half-Space Shear Moduli

Structure Degree-of-Freedom	Dynamic Soil Shear Modulus, G_{eff}		
	Soft Site Soil Profile (KSF)	Intermediate Soil Profile (KSF)	Stiff Site Soil Profile (KSF)
Horizontal Translation	2,400	5,300	7,800
Vertical Translation, Rocking	2,800	7,300	11,800

TABLE II-2-2

Reactor Building Seismic Margin Evaluation
Equivalent Elastic Half-Space Shear Moduli

Structure Degree-of-Freedom	Dynamic Soil Shear Modulus, G_{eff}		
	Lower Bound Soil Case (KSF)	Intermediate Soil Case (KSF)	Upper Bound Soil Case (KSF)
Horizontal Translation	1,400	5,300	10,100
Vertical Translation, Rocking	1,700	7,300	15,300

TABLE II-2-3

Frequency Dependent Elastic Half-Space Impedance

Direction of Motion	Equivalent Spring Constant For Rectangular Footing	Equivalent Spring Constant For Circular Footing	Equivalent Damping Coefficient
Horizontal	$k_x=k_1 2(1+\nu)G\beta_x\sqrt{BL}$	$k_x=k_1\frac{32(1-\nu)GR}{7-8\nu}$	$c_x=c_1 k_x(\text{static})R\sqrt{\rho/G}$
Rocking	$k_\psi=k_2\frac{G}{1-\nu}\beta_\psi B^2 L$	$k_\psi=k_2\frac{8GR^3}{3(1-\nu)}$	$c_\psi=c_2 k_\psi(\text{static})R\sqrt{\rho/G}$
Vertical	$k_z=k_3\frac{G}{1-\nu}\beta_z\sqrt{BL}$	$k_z=k_3\frac{4GR}{1-\nu}$	$c_z=c_3 k_z(\text{static})R\sqrt{\rho/G}$
Torsion	———	$k_\theta=k_4\frac{16}{3}GR^3$	$c_t=c_4 k_t(\text{static})R\sqrt{\rho/G}$

in which:

ν = Poisson's ratio of foundation medium,

G = shear modulus of foundation medium,

R = radius of the circular base mat,

ρ = density of foundation medium,

B = width of the base mat in the plane of horizontal excitation,

L = length of the base mat perpendicular to the plane of horizontal excitation,

k_1, k_2, k_3, k_4
c_1, c_2, c_3, c_4 = frequency dependent coefficients modifying the static stiffness or damping.

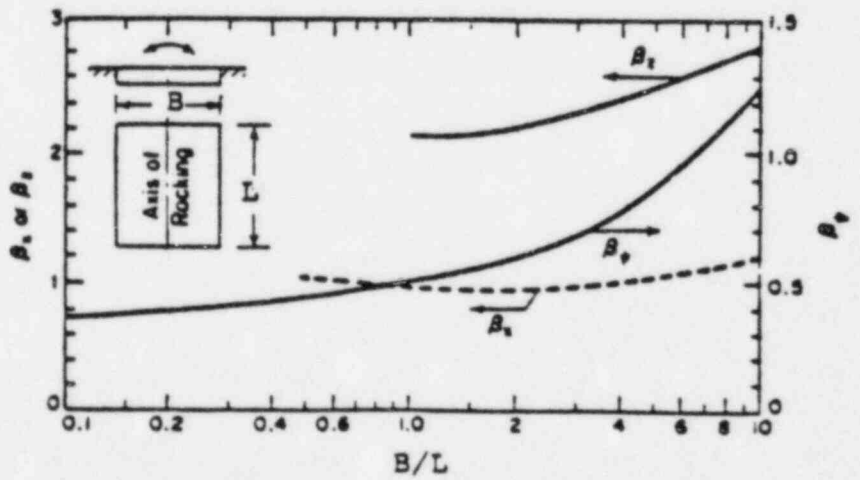

Constants β_x, β_ψ and β_z for Rectangular Base

TABLE II-2-4

Reactor Building Soil Stiffnesses

Motion	Non-Embedded Stiffnesses			Embedment Factor	Embedded Stiffnesses		
	Lower Bound Soil	Intermediate Soil	Upper Bound Soil		Lower Bound Soil	Intermediate Soil	Upper Bound Soil
Translational							
North-South and East-West	4.55×10^5	1.65×10^6	3.16×10^6	1.06	4.83×10^5	1.75×10^6	3.35×10^6
Vertical	6.00×10^5	2.65×10^6	5.38×10^6	1.04	6.24×10^5	2.76×10^6	5.60×10^6
Rotational							
North-South and East-West	1.96×10^9	6.90×10^9	1.50×10^{10}	1.13	2.21×10^9	7.78×10^9	1.69×10^{10}

Notes: 1. Units for Translational Soil Springs are K/ft.

2. Units for Rotational Soil Springs are K-ft/rad.

TABLE II-2-5

Reactor Building Damping

Motion	Non Embedded Dashpot			Embedment Factor	Embedded Dashpot (3)		
	Lower Bound Soil	Intermediate Soil	Upper Bound Soil		Lower Bound Soil	Intermediate Soil	Upper Bound Soil
Translational							
North-South and East-West	1.77×10^4	3.06×10^4	4.23×10^4	1.15	2.28×10^4	4.33×10^4	5.95×10^4
Vertical	4.96×10^4	1.06×10^5	1.49×10^5	1.07	5.36×10^4	1.16×10^5	1.66×10^5
Rotational							
North-South and East-West	5.02×10^6	8.48×10^6	1.48×10^7	1.39	2.81×10^7	6.42×10^7	1.01×10^8

Notes:
1. Units for Translational Dashpots are K-sec/ft
2. Units for Rotational Dashpots are K-sec-ft/rad
3. Includes 5% Soil Hysteretic Damping

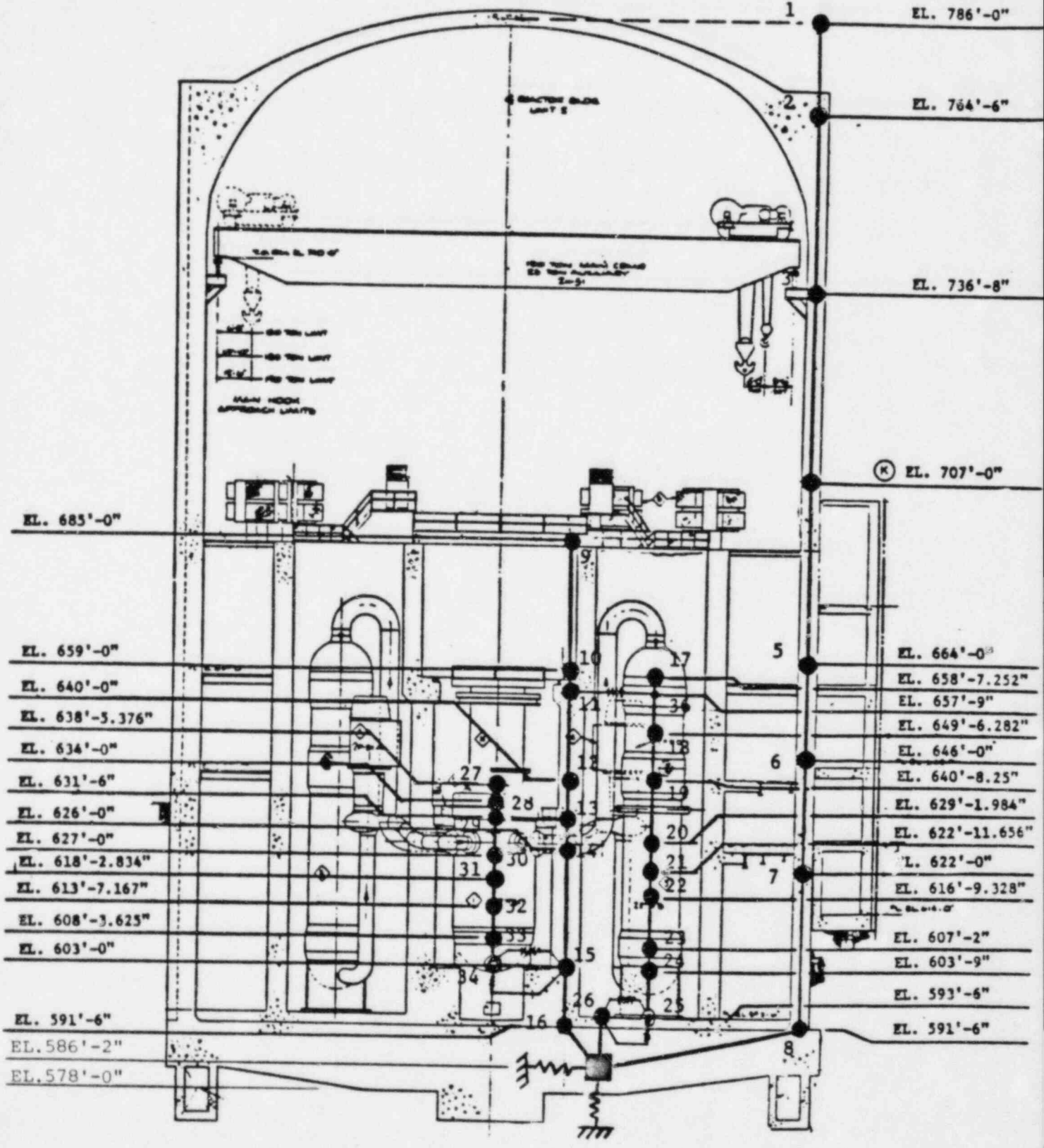

FIGURE II-2-1. REACTOR BUILDING LUMPED MASS MODEL

FIGURE II-2-2. HORIZONTAL TRANSLATION SOIL IMPEDANCE
SOFT SITE LAYERED SOIL PROFILE

FIGURE II-2-3. VERTICAL TRANSLATION SOIL IMPEDANCE
SOFT SITE LAYERED SOIL PROFILE

FIGURE II-2-4. ROCKING SOIL IMPEDANCE SOFT SITE LAYERED SOIL PROFILE

FIGURE II-2-5. HORIZONTAL TRANSLATION SOIL IMPEDANCE
INTERMEDIATE CASE LAYERED SOIL PROFILE

FIGURE II-2-6. VERTICAL TRANSLATION SOIL IMPEDANCE
INTERMEDIATE CASE LAYERED SOIL PROFILE

FIGURE II-2-7. ROCKING SOIL IMPEDANCE INTERMEDIATE CASE LAYERED SOIL PROFILE

FIGURE II-2-8. HORIZONTAL TRANSLATION SOIL IMPEDANCE
STIFF SITE LAYERED SOIL PROFILE

FIGURE II-2-9. VERTICAL TRANSLATION SOIL IMPEDANCE
STIFF SITE LAYERED SOIL PROFILE

FIGURE II-2-10. ROCKING SOIL IMPEDANCE STIFF SITE LAYERED SOIL PROFILE

3. SEISMIC RESPONSE

3.1 MODAL CHARACTERISTICS

The reactor building natural frequencies, percentage of total structure mass participating in each mode, and mode description are presented in Tables II-3-1 to II-3-3. Results for the lower bound, intermediate, and upper bound soil cases for the East-West two-dimensional dynamic model are presented in Table II-3-1. East-West fundamental structure natural frequencies range from 1.13 hertz for the lower bound soil case to 2.60 hertz for the upper bound soil case results. This fundamental structure mode is an overall soil-structure rocking mode of the reactor building. The percentage of total structure mass participating in this mode ranges from 58.5 percent for the upper bound soil case to 66.8 percent for the lower bound soil case. The second mode of the reactor building is an out-of-phase soil-structure translational mode. Most of the remaining structure mass participates in this mode with the percentage of total structure mass in this mode varying from 31.2 to 35.3 percent. Higher frequency structure modes are associated with steam generator, reactor vessel, reactor internal structure, and containment response. The percentage of total structure mass participating in these higher modes is 7.3 percent or less for any individual mode. By using 8 modes of the East-West dynamic model in response spectrum analyses, at least 99.9 percent of the structure mass was included.

The results for the North-South reactor building dynamic model presented in Table II-3-2 are virtually identical to the results presented for the East-West model. The fundamental structure natural frequencies range from 1.13 hertz for the lower bound soil case to 2.60 hertz for the upper bound soil case. The fundamental structure mode is an overall soil-structure rocking mode. Between 58.3 and 66.7 of the total structure mass participates in this mode. The second mode of the structure is an out-of-phase soil-structure translational mode. The

percentage of total structure mass participating in this mode varies from 32.4 to 36.0 percent. Higher frequency modes are associated with reactor vessel, steam generator, reactor internal structure, and containment response. The percentage of total structure mass participating in these higher modes is 5.2 percent or less for any individual mode. Eight structure modes were used in response spectrum analyses for the North-South dynamic model which results in at least 99.9 of all structure mass being included.

Reactor building response in the vertical direction is primarily in a soil-structure translation mode. As shown by Table II-3-3, the fundamental vertical natural frequency ranges from 2.16 hertz for the lower bound soil case to 6.16 hertz for the upper bound soil case. Approximately 99 percent of the total structure mass participates in this fundamental vertical mode. Use of three structure modes in the response spectrum analysis for this structure model resulted in 99.9 percent of the total structure mass being included in the results.

3.2 COMPOSITE MODAL DAMPING

Response spectrum analysis techniques assume the structure has classical normal modes. In other words, the equations of motion are assumed to uncouple and the response of the structure can be calculated as the superimposed response of a series of single-degree-of-freedom systems. For multi-degree-of-freedom structures with more than approximately 20 percent critical damping, the structure may not possess classical normal modes. Structural response can then be rigorously computed only by a step-by-step technique such as direct integration time history analysis. However, when modal damping values are appropriately selected, normal mode techniques such as response spectrum analysis can be used to calculate accurate seismic response loads. The use of response spectrum analysis techniques to compute the structure seismic loads allows a more accurate representation of the SME input characteristics without the peaks and valleys associated with an artificial time history input.

Reactor building seismic response loads were determined from response spectrum analysis using composite modal damping techniques to define modal damping for the combined soil-structure modes. Typically, composite modal damping for the structure is defined by an empirical technique such as stiffness proportional damping. This technique works well for determining structural modal damping for buildings comprised of structural systems which have different element damping ratios associated with each load-carrying subsystem. However, experience with these techniques has shown that when a structure with relatively low overall damping (≈4 to 7 percent of critical damping) is coupled to a soil model with large radiation and material damping (≈15 to 20 percent of critical damping), resulting composite modal damping values may lead to underprediction of structural response for locations high in the structure. The procedure presented in Volume I of this report avoids this difficulty and was used to define composite modal damping for the coupled soil-structure model or the reactor building. This method is based on matching the response computed from the coupled equations of motion with the modal response at selected locations. Soil impedances are considered to act at the centroid of the overall foundation in determining structure dynamic characteristics. Structure response transfer functions are developed at a number of locations in the structure for both the rigorous and normal mode solutions. Modal damping values for the normal mode solution are iterated upon until the transfer functions for the two solutions match. By choosing locations which are sensitive to damping, composite modal damping values are determined which generally predict conservative response at all locations.

Composite modal damping values were determined using the program SOILST (Reference 15). The embedded stiffnesses and dashpots presented in Tables II-2-4 and II-2-5 defined the soil impedances beneath the structure in this analysis. The prestressed containment structure was considered to be damped at five percent of critical damping. The reinforced concrete internals structure was damped at seven percent of critical damping. These damping levels are consistent with SME damping

for structures above one-half yield. The reactor vessel and steam generators were conservatively damped at two percent of critical damping. These damping levels were chosen consistent with Regulatory Guide 1.61 damping for equipment and large diameter piping systems below one-half of yield. Stiffness proportional damping techniques were used in conjunction with the structure element dampings presented above to determine structural modal damping for the fixed base structure model. The fixed base structure modes and corresponding structural modal damping were used as input to program SOILST to determine composite modal damping which accounted for both structural damping and soil radiation and material damping.

Composite modal damping values were determined for a number of locations in the structure. Typical floors were chosen on both the containment structure and the reinforced concrete internals that were relatively high in the structure and were judged to have dynamic response sensitive to modal damping. Additional locations on the steam generators and the reactor vessel were also evaluated. Composite modal damping values for all modes were chosen based on a conservative fit of the data for all locations studied.

Composite modal damping values were determined using the methodology described above for all modes contributing more than about 10 percent of the total degree-of-freedom response at the structure location studied. Local high frequency structure modes were conservatively damped at 2-1/2 percent of critical damping. The rational for lightly damping these higher frequency modes is based on a parametric study of Auxiliary Building response as discussed in Section 3.2 of Volume II and will not be repeated here. The use of 2-1/2 percent critical damped higher modes for the reactor building model instead of the 3-1/2 percent critical damped modes used for the auxiliary building reflects the lower overall structural damping specified for this structure.

The composite modal damping values used to determine seismic response loads in the reactor building are presented in Tables II-3-1 to II-3-3. In all cases, the fundamental structure rocking mode for both the North-South and East-West dynamic models is damped at 6 percent of critical damping. This low damping value reflects the low radiation damping determined for the reactor building for this degree-of-freedom. Composite modal damping values for second mode horizontal translation soil response ranges from a low of 15 percent of critical damping for the upper bound soil case to a high of 28 percent of critical damping for the soft soil case. Damping for higher frequency structure modes associated with coupled equipment and structure response varies from 2 percent of critical damping to 10 percent of critical damping.

In the vertical direction, structural response is almost entirely due to the fundamental vertical mode. Composite modal damping used for this mode ranges from 40 percent of critical damping for the upper bound soil case to 55 percent of critical damping for the lower bound soil case.

To ensure that composite modal damping values were conservatively chosen for all structure modes, comparisons of structural response predicted by direct integration time history analysis using concentrated dashpots to model the soil damping were made with the seismic response determined by modal superposition using composite modal damping. Response accelerations at typical locations in the structure were determined from direct integration of the coupled equations of motion. At these same locations, response accelerations were then developed from a modal superposition time history analysis of the flexible base structure model using the modal damping values defined for each soil case by Tables II-3-1 to II-3-3. The same input time history was used in both time history analyses. Response accelerations from the two analyses were compared to ensure the accelerations based on the composite modal damping values approximately met or exceeded those determined from the direct integration time history analyses. Table II-3-4 presents comparisons of zero period

accelerations in the structure obtained by these two procedures for the upper bound soil case. The results for the upper bound soil case are presented since seismic response loads throughout the structure are controlled by this soil case. Results for the other soil cases were similar.

3.3 STRUCTURE SEISMIC RESPONSE

Seismic loads throughout the reactor building were determined from the planar dynamic models of the structure developed for the East-West, North-South, and vertical directions. The overall seismic loads computed for the containment and reactor internal support structure were distributed to the individual structural elements as described in Section 3.3.3 of this volume. Loads in the reactor vessel and the steam generator computed from these analyses were not evaluated. Instead a more refined analysis was conducted and the SMR was based on the refined loads as discussed in Volume VIII of this report.

The overall seismic loads in the reactor building were developed from the square-root-of-the-sum-of-the-squares (SRSS) of the modal responses including consideration of closely spaced modes as discussed in Section 6.4 of Volume I. The structural response loads were determined for each of the three earthquake direction components acting independently. For the SMR, the highest load computed for the structural element from any of the three soil cases was used to determine its code margin.

3.3.1 Effects of Soil Conditions on Seismic Loads

Seismic response loads in the containment structure are presented in Figures II-3-1 to II-3-5 for the three soil cases studied. Figure II-3-6 to II-3-10 present the corresponding results for the reactor internal support structure. In all cases, the upper bound soil case results in the highest seismic response loads. Shears, overturning moments, and vertical axial forces are all greatest for the upper bound soil case. Torsional response loads were not dynamically developed

because the structure is symmetric. A five percent increase in loads for both the reactor containment building and concrete internal structure was included to account for torsion. The seismic code margin evaluation is based on the worst case condition for all elements which for this structure corresponds to upper bound soil case results.

3.3.2 Comparison of SME and FSAR SSE Design Loads

One basis for selecting various elements for code margin evaluation for the SME was the ratio of SME seismic load to the seismic load used for design. In order to determine the relative magnitudes of the SME loads to the corresponding FSAR SSE design loads, comparisons of the lateral shear forces, and overturning moments throughout the structure are shown in Figures II-3-11 through II-3-18.

Figure II-3-11 through II-3-14 present comparisons of the lateral seismic shear forces and corresponding overturning moments throughout the containment dome and shell. Between Elevation 587' and 764'-6", design shear loads exceed the SME values by about 10 to 20 percent throughout the structure. In the containment dome, above Elevation 764'-6" the design shear loads exceed SME loads by about 5 percent. Below approximately Elevation 700' on the shell, design overturning moments exceed the SME values by about 5 to 10 percent. Between Elevations 700' and 764'-6" SME overturning moments slightly exceed design values. Above Elevation 764'-6" both the design overturning moments in the dome and SME values are about the same.

Figures II-3-15 through II-3-18 show similar comparisons of SME and design seismic loads throughout the reactor internal support structure. Both the lateral shear loads and the overturning moments determined for the SME exceed the corresponding design loads. Throughout the internal structure SME lateral shear loads exceed design values by about 20 to 30 percent. The corresponding overturning moments show SME seismic moments exceeding design moments by about 30 to 40 percent. In addition to the shell, several structural elements on the internal structure were evaluated to determine the effects of these increased loads on code margins.

3.3.3 Element Loads

The dynamic model used for the seismic analysis of the reactor building consisted primarily of interconnected vertical stick elements representing the stiffness properties of the containment structure, concrete internal structures, reactor vessel, and steam generators. A single stick of elements modeled the containment structure alone. The stick modeling the internal structures represented the combined stiffnesses of the various structural elements occurring at each level. Included in the internal structures were the primary and secondary shield walls and the refueling canal walls. Overall seismic loads acting on the containment and internal structures were developed from the response spectrum analyses. Seismic stresses and loads acting on the individual structural elements due to these overall loads were determined using techniques appropriate for the load-resisting systems evaluated.

The dynamic model stiffness properties of the containment structure were represented by elastic beam properties consisting of axial and shear areas and moments of inertia. For an open, hollow section such as the containment wall, the elastic seismic stress distributions are predicted with sufficient accuracy by elementary beam theory. Overall seismic loads acting on the containment consist of vertical axial force, horizontal shears, torsional moments, and overturning moments. The vertical axial forces due to vertical seismic response and overturning moments due to horizontal seismic response primarily induce meridional membrane stresses in the containment wall. The stresses due to the vertical axial force acting at a particular elevation of the containment wall were distributed uniformly across the entire cross-section at that elevation. The stresses due to the overturning moments were distributed linearly over the cross-section according to the first harmonic. The horizontal shear forces and torsional moments primarily induce tangential membrane shear stresses in the containment wall. In accordance with elementary beam theory, the tangential shear stresses due to the horizontal shear forces were distributed by the first harmonic while the stresses due to the torsional moments were distributed uniformly around

the containment cross-section. Because seismic response of the reactor building was predicted by a series of planar models, torsional moments were not generated by the response spectrum analyses. To account for the possibility of accidental torsion, torsional moments were determined by factoring the horizontal shears by an eccentricity equal to five percent of the containment structure diameter.

A summary of the derivation of the seismic stress distributions through the containment wall is shown in Figure II-3-19. For use in the structure capacities evaluation, these stresses were converted to loads acting on a unit length of wall section by factoring them by the wall thickness. Resulting seismic loads used in developing the containment wall code margins are listed in Tables II-4-1, II-4-3, and II-4-4. Based on the results of Bechtel's finite element analysis of the axisymmetric containment structure for the nonaxisymmetric design seismic loads transmitted with Reference 20, membrane hoop forces, hoop and meridional moments, and radial shears are also expected in the wall, particularly near discontinuities such as the wall-dome and wall-base mat intersections. However, these additional loads are relatively small and were neglected with little resulting error. SME loads acting on the containment wall account for overall structure behavior and are applicable to typical wall sections. Wall discontinuities, such as the equipment hatch and pipe penetrations, introduce additional stresses, but additional reinforcement is typically provided at these locations to resist these stresses.

The dome of the containment structure was included in the reactor building dynamic model as a part of the containment vertical stick. Seismic response of a shallow, spherical shell segment such as the dome is expected to be due primarily to the vertical vibration. Reference 16 notes that the frequency of a shallow, spherical shell segment with a rise less than one-eighth of its lateral projection can be

expressed in terms of the frequency of the flat plate having the same thickness, material properties, boundary conditions, and projected lateral dimensions as follows:

$$\omega_{ij} \text{ (shallow spherical shell)} = \left[\omega_{ij}^2 \text{ (flat plate)} + \frac{E}{\mu R^2}\right]^{1/2}$$

where

ω_{ij} = Circular natural frequency in the ij mode

E = Modulus of elasticity

μ = Material mass density

R = Radius to the midsurface of the shallow, spherical shell segment

The frequency of the circular flat plate with boundary rotational stiffness provided by the cylinder, a typical thickness of 3 feet, a radius of 58 feet, a mass density of 4.66 lb-sec^2/ft^4 for concrete weighing 150 lb/ft^3, and a modulus of elasticity of 6.3×10^8 lb/ft^2 for 6,000 psi concrete was found to be 5.0 Hz (from Reference 17). Using a radius of 89 feet to the midsurface of the spherical shell segment, the frequency of the dome was calculated to be approximately 21.4 Hz using the analogy in Equation 3-1. Vertical response of the dome was determined to occur in the rigid response region based upon an inspection of the vertical response spectra at the top of the containment. Seismic forces in the dome were then calculated using equations presented in Reference 18 for a spherical shell loaded by its own weight. The inertial loading was defined by factoring the dome mass by the vertical ZPA of 0.14g. Seismic forces used in the capacities evaluation of the dome are reported in Section 4.1.2.

The base mat of the reactor building serves to transmit loads from the containment wall and the internal structures to the supporting soil medium. Seismic forces acting normal to the base mat consist of

vertical membrane forces from the containment wall and primary and secondary shield walls along with resulting soil bearing pressures. The base mat is a concrete slab varying in thickness from 9 to 13 feet and is stiffened transversely by the walls it supports. The base slab is quite stiff compared to the soil below. For rigid foundations, a common design practice is to treat the soil bearing pressures due to structure loads as being distributed linearly across the contact surface. This approximation was used in the SME definition of base mat forces due to seismic loads.

Seismic forces acting on the base mat were determined using classical solutions predicted by the theory of elasticity appropriate for the geometry and applied loading. The overturning moments from the containment wall cause vertical wall membrane forces varying according to the first harmonic as shown in Figure II-3-19 and linearly varying soil pressures symmetric about the diameter parallel to the axis about which the moment acts. Radial and tangential moments in the base mat were determined using the closed-form solutions for a circular plate simply-supported at the edges loaded in this manner presented in Section 63 of Reference 19. The meridional wall membrane force due to vertical seismic response is uniformly distributed and results in uniformly distributed soil pressures. Solutions for the base mat forces for this loading were taken from Section 16 of Reference 19. Overall seismic loads at the bottom node of the lowest element of the dynamic model representing the containment wall were taken as load input to the classical solution equations used to determine base mat moments.

Similar to the containment wall, vertical membrane forces in the walls of the internal structures result from seismic overturning moments and vertical axial forces. These loads were distributed to the primary and secondary shield walls as described later in this section. The resulting load distributions indicate that the secondary shield walls transmit most of these loads to the base mat. Base mat forces due to overall loads from the internal structures were developed from classical solutions for circular plates loaded centrally through a portion of the

plate that is rigid. Load input to the classical solution equations used to determine base mat moments consisted of overall seismic loads at the bottom node of the lowest element of the dynamic model representing the internal structures. The combined stiffness of the primary and secondary shield walls is expected to be sufficient to permit the base mat to be modeled as being rigid within the outer boundaries of the internal structures. The radius of the rigid central portion of the base mat was taken to be 44 feet and corresponds to the radius of the circle having the same perimeter as the box structure formed by the secondary shield walls. The solution for the internal forces in a circular plate subjected to a moment imparted by a rigid central portion that in turn is resisted by linearly varying pressures across the face of the plate is contained in Section 63 of Reference 19. Base mat forces due to overturning moments from the internal structures were calculated using this solution. The maximum stress occurs at the edge of the rigid plate portion and can also be calculated from parameters listed for Case 23 of Table 24 in Reference 17. The radial moment at the edge of the rigid plate portion due to uniform pressure against the face of the plate is available from the solution given by Case 21 of Table 24 of Reference 17. The base mat radial moment due to vertical seismic load from the internal structures was calculated using this solution.

Base mat forces due to overall seismic overturning moments and vertical forces from the containment wall and the internal structures were calculated separately. The base mat forces resulting from seismic response of the containment and internal structures due to a single ground motion component were superposed. The forces from the different ground motion components were combined by SRSS. The sum of the overturning moments from the containment wall and internal structures was found to exceed the corresponding moment in the soil spring beneath the reactor building. This indicates that the superposition of the loads from the containment and internal structures is conservative. Inertial forces associated with vertical response of the base mat are approximately uniformly distributed. For a uniformly distributed soil bearing pressure

resistance due to this loading, moments do not occur in the base mat due to its own inertia The sum of the vertical seismic forces from the containment wall, internal structures, and base mat was found to exceed the soil spring reaction. This indicates the conservatism inherent in the superposition of the base mat forces from the containment and internal structures. Seismic loads from the steam generators were found to be small and were neglected with little error. Resulting base mat forces used in the capacities evaluation are reported in Section 4.1.3.

The general load combination used in the structure capacities evaluation is discussed in Section 7.1 of Volume I. The dead and live load cases account for loads occurring at normal operating conditions. In addition to the dead, live, and operating thermal loads on the containment, forces acting on the structural elements due to the design accident internal pressure and thermal gradient were included. The full design accident pressure and thermal gradient were conservatively used. The code margins for the structural elements at the containment were determined for the worst case obtained from the following load combinations:

$$U = D + F + L + T_o + SME \qquad (3\text{-}2)$$

$$U = D + F + L + P + T_A + SME \qquad (3\text{-}3)$$

where

U = Limiting load on the structure

D = Dead loads

F = Prestress loads

L = Live loads

T_o = Thermal effects during normal operating conditions

P = Design accident internal pressure loads

T_A = Total thermal effects which may occur during a design accident

SME = Seismic Margin Earthquake loads

The accident pressure and thermal effects are based on the FSAR conditions for a large LOCA rather than small break LOCA. A small break LOCA is considered somewhat more realistic but would have been conservative since the probability of peak earthquake loads occurring coincidently with those from any LOCA is considered remote. Thus, the load combination assuming the simultaneous occurrence of the design basis LOCA with the peak SME loads is considered to be very conservative.

Forces acting at various locations of the wall, base mat, and dome of the containment structure are reported in the FSAR (Reference 1) for the design load combinations. Different forces were presented for the different thermal gradients resulting from summer and winter temperature conditions. Forces due to the axisymmetric loads (dead, accident pressure, etc.) were predicted by finite element analyses using a computer program capable of accounting for material nonlinearities. The forces due to the design seismic loads were determined by separate static finite element analyses performed for an elastic, axisymmetric structure subjected to nonaxisymmetric loads. These forces were superposed on those from the axisymmetric analyses to arrive at forces for the design load combinations involving the design OBE and SSE. Containment forces due to the design SSE included in the design load combinations were supplied as a part of Reference 20.

Forces acting on the containment structure for the load combinations used in this evaluation as specified in Equations 3-2 and 3-3 were determined by superposing the forces occurring during normal operating and accident conditions listed in the FSAR on those due to the SME. For the load combination defined in Equation 3-2, forces due to the normal operating conditions were taken from Tables 3.8-3 and 3.8-4 of the FSAR. For the load combination defined in Equation 3-3, forces occurring at accident conditions were taken from Tables 3.8-5 and 3.8-6. Forces consisting of meridional and hoop membrane forces, meridional and hoop moments, and radial or transverse shears are listed in these tables for 15

different cross-sections through the dome, wall, and base mat. The locations of these sections are shown in Figure II-4-3. Seismic forces due to the SME were calculated for these locations and superposed on the forces at normal operating or accident conditions. The distinction between summer and winter temperature conditions was retained in this evaluation. The sign convention used in defining the FSAR forces was also adopted. Seismic forces were taken to add to or subtract from the forces at normal operating or accident conditions since seismic effects can cause forces having either positive or negative signs. Forces acting on the selected containment wall sections due to the SME, normal operating conditions, and accident conditions are listed in Tables II-4-1, II-4-3, and II-4-4. The net forces on the wall sections corresponding to the load combinations used in this study are listed in Tables II-4-2, II-4-3, and II-4-4. Similar forces acting on the selected base mat and dome sections are reported in Sections 4.1.2 and 4.1.3.

A single vertical stick was used to model the combined stiffness and mass properties of the internal structures. Similar to the containment structure, the dynamic model stiffness properties of the internal structures consisted of axial and shear areas and moments of inertia. The axial area and moments of inertia were based on elementary beam theory with all of the walls at a given horizontal section combined to form a single beam cross-section. The shear area for response in a given horizontal direction was defined as the sum of the areas of the walls loaded in-plane in that direction. As an example, the internal structures cross-section used to develop the dynamic model properties between Elevation 603'-0" and 626'-0" is shown in Figure II-3-20.

The reactor building internal structures essentially form an open, hollow section generally lacking the horizontal diaphragms of a conventional building structure that would distribute the seismic inertial loads to the vertical load-resisting elements. As with the containment structure, the elastic seismic stress distributions are predicted with sufficient accuracy by elementary beam theory for this type of structure. Vertical membrane stresses in the walls due to overall

seismic overturning moments and vertical axial loads were determined in the same manner as the containment wall meridional membrane stresses. Consistent with the derivation of the dynamic model shear areas, overall seismic horizontal shears were distributed to the individual walls in proportion to their contributions to the total shear areas. Torsional moments were not generated by the response spectrum analyses. To account for the possibility of accidental torsion, torsional moments were determined for the internal structures in the same manner as previously described for the containment wall. Polar moments of inertia were calculated for the same cross-sections used to develop the other stiffness properties of the dynamic model. Shear stresses due to the accidental torsional moments were then calculated for walls using these polar moments of inertia. As noted in Section 4.2.2, the shear strengths of the secondary shield walls were developed in terms of load capacities rather than stress capacities. The accidental torsion contributions to the seismic shear loads were determined by factoring the shear stresses due to torsion by the wall areas. The total shear force on a wall due to a single ground motion component was taken as the sum of the contributions from the direct horizontal shear and the torsional moment.

Forces acting on the structural members of the internal structures due to loads occurring at normal operating conditions were taken from the results of static finite element analyses supplied by Bechtel (Reference 21). Load cases occurring at normal operating conditions consisted of dead load, live load, and thermal effects at normal operation. The code margins for the structural elements of the internal structures were calculated for the worst case from the following load combinations:

$$U = D + T_o + SME \qquad (3\text{-}4)$$

$$U = D + L + T_o + SME \qquad (3\text{-}5)$$

1

The terms used in the load combination equations were previously defined in the discussion on the containment structure load combinations.

The three-dimensional finite element model used for these static analyses generally consisted of plate elements representing the walls and beam elements representing the beams and columns. Results from the static analyses for the plate elements modeling the concrete walls and slabs consisted of membrane normal and shear forces per unit length and out-of-plane bending and twisting moments per unit length. The element stresses due to the normal operating condition load cases were used to define stresses and loads consistent with the definition of the member capacities in the in-plane shear code margin calculations (see Section 4.2). Shear capacities for rectangular walls such as the secondary shield walls were defined in terms of the total in-plane shear force. Shear forces due to the normal operating condition load cases were determined by integrating the in-plane shear stresses over the lengths of the walls. As described in Section 4.2, capacities of the other members were defined at the local level in terms of forces per unit member length. For these capacities, the membrane shear forces, vertical membrane forces, and out-of-plane bending moments about the horizontal axis from the static analyses acting on a unit member length were used directly in the load combination equations. Forces and forces per unit member length due to seismic and normal operating condition loads for the members of the internal structures evaluated are reported in Section 4.2.

TABLE II-3-1

REACTOR BUILDING NATURAL FREQUENCIES, MODAL MASSES, AND MODAL DAMPING

EAST-WEST DYNAMIC MODEL

Mode	Lower Bound Soil			Intermediate Soil			Upper Bound Soil			Mode Description
	Frequency (Hertz)	Modal Mass (%)	Modal Damping (% Critical)	Frequency (Hertz)	Modal Mass (%)	Modal Damping (% Critical)	Frequency (Hertz)	Modal Mass (%)	Modal Damping (% Critical)	
1	1.13	66.8	6	1.98	62.1	6	2.60	58.5	6	Soil-Structure Rocking Mode
2	2.87	33.0	28	4.97	35.3	22	6.05	31.2	15	Out-of-Phase Soil-Structure Translation
3	7.22	---	2	7.32	0.6	2	7.42	2.3	3	Reactor Vessel Mode
4	7.94	0.1	2.5	8.49	1.8	8	9.47	7.3	10	In-Phase Reactor Internal, Steam Generator Mode
5	13.63	---	2.5	13.64	---	2	13.64	---	2	Steam Generator Mode
6	15.63	---	2.5	15.85	0.1	3	16.20	0.6	2.5	Containment Mode
7	20.94	-	2.5	21.63	---	2.5	22.47	---	2.5	
8	26.79	-	2.5	26.82	---	2.5	26.85	---	2.5	

Note: 1. Modal mass percentage is defined as the percentage of the total structure mass participating in the mode. Modal mass percentages less than 0.1 percent are not shown.

TABLE II-3-2

REACTOR BUILDING NATURAL FREQUENCIES, MODAL MASSES, AND MODAL DAMPING

NORTH-SOUTH DYNAMIC MODEL

Mode	Lower Bound Soil			Intermediate Soil			Upper Bound Soil			Mode Description
	Frequency (Hertz)	Modal Mass (%)	Modal Damping (% Critical)	Frequency (Hertz)	Modal Mass (%)	Modal Damping (% Critical)	Frequency (Hertz)	Modal Mass (%)	Modal Damping (% Critical)	
1	1.13	66.7	6	1.98	61.9	6	2.60	58.3	6	Soil-Structure Rocking Mode
2	2.87	33.2	28	5.01	36.0	24	6.16	32.4	17	Out-of-Phase Soil-Structure Translation
3	7.24	---	2	7.33	0.6	2	7.44	3.4	3	Reactor Vessel Mode
4	8.33	---	3	8.92	1.2	6	9.87	5.2	10	In-Phase Reactor Internal, Steam Generator Mode
5	13.62	---	2.5	13.62	---	2	13.63	---	2	Steam Generator Mode
6	15.63	---	2.5	15.87	0.1	3	16.23	0.7	6	Containment Mode
7	21.16	---	2.5	21.76	---	2.5	22.52	---	2.5	
8	26.27	---	2.5	26.28	---	2.5	26.29	---	2.5	

Note: 1. Modal mass percentage is defined as the percentage of the total structure mass participating in the mode. Modal mass percentages less than 0.1 percent are not shown.

TABLE II-3-3

REACTOR BUILDING NATURAL FREQUENCIES, MODAL MASSES, AND MODAL DAMPING

VERTICAL DYNAMIC MODEL

Mode	Lower Bound Soil			Intermediate Soil			Upper Bound Soil			Mode Description
	Frequency (Hertz)	Modal Mass (%)	Modal Damping (% Critical)	Frequency (Hertz)	Modal Mass (%)	Modal Damping (% Critical)	Frequency (Hertz)	Modal Mass (%)	Modal Damping (% Critical)	
1	2.16	99.9	55	4.46	99.7	48	6.16	98.7	40	Vertical Soil-Structure Translation
2	15.90	---	2.5	16.06	0.2	2	16.28	0.9	3	Vertical Soil-Structure mode with containment out-of-phase
3	19.26	---	.	19.29	---	2.5	19.35	0.1	2.5	Vertical structure mode with reactor vessel and reactor internals out-of-phase

Note: 1. Modal mass percentage is defined as the percentage of the total structure mass participating in the mode. Modal mass percentages less than 0.1 percent are not shown.

Table II-3-4

Comparison of In-Structure Zero Period Accelerations Determined by Direct Integration and Modal Superposition

Upper Bound Soil Case

Location	North-South Response Due to North-South Excitation		East-West Response Due to East-West Excitation		Vertical Response Due to Vertical Excit tion	
	Direct Integration	Modal Superposition	Direct Integration	Modal Superposition	Direct Integration	Modal Superposition
Containment - Elev. 786' - 0"	0.385	0.386	0.389	0.392	0.114	0.114
Containment - Elev. 664' - 0"	0.170	0.167	0.177	0.181	0.106	0.109
Containment - Elev. 591' - 6"	0.139	0.159	0.138	0.154	0.099	0.105
Reactor Internals - Elev. 685' - 0"	0.270	0.284	0.277	0.292	0.099	0.107
Reactor Internals - Elev. 640' - 0"	0.188	0.205	0.184	0.199	0.098	0.106

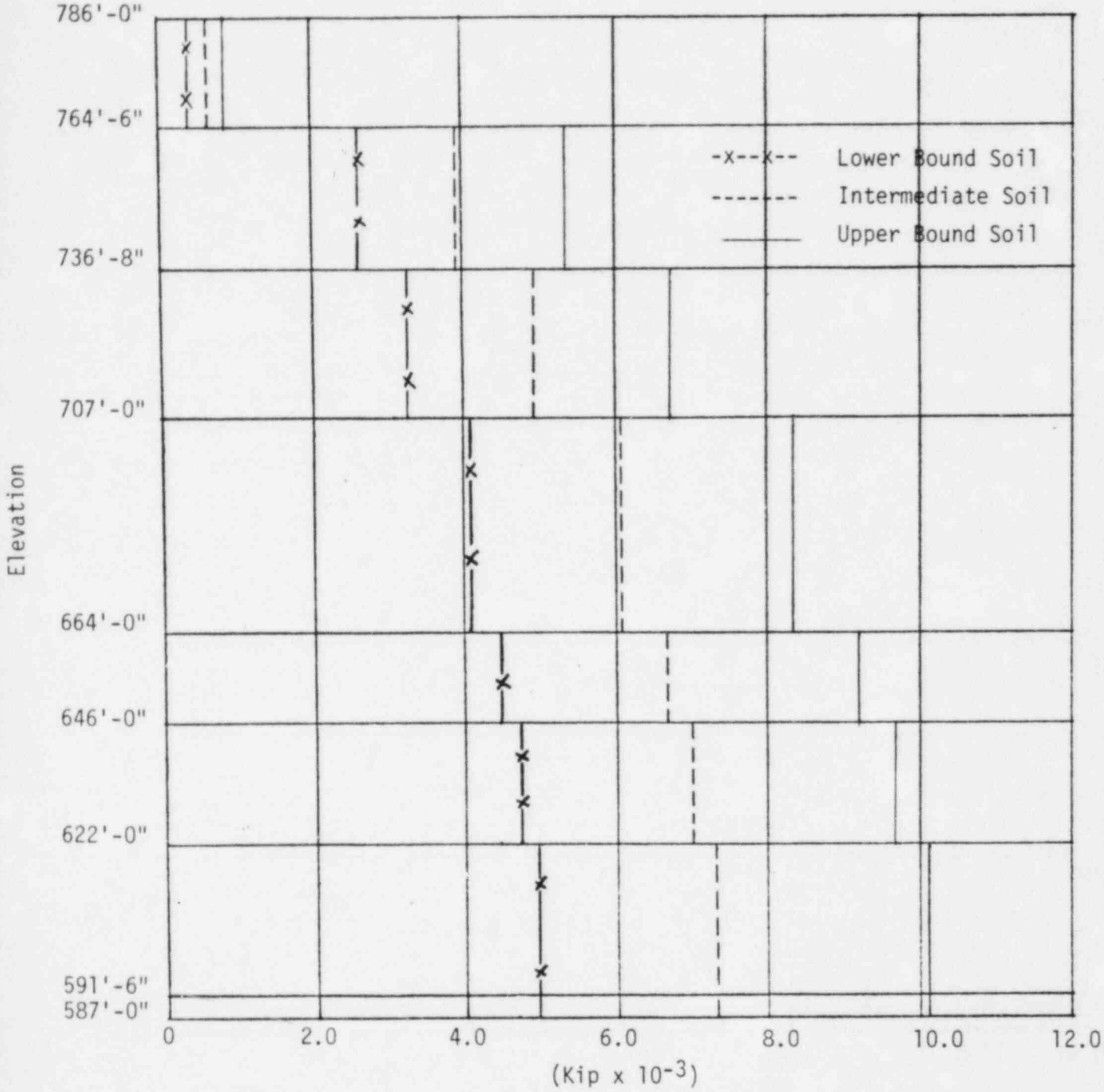

FIGURE II-3-1. CONTAINMENT DOME AND SHELL N-S SHEAR

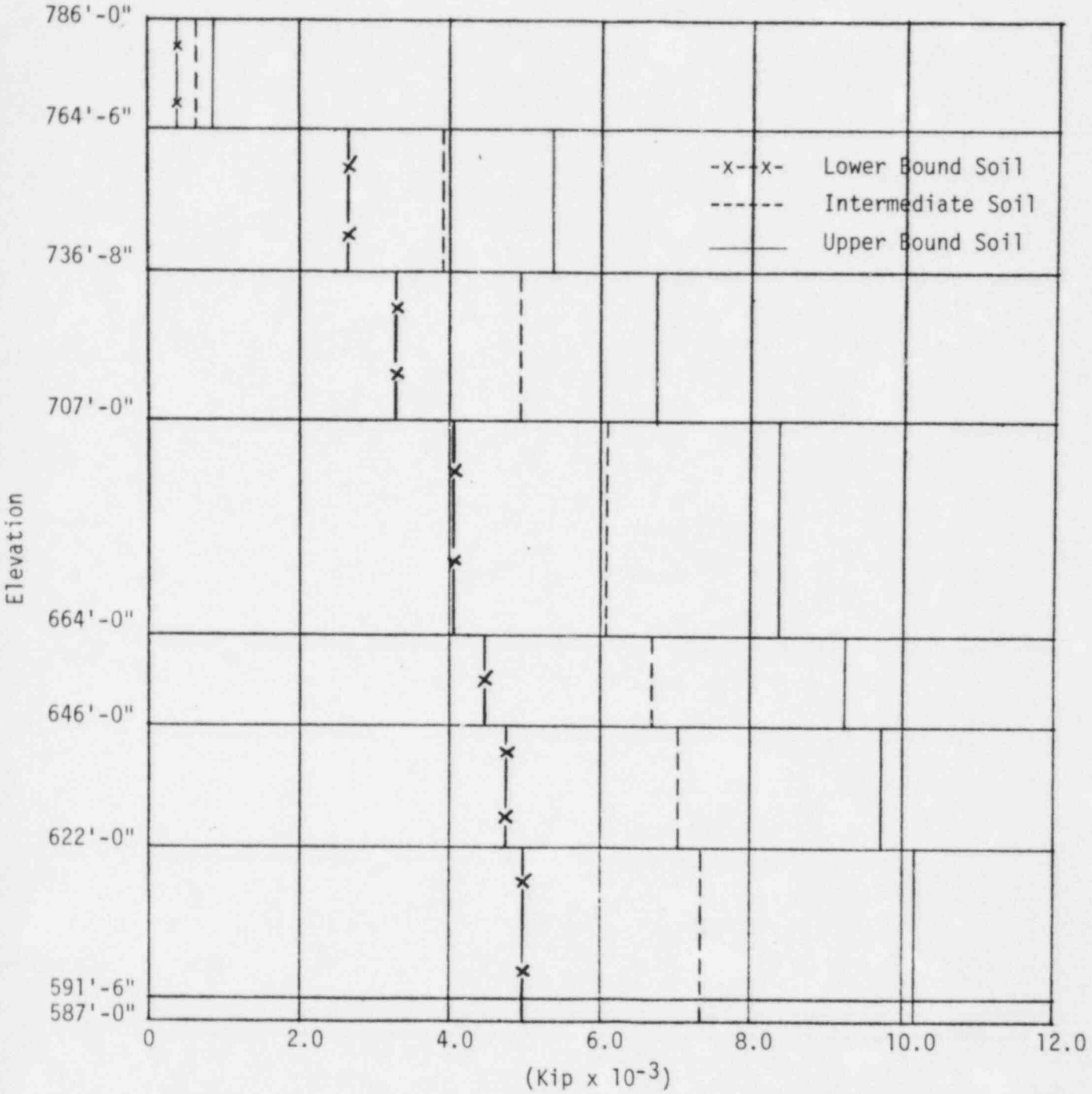

FIGURE II-3-2. CONTAINMENT DOME AND SHELL E-W SHEAR

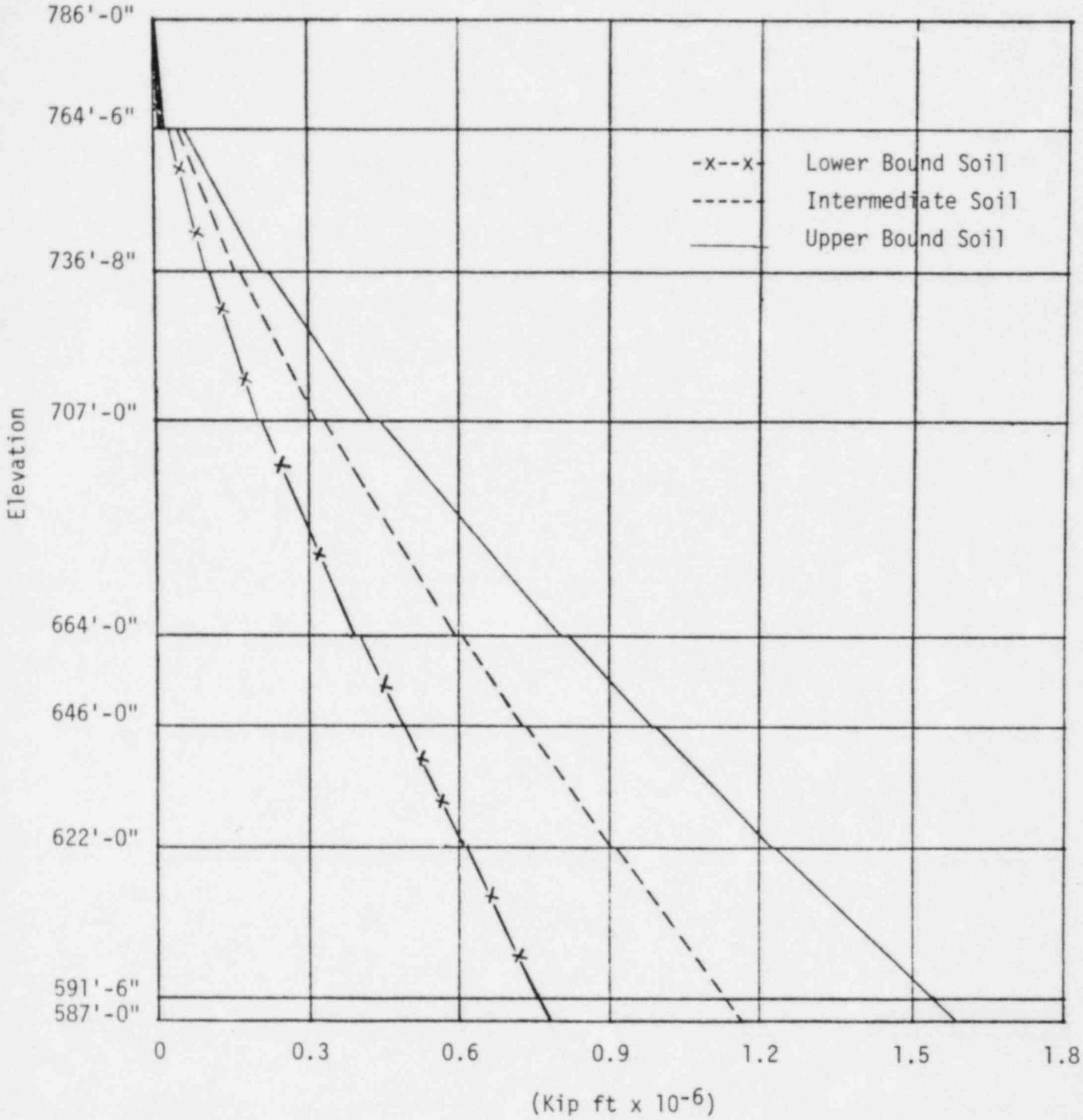

FIGURE II-3-3. CONTAINMENT DOME AND SHELL MOMENT ABOUT N-S AXIS

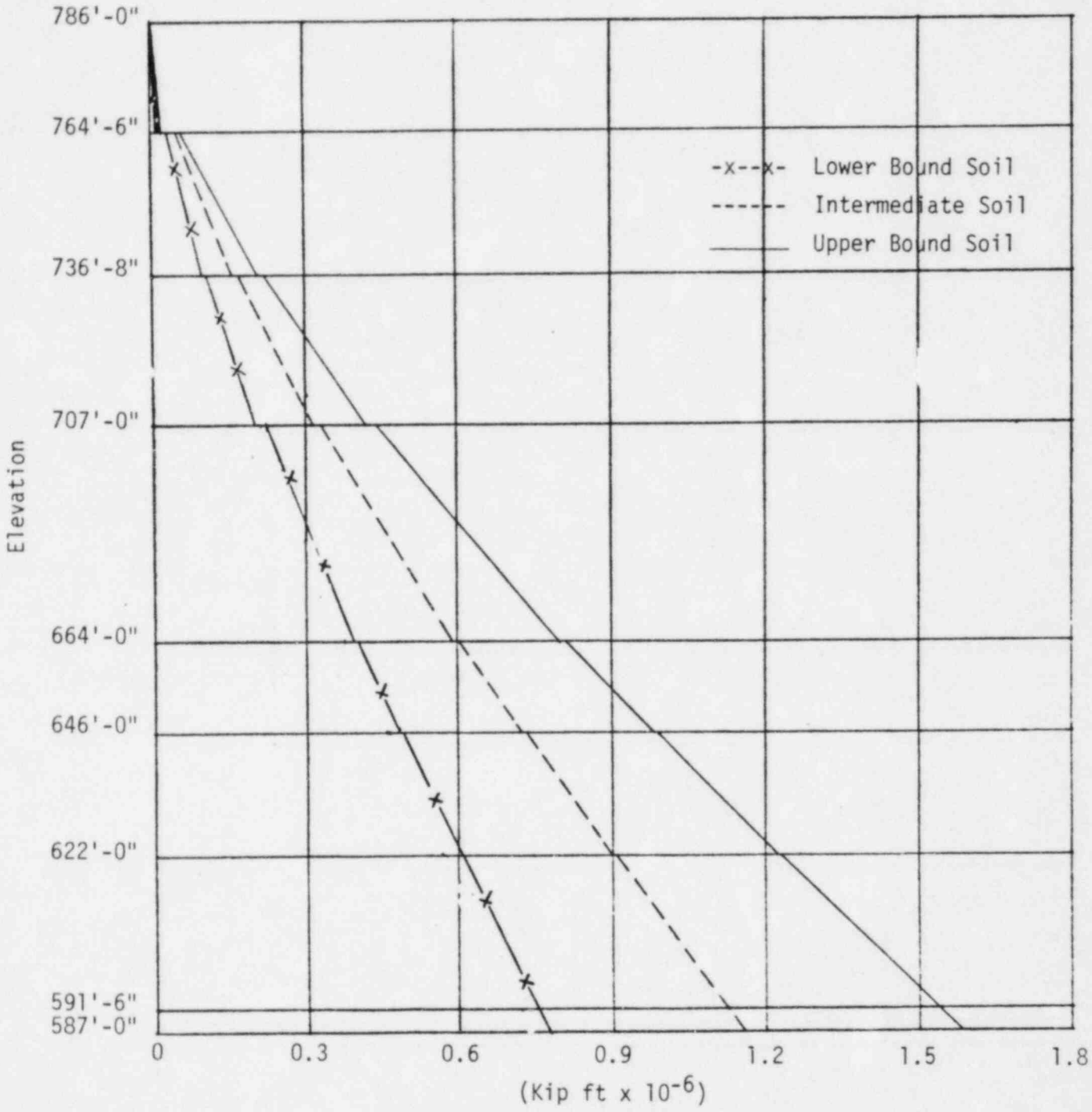

FIGURE II-3-4. CONTAINMENT DOME AND SHELL MOMENT ABOUT E-W AXIS

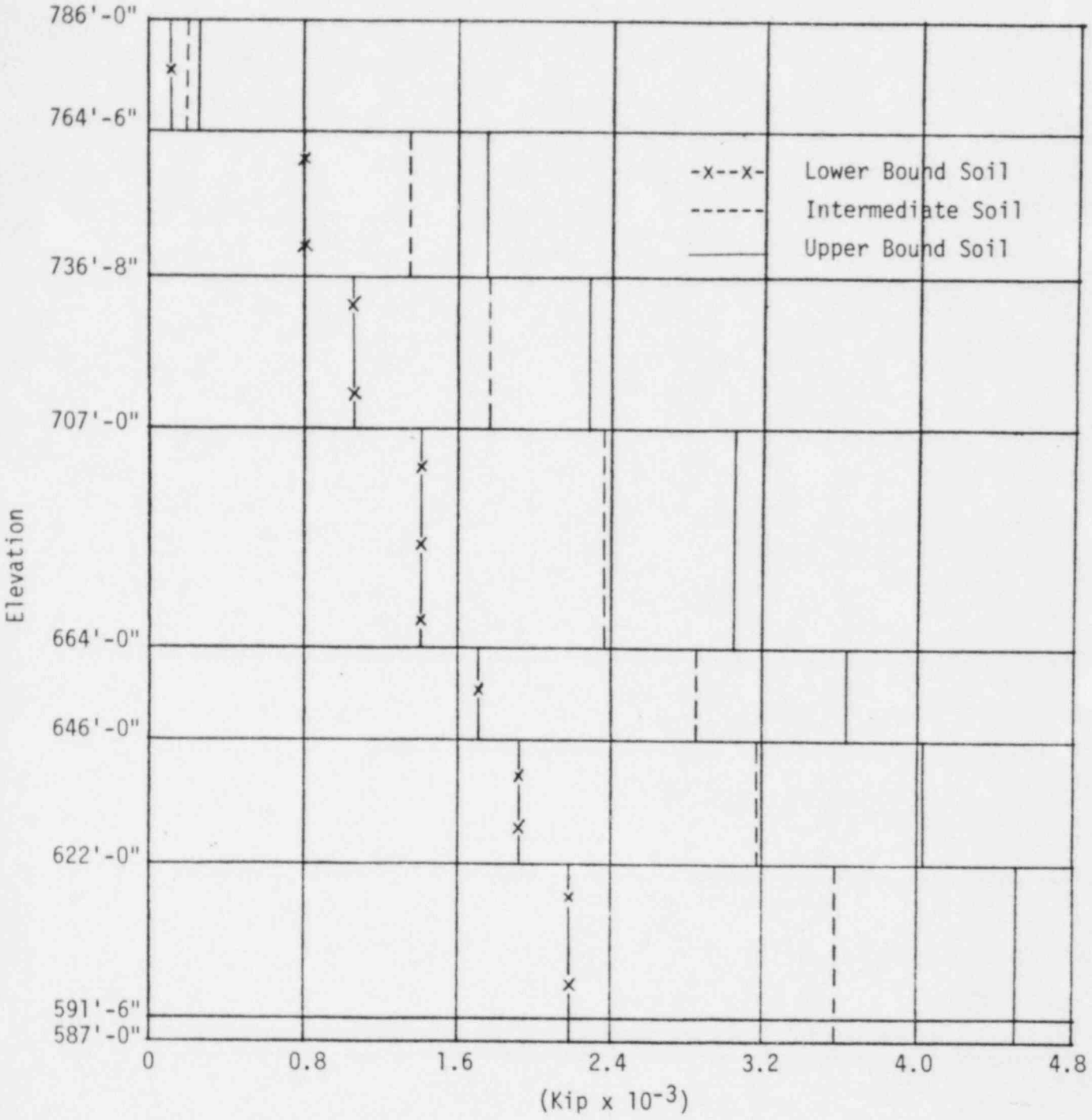

FIGURE II-3-5. CONTAINMENT DOME AND SHELL AXIAL FORCE

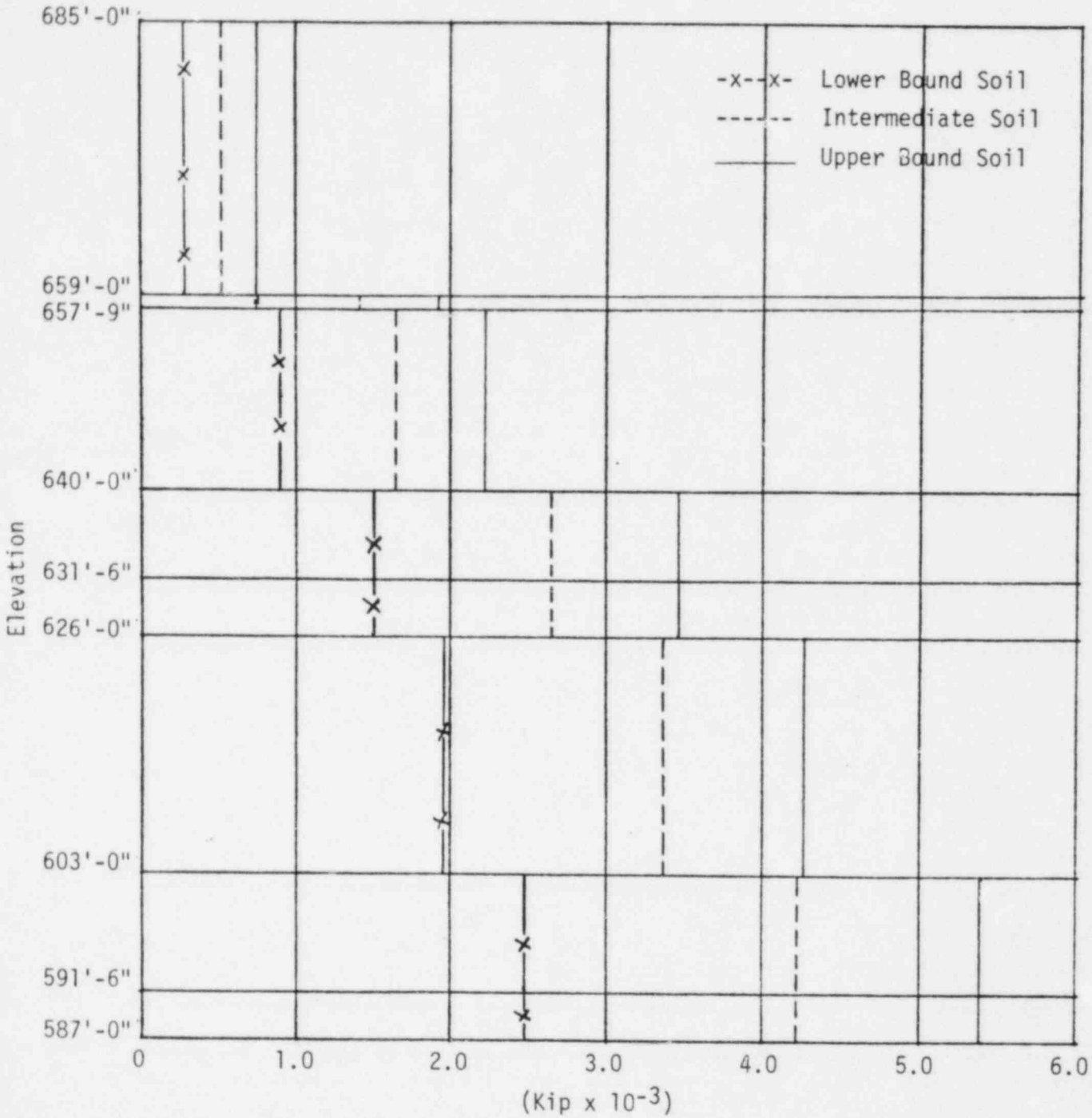

FIGURE II-3-6. INTERNAL STRUCTURE N-S SHEAR

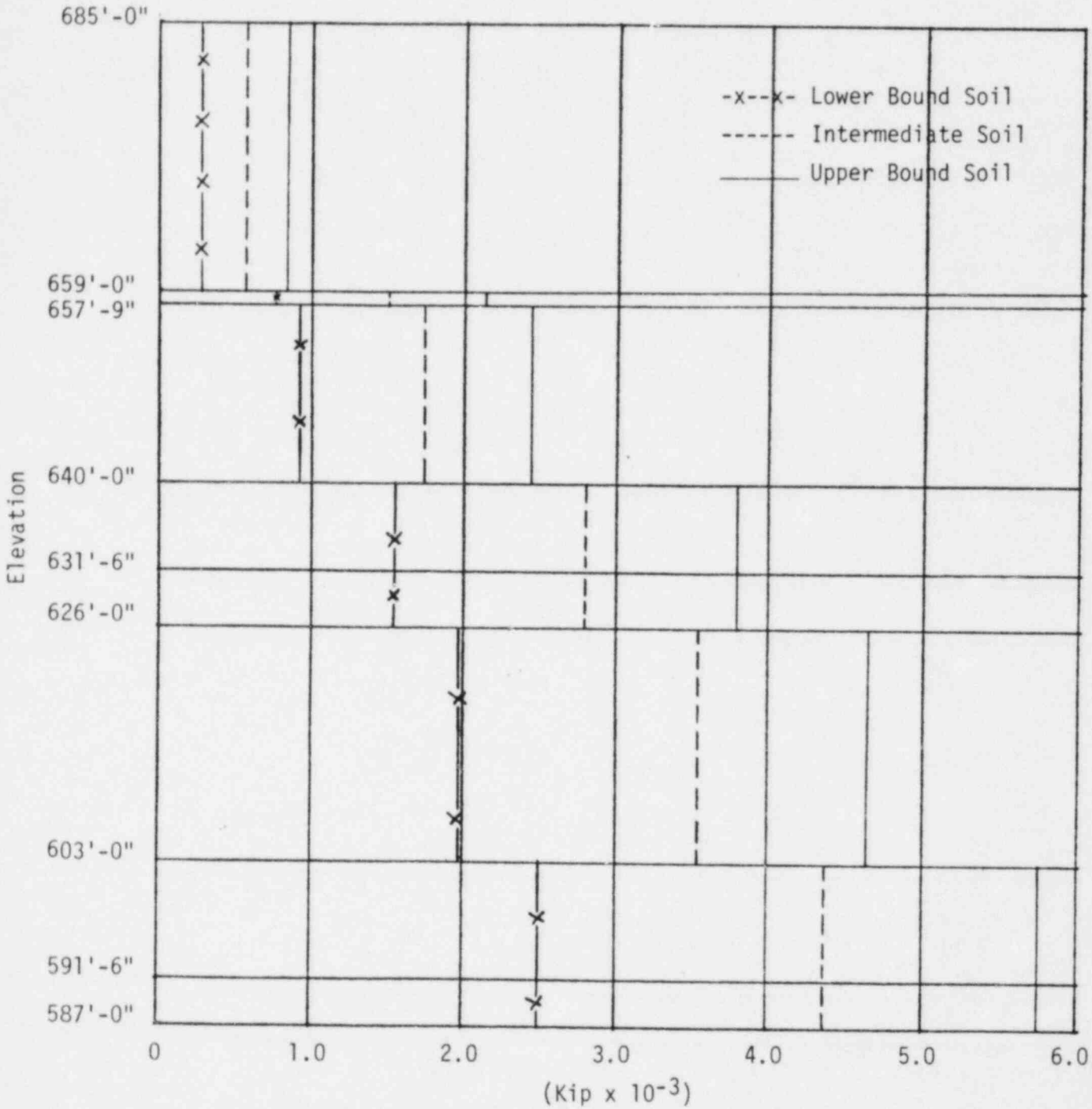

FIGURE II-3-7. INTERNAL STRUCTURE E-W SHEAR

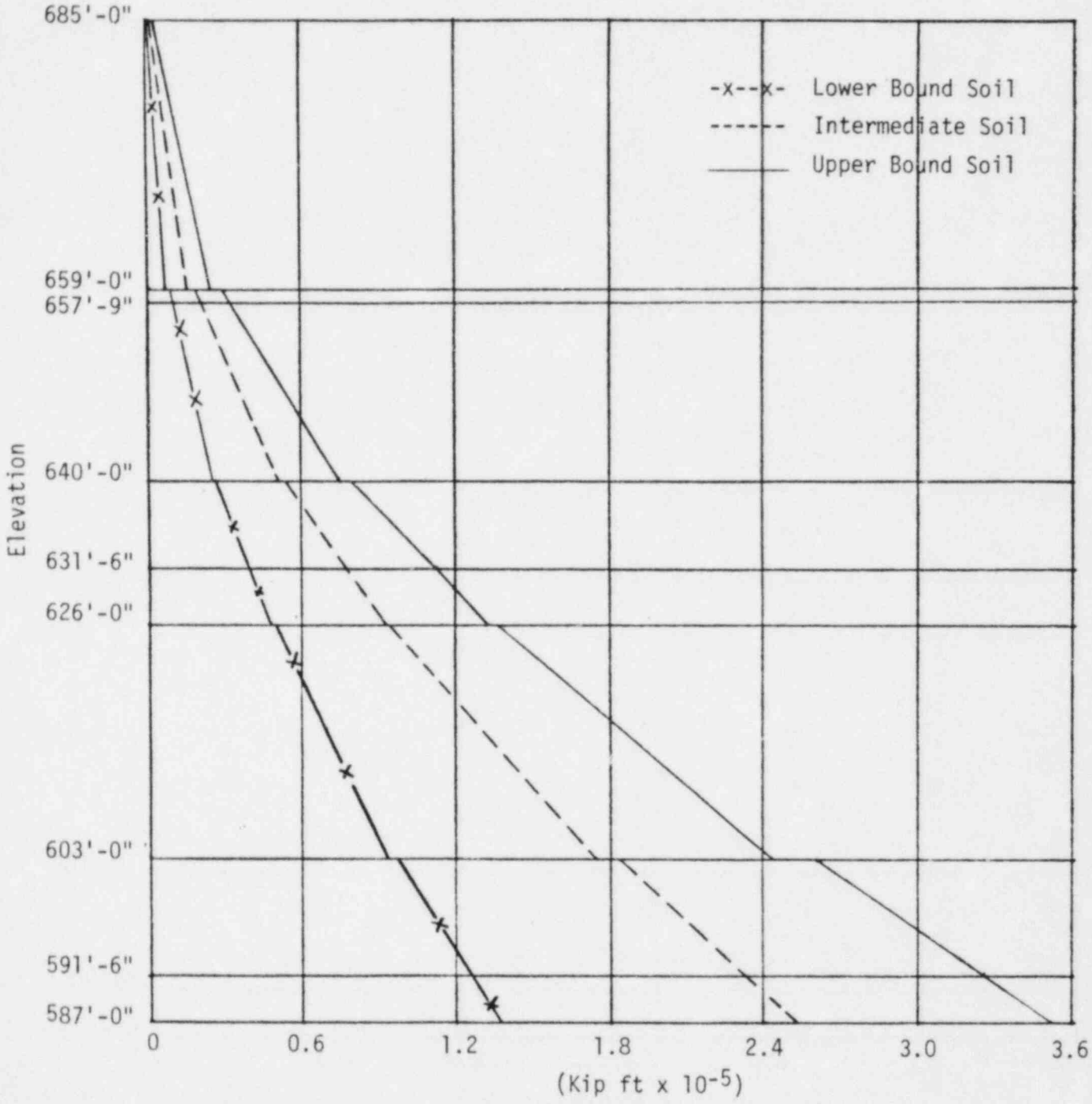

FIGURE II-3-8. INTERNAL STRUCTURE MOMENT ABOUT N-S AXIS

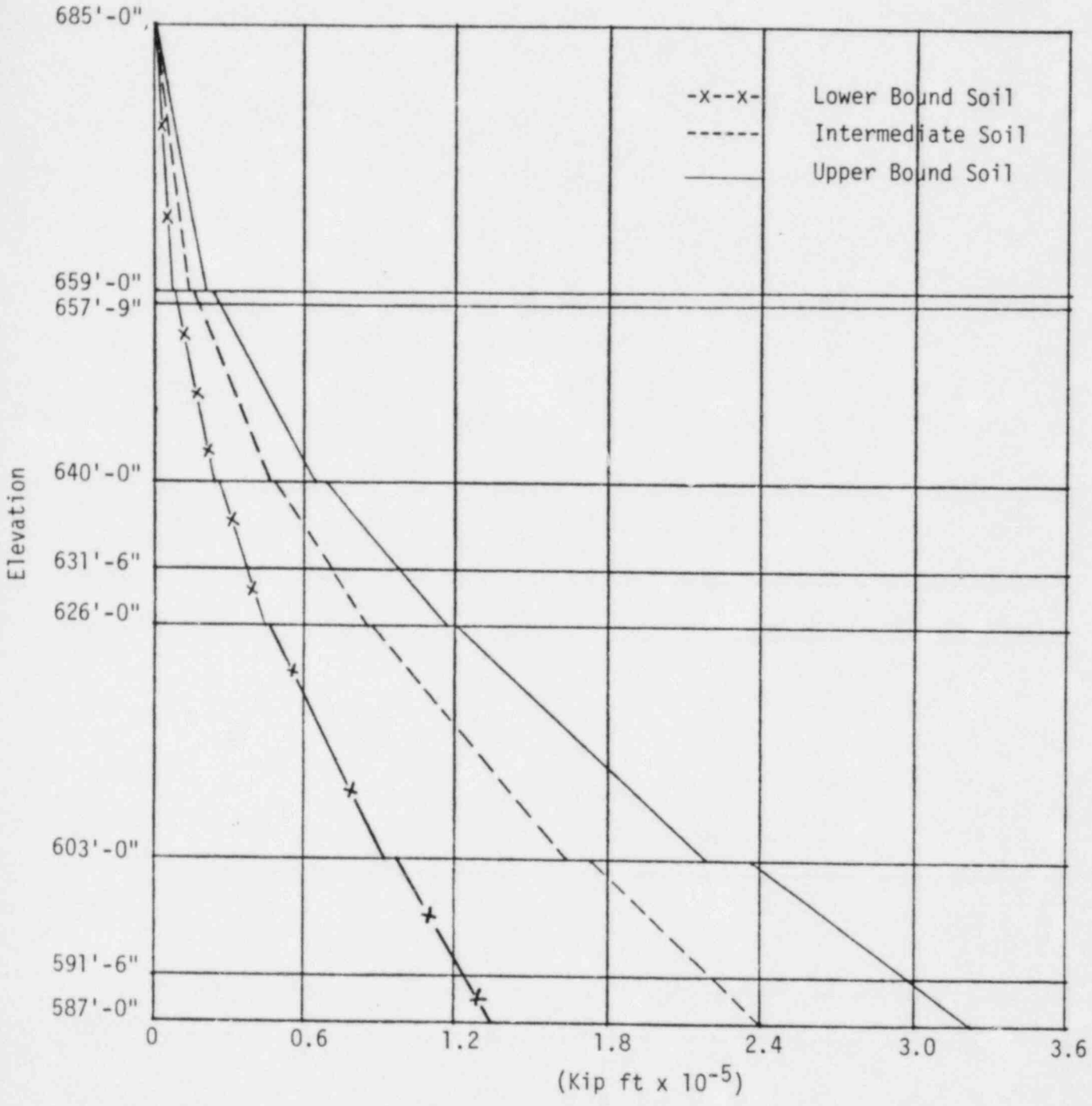

FIGURE II-3-9. INTERNAL STRUCTURE MOMENT ABOUT E-W AXIS

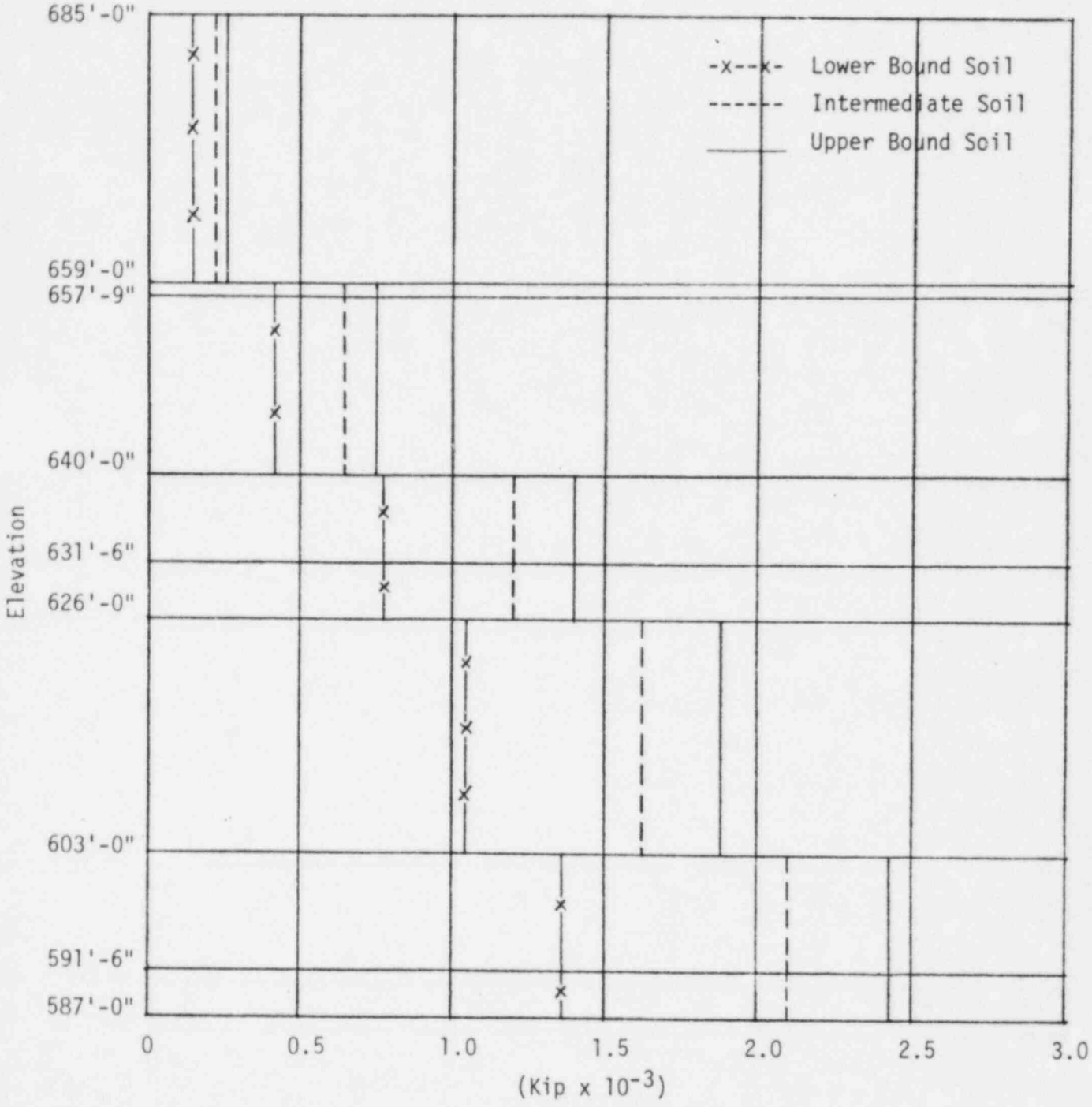

FIGURE II-3-10. INTERNAL STRUCTURE AXIAL FORCE

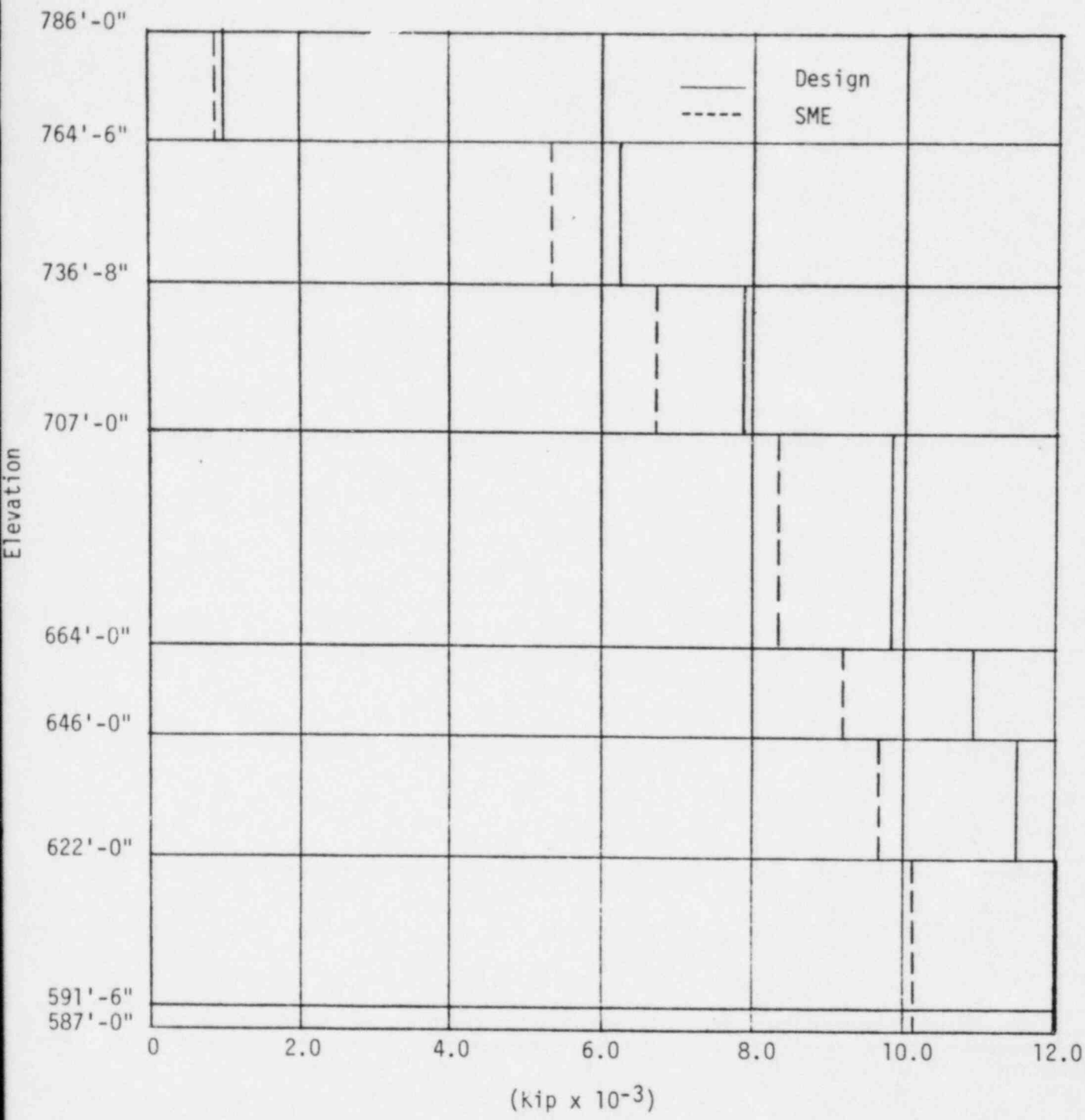

FIGURE II-3-11. CONTAINMENT DOME AND SHELL N-S SHEAR COMPARISON

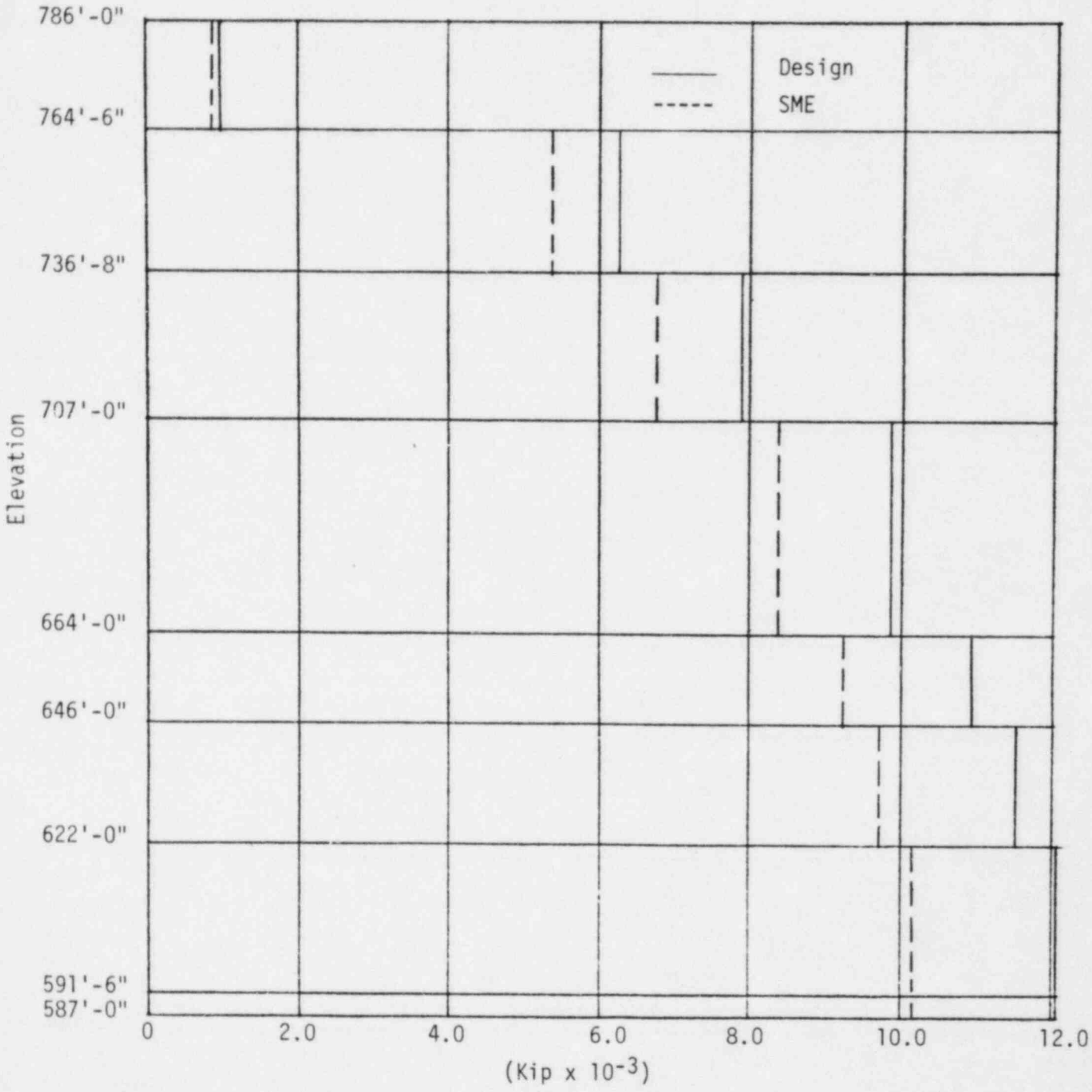

FIGURE II-3-12. CONTAINMENT DOME AND SHELL E-W SHEAR COMPARISON

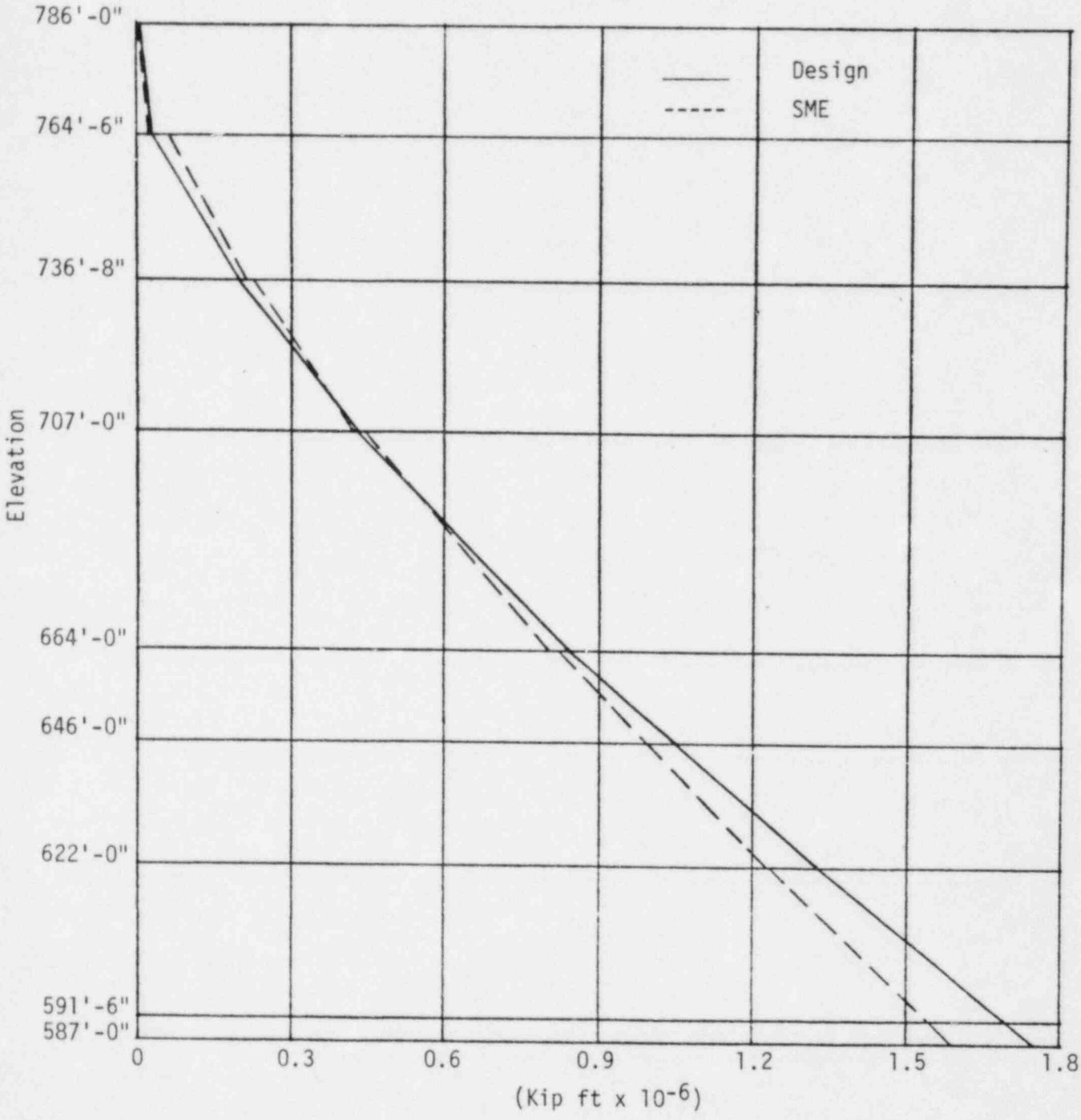

FIGURE II-3-13. CONTAINMENT DOME AND SHELL MOMENT ABOUT N-S AXIS COMPARISON

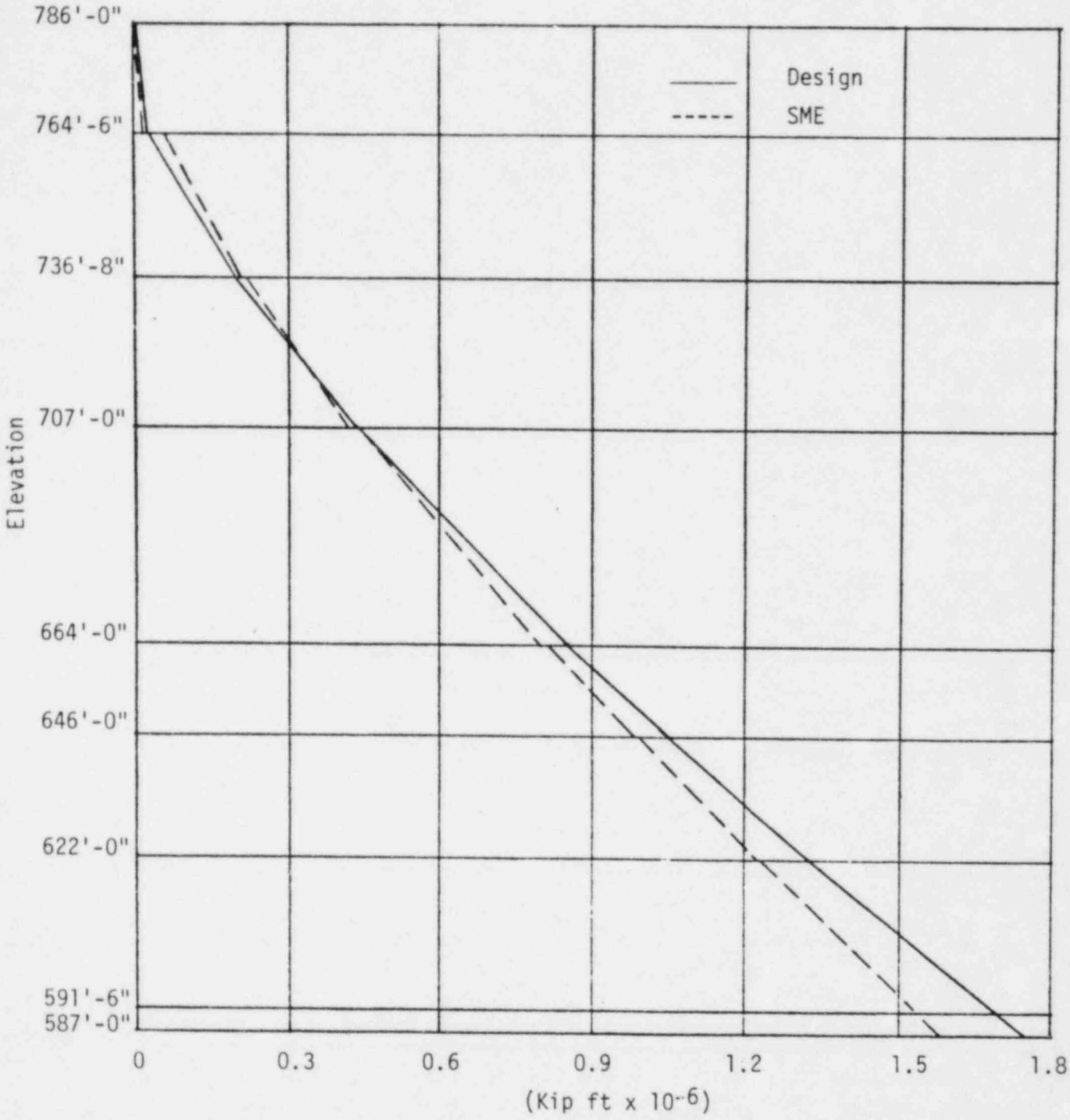

FIGURE II-3-14. CONTAINMENT DOME AND SHELL MOMENT ABOUT E-W AXIS COMPARISON

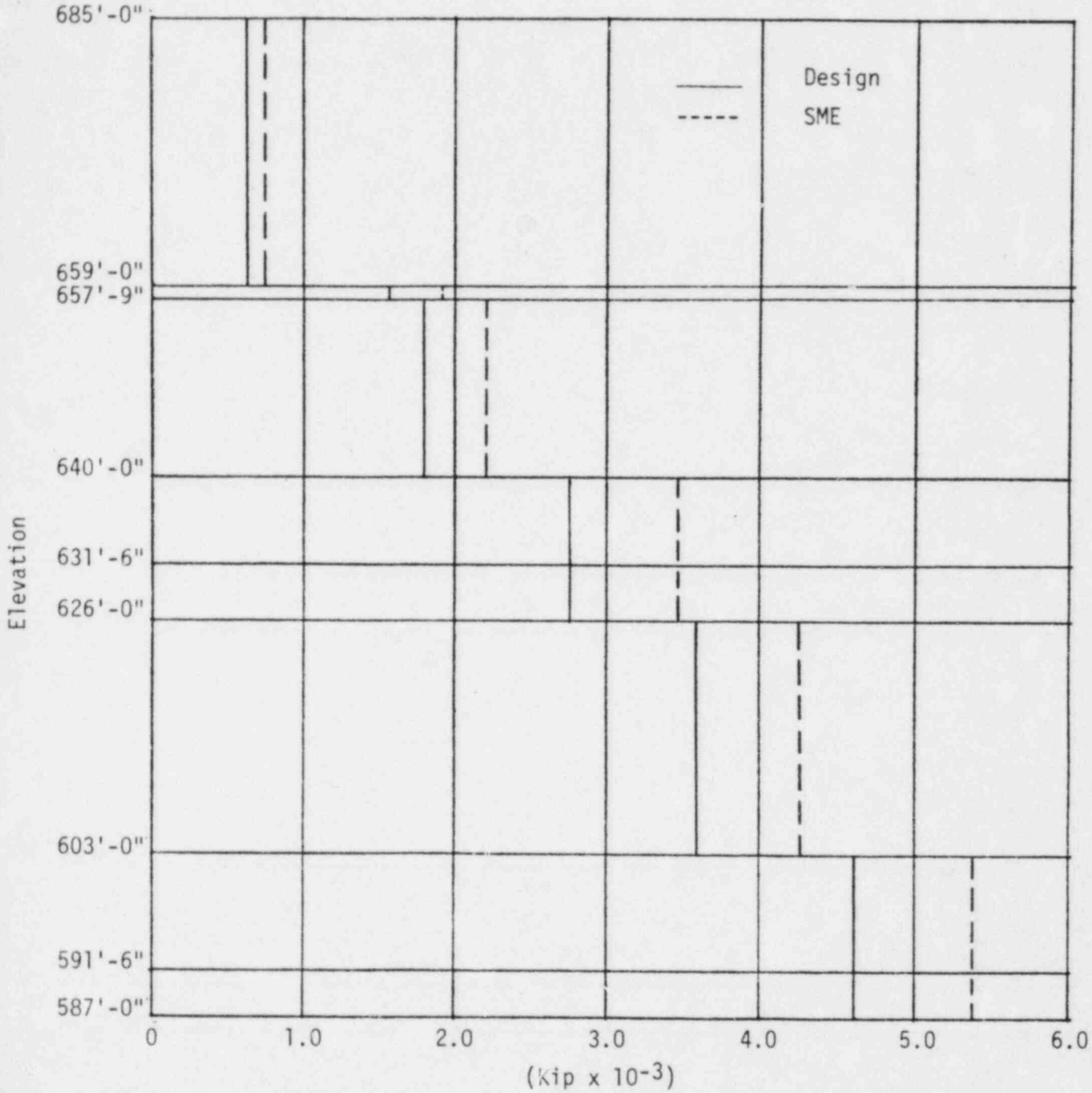

FIGURE II-3-15. INTERNAL STRUCTURE N-S SHEAR COMPARISON

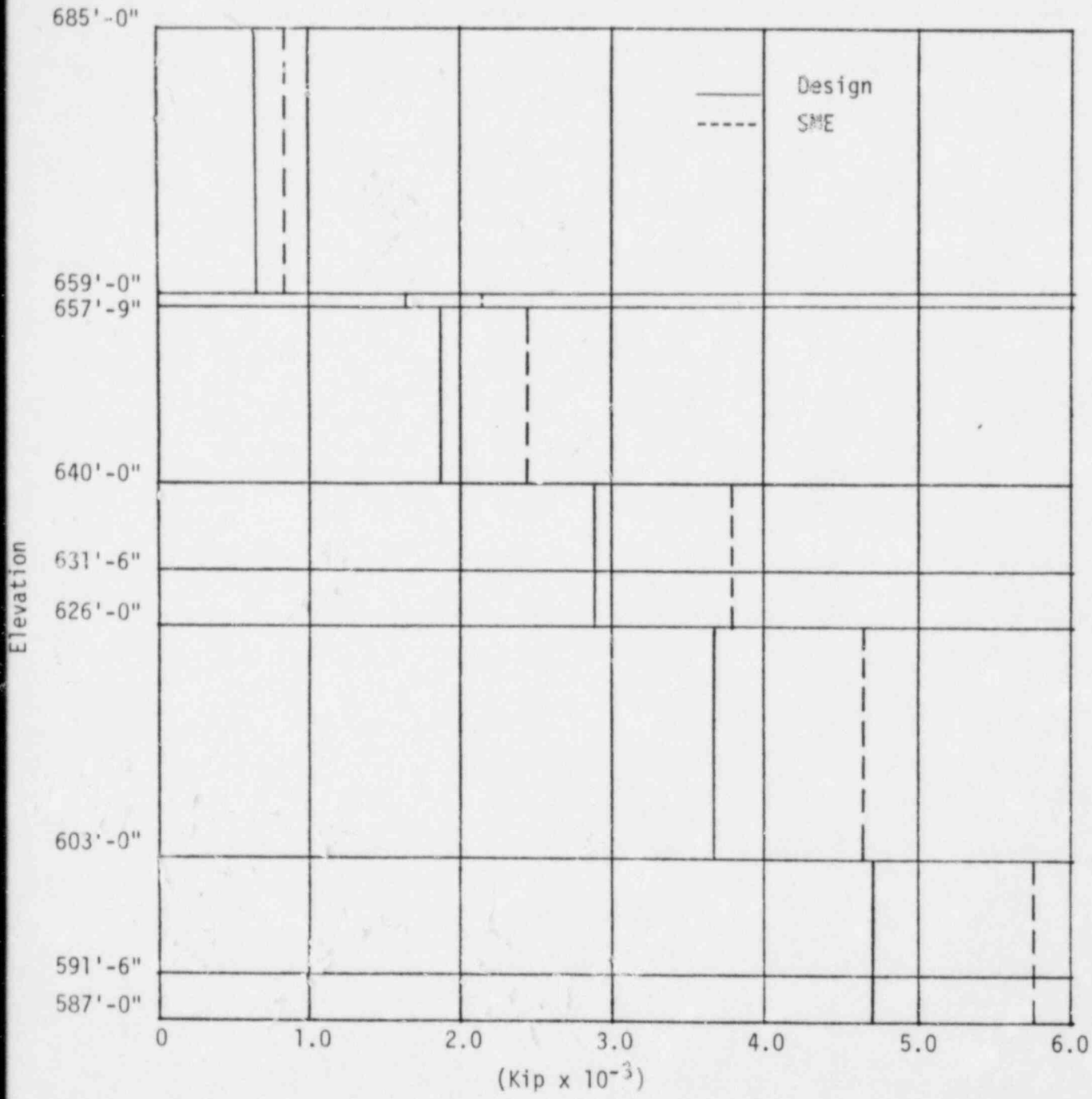

FIGURE II-3-16 INTERNAL STRUCTURE E-W SHEAR COMPARISON

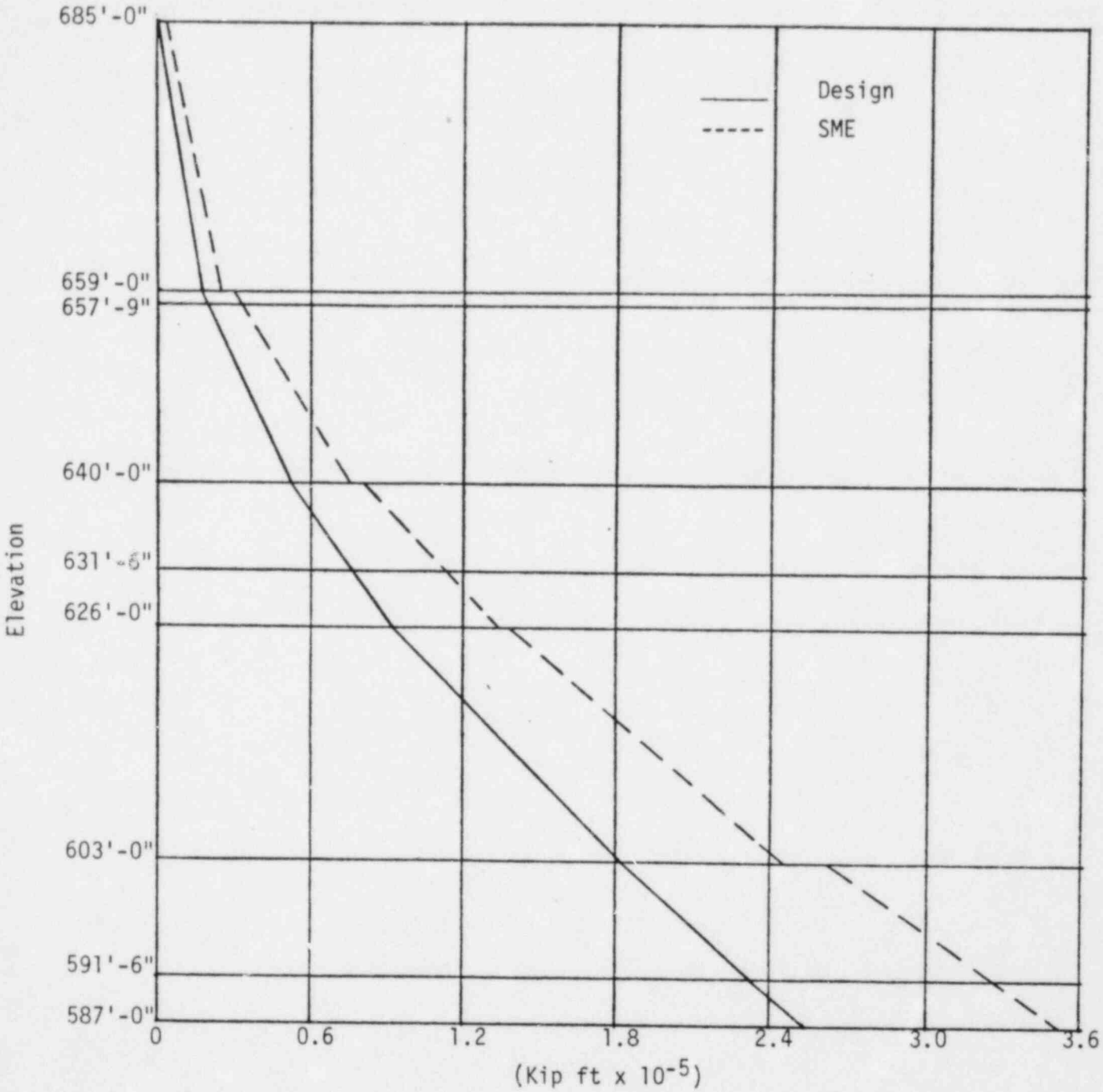

FIGURE II-3-17. INTERNAL STRUCTURE MOMENT ABOUT N-S AXIS COMPARISON

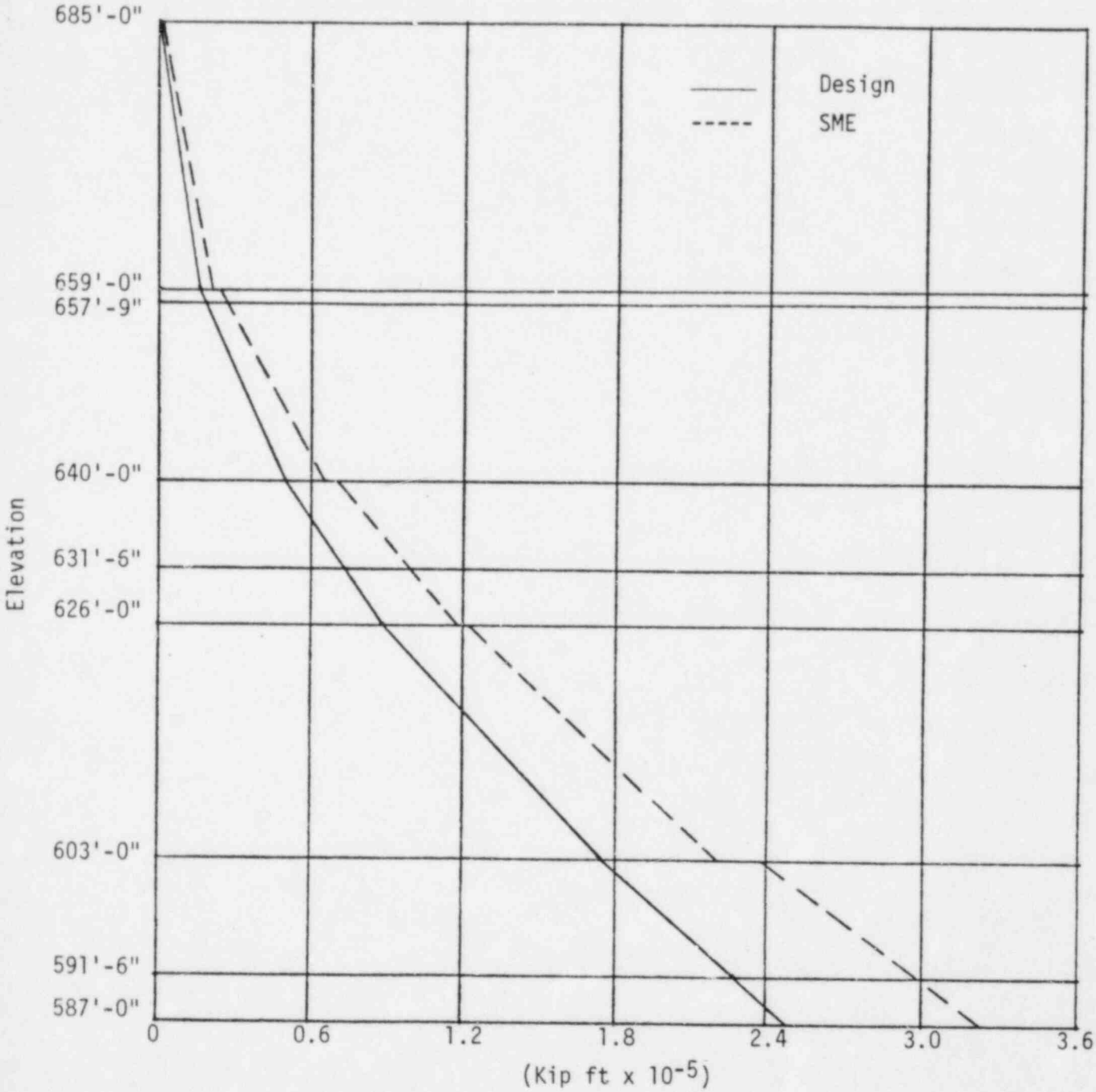

FIGURE II-3-18. INTERNAL STRUCTURE MOMENT ABOUT E-W AXIS COMPARISON

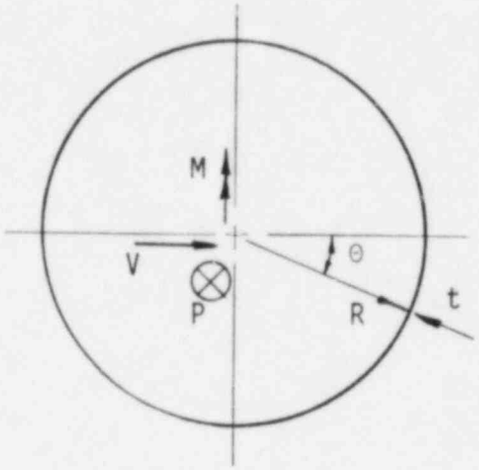

PLAN

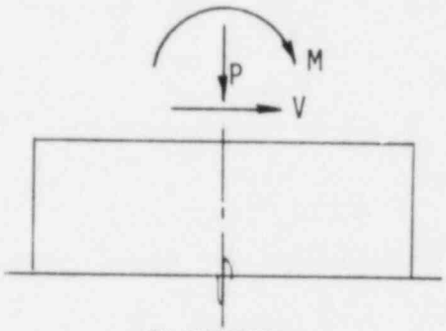

ELEVATION

σ_P = Meridional membrane stress due to vertical force P

$$= \frac{P}{2\pi Rt}$$

σ_M = Meridional membrane stress due to overturning moment M

$$= \frac{M}{\pi R^2 t} \cos\theta$$

τ = Tangential shear stress due to horizontal shear V

$$= \frac{V}{\pi Rt} \sin\theta$$

FIGURE II-3-19. CONTAINMENT WALL SEISMIC STRESS DISTRIBUTION

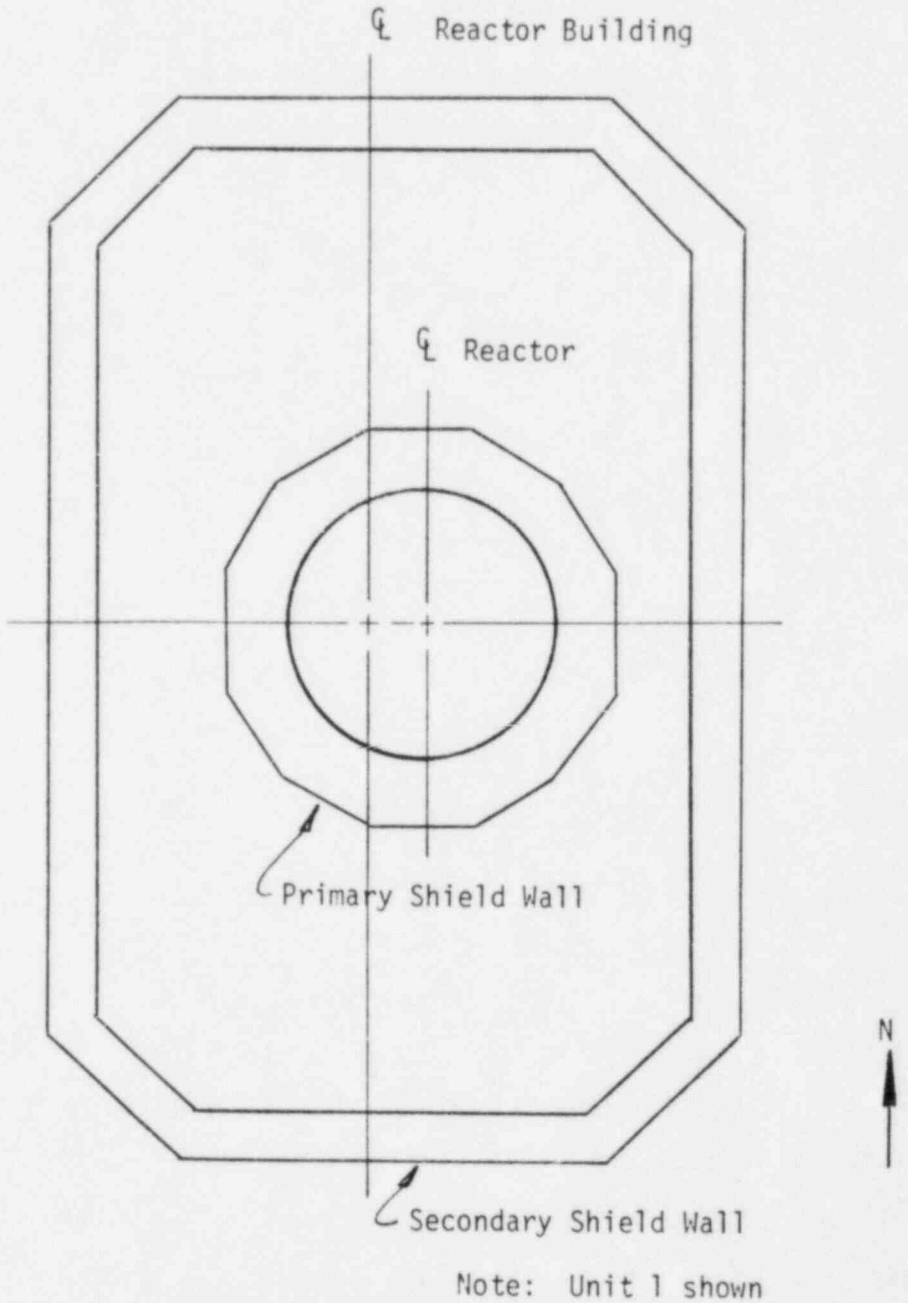

FIGURE II-3-20. INTERNAL STRUCTURES CROSS-SECTION FROM ELEVATION 603'-0 TO ELEVATION 626'-0

4. CODE MARGINS

For the reactor building structure code margins evaluation, a number of structural elements composing the containment structure and the internal structures were selected to compare their capacities as prescribed by the acceptance criteria agaist their loads or stresses due to the SME combined with those occurring at normal operating or accident conditions. Descriptions of the structural elements selected for review are contained in the following sections. These elements are those expected to be more highly stressed due to seismic loads relative to other elements within the reactor building.

General criteria used to identify structural elements to be included in the SMR structures capacities evaluation considered both comparisons of load distributions and structural resistances. The selected locations of the containment wall occur towards the lower elevations where seismic loads are greater compared to those occurring towards the dome. The reinforcement layout through the height of the wall was reviewed to provide an approximate assessment of the distribution of structural resistance. The selected wall locations correspond to typical cross-sections and account for overall behavior of the containment structure. Additional reinforcement is typically provided at discontinuities such as the equipment hatch and pipe penetrations to resist the additional stresses introduced at these locations. Review of the reinforcement around these large penetrations indicated that sufficient capacity is available to resist the applied loading. As with the containment wall, the distribution of loads and available structural resistance through the base mat and dome were reviewed to select sections for detailed evaluation.

The internal structures were reviewed on a similar basis to select elements for detailed evaluation. A sampling of locations from the primary and secondary shield walls was made since these are the major

load-resisting members. As with the containment wall, the lower elevations are subjected to greater seismic load as compared to the upper elevations. The physical conditions of the walls were reviewed to provide an approximate assessment of the relative wall capacities. This included considerations such as wall thickness, reinforcement patterns, and the presence of openings which would tend to reduce the amount of material available for load resistance. The availability of load paths to provide the means for transmitting the seismic forces down to the base mat led to the selection of the refueling canal slab and the interfaces between the primary and secondary shield walls and the base mat liner plate for review.

Capacities for the structural elements selected for review were developed in accordance with the structural acceptance criteria described in Section 7.2 of Volume I. For the concrete containment, the provisions specified by Article CC-3000 of the ASME Section III, Division 2, "Code for Concrete Reactor Vessels and Containments" (Reference 22) were followed. Stresses in the concrete, steel reinforcement, and prestress tendons were limited to the allowable stresses for factored loads. In addition, the tangential shear stress in the prestressed containment wall was limited to that value causing a principal tensile stress of $4\sqrt{f'_c}$ where f'_c is the concrete compressive strength in psi. This requirement is specified in subsection II.5 of Section 3.8.1 of the Standard Review Plan. For the concrete internal structures, the section strength available for resisting loads was based on the ultimate strength design methods contained in ACI 349-80, "Code Requirements for Nuclear Safety Related Concrete Structures" (Reference 23). Additional details concerning application of the acceptance criteria to the capacities evaluation calculations are discussed in the following subsections.

The ultimate strengths and allowable stresses were conservatively based on minimum specified crushing strengths or material yield stresses. The concrete used in the construction of the reactor building was typically specified to have a minimum compressive strength of 6000 psi for

the containment wall and dome, 5000 psi for the internal structures, and 4000 psi for the base mat. Deviations from these typical values were noted on the structural drawings. Reinforcing steel used was required to conform to ASTM Designation A615, Grade 60 and has a specified minimum yield stress of 60,000 psi. The wire forming the tendons used to posttension the containment wall and dome was required to conform to ASTM A421, Type BA, with intermediate relaxation properties. This material has a minimum specified tensile strength of 240,000 psi and a minimum yield strength not less than 80 percent of this minimum tensile strength.

4.1 CONTAINMENT CAPACITIES

Evaluation of the selected elements of the containment structure was conducted on the basis of the requirements contained in Article CC-3000 of the ASME Section III, Division 2 code (ASME Code). The load combinations used in this study include the SME and the internal pressure and thermal gradient associated with the design basis accident. These loads are defined as factored loads in Article CC-3222 of the ASME Code. Code margins for the structural elements of the containment were developed by comparing stresses in the concrete, reinforcing steel, and prestress tendons due to the applied loads against the ASME Code allowable stresses permitted at factored load conditions.

4.1.1 Wall Capacities

Definition of the stresses due to the applied meridional membrane forces and bending moments per unit length of wall is dependent on assumptions regarding behavior of the cross-sections being evaluated. General requirements for factored load design assumptions are contained in Article CC-3511.1 of the ASME Code and were followed in this study. These requirements specify that equilibrium and strain compatibility must be satisfied. Strains were assumed to vary linearly across the thickness of the section being evaluated. The reinforcement stress-strain behavior was based on Article CC-3511.1(c):

$$f_s = E_s \varepsilon_s \qquad \text{for } \varepsilon_s < 0.9\ \varepsilon_y \qquad (4\text{-}1)$$

or

$$f_s = 0.9\ f_y \qquad \text{for } \varepsilon_s \geq 0.9\ \varepsilon_y \qquad (4\text{-}2)$$

where

f_s = Stress in steel reinforcement, psi

ε_s = Strain in steel reinforcement, in/in

E_s = Reinforcement modulus of elasticity, psi

f_y = Reinforcement yield stress, psi

ε_y = Reinforcement strain at yield, in/in

This stress-strain relationship is shown in Figure II-4-1. Article CC-3511.1(c) permits the relationship between the concrete compressive stress and the concrete strain to be assumed to be triangular, parabolic, or any other shape resulting in a prediction of the stresses and strains in substantial agreement with test results. Reference 24 notes that an acceptable concrete stress-strain relationship is parabolic up to a strain limit of 0.002 in/in. The concrete stress at this strain level is 0.85 times the compressive strength f'_c. This relationship, shown in Figure II-4-2, was used and is expressed as follows (from Reference 25):

$$f_c = f''_c \left[\frac{2\varepsilon_c}{\varepsilon_o} - \left(\frac{\varepsilon_c}{\varepsilon_o} \right)^2 \right] \qquad (4\text{-}3)$$

where

f_c = Concrete compressive stress corresponding to strain ε_c, psi

f''_c = $0.85\ f'_c$ psi

f'_c = Concrete compressive strength, psi

ε_o = 0.002 in/in

The tensile strength of concrete was neglected.

Treatment of the prestress tendons in the wall necessitated additional, conservative assumptions on the structural section behavior under meridional membrane forces and bending moments. The tendons were posttensioned and remained ungrouted following anchorage. The prestress forces were included in the axisymmetric finite element design model (Reference 1). The additional stress induced in an ungrouted tendon due to applied loading is a function of the total elongation between the anchorages. This stress is typically less than that for a grouted tendon for the same applied loading. The strains in the ungrouted tendon are distributed along the entire length whereas the strains in the grouted tendon will be more concentrated in the vicinities of the cracks similar to bonded reinforcement. To calculate the stress in the tendon due to the applied loading on the prestressed member, it is necessary to integrate the strains along the entire tendon length. As an alternative, strains across the sections evaluated in this study due to applied membrane forces and bending moments and stresses in the concrete and steel reinforcement were determined by neglecting the additional stiffness provided by the prestress tendons. In reality, the tendons will also restrain deformations of the wall sections. Neglecting the restraint provided by the tendons, therefore, leads to conservative concrete and reinforcement stresses. The tendons themselves were evaluated in a separate calculation as discussed later in this section.

Meridional membrane forces and bending moments per unit wall length due to the SME, normal operating conditions, and accident conditions acting on the containment wall sections selected for evaluation are listed in Table II-4-1. The wall section numbers used are those assigned in the FSAR and are located as shown in Figure II-4-3 and Figures 3.8-25 and 26 of the FSAR. The basis for these forces is described in Section 3.3.3. Net membrane forces and bending moments per unit wall length for the load combinations used in this evaluation are listed in Table II-4-2. The membrane force due to the SME can be either tensile or compressive.

For the load combinations listed in Table II-4-2, a +SME signifies that the membrane force was taken to be tensile while a -SME signifies that the force was taken to be compressive. Thermal gradients occurring during both winter and summer conditions were considered. Only the forces and stresses for the temperature condition leading to the governing code margins are listed in Table II-4-2.

Stresses in the concrete and steel reinforcement were calculated using the analytical techniques previously described. At each section evaluated, the materials available to resist the applied forces were defined. This information consisted of concrete thickness and the amount and location of the steel reinforcement. A total wall thickness of 42.25 inches including the 0.25-inch thick liner plate was typical through the height of the containment up to the springline. Vertical reinforcement through the midheight section of the wall typically consisted of #11 bars spaced at 8 inches at the outside face. More reinforcement was provided at both faces towards the dome and base mat. In accordance with Article CC-3121 of the ASME Code, the liner plate was not included as a strength element. The calculated forces per unit wall length were applied to the material at each wall section considered. Strains and stresses due to these forces satisfying the conditions of equilibrium and strain compatibility as specified in Article CC-3511.1 of the ASME Code were then determined. | 1

Maximum stresses occurring for each wall section and load combination considered are listed in Table II-4-2. These stresses were compared to allowable values permitted by the ASME Code to determine code margins and F_{SME} factors. The allowable concrete compressive stresses for factored load conditions are specified in Table CC-3421-1 of the ASME Code as amended by the Summer 1981 Addenda. Different allowable values are permitted depending on whether the stress calculated is membrane only or membrane plus bending and due to primary loads or primary plus secondary loads. In general, the critical stress was found to be membrane plus bending. The classification of forces as either primary or

secondary is delineated in Table CC-3136.5-1 of the ASME Code. The classifications are functions of location, origin of the loads, and the type of force. Based on these classifications, the concrete stress at Section 9, which is located away from the discontinuities towards midheight of the wall, was compared against the allowable value for primary forces of 0.75 f'_c which equals 4500 psi. This allowable stress is conservative since the applied forces include some contribution from thermal effects which are classified as secondary and would permit an allowable stress of 0.85 f'_c. However, the concrete stress due to the applied forces, not including the thermal effects, would still have to be compared against the 0.75 f'_c allowable value. Since the contribution to the applied forces from the design basis accident thermal effects alone at Section 9 is not known from the information available, the conservative stress allowable of 0.75 f'_c was retained. Although loads due to the thermal strains at normal operating conditions could presumably be back-calculated from the available information, the lower allowable stress was used for simplicity. It should be noted that the lowest code margin at Section 9 occurs for the reinforcement stress. The selection of the more conservative concrete allowable stress does not lead to excessive conservatism in the final results. Both Sections 10 and 11 are located within about 15 feet from the top of the base mat and are thus sufficiently close to the discontinuity that they can be considered to be "regions at or near gross charges in the shell geometry" for ASME Code classification purposes. For these locations, bending moments due to both external loads and thermal strains are classified as being secondary forces so the allowable concrete stress of 0.85 f'_c, which equals 5100 psi, was used. In accordance with Articles CC-3422.1(b) and CC-3422.2(a), the allowable stress in the reinforcement for tension and compression was taken to be 0.9 times the yield strength which equals 54,000 psi.

Code margins and F_{SME} factors, presented in Table II-4-2, were developed from the calculated stresses and their allowable values. The code margin is defined as the ratio of the allowable stress to the stress due to the total applied forces for the load combinations considered:

$$\text{Code Margin} = \frac{f_{all}}{f} \qquad (4\text{-}4)$$

where

f_{all} = Allowable stress

f = Stress due to the total applied forces

The F_{SME} factor is the factor by which the SME ground motion would have to be increased to cause a stress equal to the allowable value. Because of the inter-relationship between the applied forces, the material stresses, and the extent of concrete cracking, a trial and error procedure was necessary to determine the F_{SME} factors. This procedure consisted of the following steps:

1. Assume a value of F_{SME}.
2. Calculate the meridional membrane force and bending moment per unit length of wall occurring for the SME ground motion factored by F_{SME}.
3. Calculate the net forces by combining the forces determined in 2 with those due to normal operating or accident conditions, depending on which load combination is being considered.
4. Determine the stresses for the solution which satisfies equilibrium and strain compatibility.
5. Compare the calculated stresses to the allowable values. Repeat the procedure using different values of F_{SME} until the solution that gives stresses equal to the allowable values is found.

The lowest code margin of 1.5 and the lowest F_{SME} factor of 2.0 were found to occur at Section 9 for the load combination D + F + L + P + T_A + SME. This code margin and F_{SME} factor are governed by stress in the reinforcement. F_{SME} factors greater than approximately 8 (corresponding to approximately a 1g earthquake) are listed as "Large."

Both the containment wall and dome were prestressed by tendons consisting of 170 wires, each wire being 0.25 inches in diameter and drawn from steel conforming to ASTM A421, Type BA. These tendons were posttensioned and ungrouted. The wall tendons were selected for evaluation since their stresses due to seismic load are expected to be greater than those for the dome tendons.

The effective stress in the wall tendons including reductions in prestress due to losses was taken from the original tendon design calculations. The initial tendon stress at the end being jacked prior to prestress losses was taken to be 168 ksi which corresponds to 70 percent of the minimum specified ultimate tensile strength of the prestressing steel. This value is the allowable stress for posttensioning tendons immediately after anchoring that was permitted by ACI 318-63 (Reference 26), the code to which the containment was designed. Prestress losses occur due to anchorage slip, elastic shortening of the concrete, frictional loss, concrete creep and shrinkage, and steel relaxation. Elastic shortening was accounted for in the usual manner while anchorage slip was conservatively neglected. Parameters used to define the losses due to friction, creep, and shrinkage correspond to values listed on Drawing C-301, Revision 3. These included a wobble friction coefficient, K, of 0.0003, a curvature friction coefficient, μ, of 0.14, a prestress loss due to creep of 0.225×10^{-6} in/in/psi, and a prestress loss due to shrinkage of 168×10^{-6} in/in. The values of these parameters are within the ranges normally expected for concrete posttensioned by ungrouted wire tendons. A loss due to steel relaxation of 4 percent of the stress at anchoring was based on the ASTM requirements for the wire material used.

Accounting for all losses, the tendon stress at the end from which the tendons were jacked was found to be 149 ksi by the original tendon design calculations. 1

Because the tendons are ungrouted, the additional stress caused by the applied loading is a function of the total tendon elongation between the anchorages. The strains are thus distributed along the entire length. To determine the additional tendon stress due to the applied loading, the strain profile through the height of the containment wall was determined. For the load combination being evaluated, strains 1
due to the applied forces were determined at the sections through the entire height of the wall for which forces due to accident conditions were available from the FSAR (Sections 5 to 11, Figure II-4-3). These applied loads consisted of membrane forces and bending moments due to $P + T_A + SME$. The meridional strains in the wall due to these loads 1
were determined using elementary beam theory along with the uncracked cross-sectional wall properties. The uncracked properties are adequate to predict the overall deformation of the wall between the tendon anchorages. The strain profile was then developed from the strain at each wall section occurring at the location of the centerline of the tendon in the wall cross-section. The tendon elongation was determined by integrating the strains from this profile over the length of the tendon. The resulting uniform tendon strain was then found by dividing the calculated elongation by the initial tendon length. The uniform tendon stress was calculated by factoring the uniform strain by the tendon modulus of elasticity. This approach for determining the additional tendon stress due to applied load is similar to the method described in Reference 33 for unbonded tendons prior to the occurrence of concrete cracking.

1

For the governing load combination, $D + F + L + P + T_A + SME$ (Winter), the additional vertical tendon stress due to the applied loads was calculated to be 6 ksi. Combining this value with the tendon stress at the end which is jacked after losses of 149 ksi leads to a net stress of 155 ksi. The allowable tendon stress permitted by Article CC-3423 of the ASME Code is 90 percent of the yield stress, or 173 ksi. The

resulting code margin is 173/155 = 1.12. It should be noted that the code margin for the effective tendon stress after losses and prior to the application of external load is already 173/149 = 1.16. Test results to verify the tendon strength properties were transmitted as a part of Reference 32. Evaluation of the tensile strength data indicates that the mean minus 1.65 standard deviations tendon ultimate tensile strength is approximately 247 ksi. Additional conservatism in the reported tendon code margin is apparent from a comparison to the minimum specified tensile strength of 240 ksi. | 1 | 1

An F_{SME} factor of 23 was found to cause a net tendon stress equal to the allowable stress of 173 ksi. Included in this evaluation is the maximum LOCA pressure and temperatures which are considered to be conservative. Although the code margin for this detail is relatively low, it is not governed by the earthquake loads. An increase in the earthquake loads of 23 would be required before the code allowable for this detail is reached and failure would not be expected until the structure is subjected to considerably greater earthquake levels. | 1 | 1

The application of horizontal seismic shear forces on the containment wall results primarily in tangential shear stresses. In accordance with Subsection II-5 of Section 3.8.1 of the Standard Review Plan, the tangential shear stress at a section of the wall was limited to the value-causing a principal tensile stress of $4\sqrt{f'_c}$ where f'_c is the concrete compressive strength in psi. The allowable tangential shear force meeting this requirement given the meridional and hoop membrane forces acting concurrently was calculated by the following expression:

$V_{t,all}$ = Allowable tangential shear force per unit wall length, k/ft

$$= \frac{4bt\sqrt{f'_c}}{1000}\left[1 - \frac{P_m+P_h}{\left(\frac{4bt\sqrt{f'_c}}{1000}\right)} + \frac{P_m P_h}{\left(\frac{4bt\sqrt{f'_c}}{1000}\right)^2}\right]^{\frac{1}{2}} \qquad (4\text{-}5)$$

P_m, P_h = Membrane forces in the meridional and hoop directions, respectively, due to the SME combined with either normal operating or accident conditions, positive in tension, k/ft

b = Wall thickness, in

t = 12 in/ft

This expression was derived from the standard stress transformation equation for principal stresses. The meridional membrane force due to the SME was always taken as being tensile since this leads to lower allowable shear forces. For the selected wall sections and their governing load combinations, the calculated applied tangential shear forces, meridional and hoop membrane forces, and allowable tangential shear forces acting on a unit length of wall are listed in Table II-4-3. Code margins, calculated as the ratios of the allowable to applied tangential shear forces, are also listed in Table II-4-3 along with the F_{SME} factors. The F_{SME} factors were determined by expressing the tangential shear and meridional membrane forces by their values due to the SME increased by an unknown F_{SME} factor, inserting these forces into Equation 4-5, and solving for F_{SME} using the quadratic equation. As an example, for Section 11:

$$V_t = 57\ F_{SME}$$

$$V_t = 156 \left[1 - \frac{(-189 + 135\ F_{SME}) - 300}{156} + \frac{(-189 + 135\ F_{SME})(-300)}{156^2} \right]^{\frac{1}{2}}$$

$$V_t = V_{t,all}$$

$$- 3250\ F_{SME}^2 - 61{,}600\ F_{SME} + 157{,}000 = 0$$

$$F_{SME} = 2.3$$

An F_{SME} factor less than the code margin occurs because increasing the SME ground motion increases the meridional membrane tension along with the tangential shear force and thus reduces the allowable tangential shear force.

Elevations of the containment wall shown on the structural drawings indicate that horizontal construction joints were used. Tangential shear forces due to horizontal seismic response and radial shear forces due to normal operating or accident condition loads must be transferred across the horizontal construction joints by shear friction. Equation 12.2 from Reference 25 gives the average shear stress that can be safely transferred across a well prepared horizontal construction joint across shear walls as:

v_{uf} = Nominal shear stress transmitted across joint

$$= \frac{N + A_{vf}\ f_y}{A_g} \qquad (4\text{-}6)$$

N = Axial force, positive in compression

A_{vf} = Total steel to be utilized for clamping force

A_g = Gross sectional area of wall

Inherent in this equation is a coefficient of friction μ of unity which is the value that ACI 349-80 specifies for concrete placed against hardened concrete. ACI 349-80 also limits the calculated shear strength V_n to lesser of $0.2f'_c\ A_c$ or $800A_c$ where A_c is the concrete area resisting shear transfer (Section 11.7.4).

The allowable shear force per unit wall length acting across a horizontal construction joint was developed from this information. The axial force was taken as the meridional membrane force acting concurrently with the applied shear force. A strength reduction factor, ϕ, of 0.85 specified for shear in Section 9.3.2 of ACI 349-80 was included.

V_{all} = Allowable shear force per unit wall length, k/ft

$$= \phi \left[A_{sm} f_y - P_m\right] \leq \phi\left[0.2f'_c\, bt\right] \qquad (4\text{-}7)$$

$$\text{and} \leq \phi\left[\frac{800\ bt}{1000}\right]$$

where

ϕ = Strength reduction factor = 0.85

A_{sm} = Area of meridional steel reinforcement, in^2/ft

f_y = Reinforcement yield strength, ksi

f'_c = Concrete compressive strength, ksi

P_m = Net meridional membrane force due to the SME combined with either normal operating or accident conditions, positive in tension, k/ft

b = Wall thickness, in

t = 12 in/ft

The same shear friction mechanism must resist both tangential and radial shear forces. The presence of radial shear due to loads occurring at normal operating or accident conditions reduces the magnitude of the

tangential shear due to the SME that can be permitted. The allowable tangential shears were calculated by deducting vectorially the radial shears acting concurrently at the sections from the total allowable shears.

$V_{t,all}$ = Allowable tangential shear force per unit length, k/ft

$$= \sqrt{V_{all}^2 - V_r^2} \qquad (4\text{-}8)$$

V_r = Radial shear acting concurrently with the applied tangential shear, k/ft

For the wall sections selected, the allowable tangential shear forces were calculated as if there were construction joints at each of the sections. Applied tangential and radial shear forces, meridional membrane forces, and allowable tangential shear forces are listed in Table II-4-4. Code margins, calculated as the ratios of the allowable to applied tangential shear forces, are also listed in Table II-4-4 along with the F_{SME} factors. Similar to the concrete tangential shear stress calculations, an F_{SME} factor less than the code margin occurs because increasing the SME ground motion increases the meridional membrane tension along with the tangential shear force and thus reduces the allowable tangential shear force.

4.1.2 Dome Capacities

The containment dome is essentially a shallow spherical shell segment typically three-feet thick with an inside radius of 87'-6". The dome is prestressed by a three-way pattern of tendons oriented at 120^{o} to each other. The tendons are anchored at the face of the ring girder provided around the dome. Conventional reinforcement is provided in a square mesh at the top at both faces in the vicinity of the ring girder. In general, the seismic forces in the dome are small and the dome design were not governed by seismic loads.

Forces for the design load combinations were reported in the FSAR at the locations identified as Section 1 to 4 in Figure II-4-3. Section 1 is closest to the dome apex and Section 4 is cut through the ring girder. Based on a comparison of loads to available capacities and safety factors reported in the FSAR for the design load combination, Section 1 subjected to meridional forces was selected for investigation in this study. The governing load combination was found to be D + F + L + T_o + SME (Winter). The membrane force and bending moment occurring at normal operating conditions for this thermal case are -608 k/ft and -330 k-ft/ft. The membrane force due to the SME, calculated as described in Section 3.3.3, was found to be only 3 k/ft. The section was evaluated for a net meridional membrane force of -605 k/ft and a net moment of -330 k-ft/ft.

Stresses in the containment dome concrete and reinforcement due to these net applied forces were determined using the same solution techniques developed for the wall evaluation. Maximum concrete and reinforcement stresses were calculated to be 2850 psi and 1.4 ksi in compression, respectively. Allowable stresses are the same as those specified for the containment wall. Similar to Wall Section 9, an allowable concrete stress of 4500 psi, corresponding to 0.75 f'_c, is appropriate. The allowable reinforcement stress is also 54,000 psi. The dome code margin of 1.6 is governed by the concrete compressive stress. Due to the small magnitude of the seismic membrane force, a very large F_{SME} factor results.

4.1.3 Base Mat Capacities

The containment base mat is a conventionally reinforced concrete circular slab varying in thickness from 9 feet at the outside edge to 13 feet towards the center. It is reinforced by an orthogonal grid oriented in the N-S and E-W directions. Two layers of #18 bars are used at the top and bottom faces in both directions. Additional reinforcement was provided at the steam generator mounting locations and the sump pit. Dowels extending into the containment wall are anchored in the base mat.

Forces for the design load combinations were reported in the FSAR for the four sections identified as Sections 12 to 15 which are located at different radii from the center, with Section 12 being closest to the outside edge (see Figure II-4-3). Section 12 was selected to be evaluated for the SME for combined radial membrane force and bending moment. This section is located at a radius of approximately 44 feet from the center of the reactor building. This radius is equal to that of the equivalent radius of the rigid plate portion used to develop base mat forces due to loads from the internal structures (see Section 3.3.3). The governing load combination was found to be $D + F + L + P + T_A + SME$ at Summer conditions. From Table 3.8-6 of the FSAR, the radial membrane force due to $D + F + L + P + T_A$ (Summer) is -126 k/ft and the moment is -1740 k-ft/ft. The moment due to the SME, calculated as described in Section 3.3.3, was found to be -1630 k-ft/ft. The combined membrane force is -126 k/ft and the moment is -3370 k-ft/ft.

Stresses in the containment base mat concrete and reinforcement due to membrane force and bending moment were determined using the same solution techniques developed for the containment wall as described in Section 4.1.1. For the applied forces noted above, the maximum concrete and reinforcement stresses were found to be 1570 psi and 30 ksi, respectively. These stresses were compared to the same allowable values used in the containment wall evaluation. As with Section 9 of the containment wall, the concrete allowable stress was taken to be $0.75\ f'_c$, which corresponds to 3400 psi. The reinforcement allowable stress was taken to be 54,000 psi. Based on these stresses and their allowable values, a code margin of 1.8, governed by the reinforcement, was calculated for the base mat. The F_{SME} factor was determined using the same procedure developed for the containment wall and was found to be 2.5.

Transverse shear forces result as the base mat distributes the vertical forces from the containment wall and internal structures into the supporting soil. Of the four base mat sections for which forces are listed in the FSAR, Section 12 was selected to compare its transverse

shear capacity against the applied loading. This section is the closest to the containment wall which is the source of much of the applied seismic forces in the vertical direction. A transverse shear of 137 k/ft occurs due to accident conditions for the governing load combination of $D + F + L + P + T_A$ + SME (Summer). A transverse shear of 34 k/ft due to the SME was calculated as described in Section 3.3.3. A net shear force of 171 k/ft was used to determine the code margin.

Resistance to transverse shear in the base mat is provided by the concrete, structural steel W6x25 sections anchored in the base mat, and additional reinforcement ties. The total concrete thickness at Section 12 is approximately 11 feet. The W6x25 sections are embedded vertically within the base mat concrete and are laid out in a horizontal grid pattern with the spacing between adjacent rows typically four feet in both plan directions. The ends of the sections are anchored in the concrete so that the members will behave as stirrups of a reinforced concrete beam. Additional reinforcement is provided in the vicinity of Section 12 to provide additional shear resistance. This reinforcement consists of 3-2 #11 bundled vertical bars within a 4'-0" by 4'-0" plan area. These bars serve as shear ties.

The base mat transverse shear capacity at Section 12 was based on the design provisions contained in the ASME Code for radial shear acting on reinforced concrete at factored load conditions. The ASME Code specifies that shear reinforcement must be provided if the nominal shear stress v_u exceeds the allowable value. For members subjected to membrane compression, the allowable value can be determined by either Equation 4-9 or 4-10, but cannot exceed the value from Equation 4-11 (from CC-3421.4.1(b) of the ASME Code).

v_c = Allowable concrete shear stress, psi

$$= 1.9\sqrt{f'_c} + 2500\,\rho\left(\frac{V_u d}{M'}\right) \qquad (4\text{-}9)$$

or

$$V_c = 2\left(1 + 0.0005\,\frac{N_u}{A_g}\right)\sqrt{f'_c} \qquad (4\text{-}10)$$

$$V_c \leq 3.5\sqrt{f'_c}\,\sqrt{1 + 0.002\,\frac{N_u}{A_g}} \qquad (4\text{-}11)$$

where

f'_c = Concrete compressive strength, psi

ρ = Tension reinforcement ratio

V_u = Factored shear force at section, lb

M' = $M_u - N_u\ (4t-d)\ /8$

M_u = Factored moment at section, lb-in

N_u = Factored axial load at section, positive in compression, lb

t = Overall member thickness, in

d = Distance from extreme compressive fiber to centroid of tensile reinforcement, in

A_g = Gross area of section, in^2

When the nominal shear stress v_u, calculated as in Equation 4-12 below, exceeds the allowable concrete shear stress v_c, shear reinforcement must be provided.

v_u = Nominal shear stress, psi

$$= \frac{V_u}{0.85\ bd} \qquad (4\text{-}12)$$

b = Member width, in

For shear reinforcement perpendicular to the containment surface, the required reinforcement area A_v is given by Equation 4-13 (from CC-3521.2.3(a)):

A_v = Required area of shear reinforcement, in^2

$$= \frac{(v_u - v_c)\, bs}{f_y} \qquad (4\text{-}13)$$

where

f_y = Reinforcement yield strength, psi

s = Reinforcement spacing parallel to longitudinal reinforcment, in

This is equivalent to defining an allowable reinforcement shear stress v_s:

v_s = Allowable reinforcement shear stress, psi

$$= \frac{A_v f_y}{bs} \qquad (4\text{-}14)$$

The net allowable shear stress is the sum of the allowable concrete and reinforcement shear stresses.

For Section 12 of the base mat, an applied nominal shear stress of 140 psi was calculated for the net transverse shear force of 171 k/ft. At this location, allowable concrete and reinforcement shear stresses of 127 psi and 358 psi were determined using Equations 4-10 and 4-14, with a resulting net allowable shear stress of 485 psi. The code margin for

transverse shear at Section 12 is, therefore, 3.5 with an F_{SME} factor of 14. It should be noted that the effect of the compressive axial load N_u was conservatively neglected in deriving the allowable concrete shear stress.

4.2 INTERNAL STRUCTURES CAPACITIES

The capacities of the structural elements of the reactor building internal structures were determined in accordance with the ultimate strength design methods contained in ACI 349-80. Loads acting on these elements due to the SME combined with normal operating conditions were determined as described in Section 3.3.3. Code margins for the structural elements of the internal structures selected for evaluation were calculated by comparing the applied loads to the code ultimate strength capacities. Descriptions of the locations of the structural members in the following discussion is with respect to the layout of the Unit 1 internal structures. Locations of the corresponding Unit 2 members are by the opposite hand.

4.2.1 Primary Shield Wall Capacities

The primary shield wall is a thick-walled reinforced concrete cylinder housing the reactor vessel. The outside face is a 12-sided polygon and the inside face is circular with a wall thickness of about 5'-6" above Elevation 602'-3" and 10'-6" below this elevation to the base mat. The primary shield wall is reinforced in the meridional and hoop directions at both faces with horizontal ties provided.

The ability of the primary shield wall to resist meridional membrane forces and bending moments as well as tangential shear forces was investigated. The meridional membrane force is composed of contributions from the SME and normal operating condition loads while the bending moment through the wall occurs due to the normal operating condition loads only. As noted in Section 3.3.3, these loads are defined as acting on unit lengths of wall. Consistent with this load definition, the capacity of a unit wall length can be determined using the basic

ultimate strength design principles contained in Section 10.2 of ACI 349-80 to account for the axial load-flexure interaction. This approach is appropriate for walls such as the primary shield wall that are significantly stressed due to loads occurring at normal operating conditions. Capacities calculated in this manner are conservative for walls subjected to vertical forces by seismic overturning moments. The limiting overturning moment determined by this approach corresponds to the value that causes sufficient meridional membrane force on a localized unit length of wall such that the ultimate strength capacity of this section is attained. However, design provisions recommended in Reference 27 indicate that the flexural strength of rectangular shear walls can be determined using the basic ACI ultimate strength design principles for reinforced concrete members. Implicit in the flexural strength equations of Reference 27 is the occurrence of stress redistribution as the distributed reinforcement along the length of the wall progressively yields in tension and the concrete progressively crushes under increasing in-plane moment. The conservatism contained in the approach for evaluating the capacity of the primary shield wall under combined meridional membrane force and moment acting on a unit length of wall is apparent. Based on the provisions of Reference 27, it can be concluded that the primary shield wall as a whole has additional capacity through stress redistribution beyond the load level at which a unit length of wall reaches its capacity.

The primary shield wall was evaluated for its capacity against applied meridional membrane force and bending moment at Elevation 603'-0". Forces due to loads occurring at normal operating conditions were taken from the results for Element 112 of Bechtel's finite element model. This element is located at the west side of the primary shield wall. The meridional membrane force and bending moment acting on this element at normal operating conditions are -206 k/ft and 10,700 k-in/ft, respectively. The membrane force due to the SME at this location was found to be $\pm$34 k/ft. Membrane forces acting on the structural elements of the internal structures are defined as being positive in tension.

In accordance with the approach adopted in this study, capacity of the wall section was based on column axial load-bending interaction curves contained in Reference 28. In this discussion, the term "axial load" is used to describe the capacity of the structural member against meridional membrane force per unit length and is positive in tension. The curves used in the evaluation of the primary shield are shown in Figure II-4-4. This figure was reproduced from Uniaxial Chart No. 94 of Reference 28, with adjustments made for an increased value of the strength reduction factor ϕ permitted by Section 9.3.2(c) of ACI 349-80 and maximum axial compressive strength set by Section 10.3.5.2 of ACI 349-80. Values of the parameters K and $K\frac{e}{t}$ were calculated to be -0.043 and 0.040, respectively. These values are located on the chart in Figure II-4-4 as Point A. The capacity of this section is defined by the locus of points drawn as Curve U in Figure II-4-4 and corresponds to a value of $P_t m$ of 0.14. The moment capacity given the applied axial load can be found by locating the intersection of Curve U with the line K = -0.043, shown as Point B. The value of $K\frac{e}{t}$ for Point B is 0.064, and gives a moment capacity of 16,700 k-in/ft. The axial load capacity given the applied moment can be found by locating the intersection of Curve U with the line $K\frac{e}{t}$ = 0.040, shown as Points C and D. The capacity of Point C is controlled primarily by axial compression while the capacity at Point D is controlled primarily by flexure. The values of K for Points C and D are -0.54 and +0.013, and lead to axial load capacities of -2100 k/ft and +53 k/ft. Rather than define the code margin in terms of the axial load capacity since two capacities are possible, the code margin was based on the moment capacity. A code margin of 1.6 was calculated for the primary shield wall. Because the effect of the SME is to cause meridional membrane stresses, the F_{SME} factor was based on the axial load capacity. For the controlling case of the seismic load causing a tensile axial load, the F_{SME} factor was found to be 7.6.

$$F_{SME} = \frac{P_u - P_{DL}}{P_{SME}}$$

$$= \frac{53 - (-206)}{34}$$

$$= 7.6$$

P_u = Axial load capacity for the section corresponding to an applied moment of 10,700 k-in/ft, k/ft

P_{NOL} = Axial load due to loads occurring at normal operating conditions, k/ft

P_{SME} = Axial load due to the SME, k/ft

The shear strength provisions for rectangular concrete walls are contained in Section 11.10 of ACI 349-80. The total ultimate strength capacity is composed of separate contributions from the concrete and the steel reinforcement. ACI 349-80 provides alternative formulations with different levels of detail required for determining the concrete shear strength. Section 11.10.5 specifies the concrete shear strength as the value corresponding to an average shear stress of $2\sqrt{f'_c}$ (psi) acting on the effective area for walls in compression.

V_c = Nominal concrete shear strength, lb

$$= 2\sqrt{f'_c}\, hd \text{ for walls in compression} \qquad (4\text{-}15)$$

f'_c = Concrete compressive strength, psi

h = Wall thickness, in

d = Effective wall depth, in

This strength is subjected to a reduction if the wall is loaded in tension. As an alternative, Section 11.10.6 of ACI 349-80 permits the use of the lesser of the concrete shear strengths defined by the following two equations:

$$V_c = 3.3\sqrt{f'_c}\ hd + \frac{N_u d}{4l_w} \qquad (4\text{-}16)$$

or

$$V_c = \left[0.6\sqrt{f'_c} + \frac{l_w\left(1.25\sqrt{f'_c} + 0.2\,\frac{N_u}{l_w h}\right)}{\frac{M_u}{V_u} - \frac{l_w}{2}}\right] hd \qquad (4\text{-}17)$$

l_w = Wall length, in

V_u = Shear force acting on the section , lb

N_u = Axial load occurring simultaneously with the shear force V_u, lb

M_u = Moment acting on the section, in-lb

As noted in Reference 27, Equation 4-16 reflects the concrete shear strength when web-shear cracking occurs as opposed to flexure-shear cracking which is represented by Equation 4-17. The contribution to shear strength for rectangular walls provided by the reinforcement is contained in Section 11.10.9 of ACI 349-80.

V_s = Nominal shear strength provided by reinforcement, lb

$$= \frac{A_v f_y d}{s_2} \qquad (4\text{-}18)$$

A_v = Area of horizontal reinforcement within a distance s_2, in^2

f_y = Reinforcement yield strength, psi

s_2 = Spacing of horizontal wall reinforcement, in

The ultimate shear strength of a rectangular wall is the sum of the concrete and reinforcement shear strengths reduced by a strength reduction factor, ϕ, of 0.85. Additional requirements for shear wall are contained in ACI 349-80.

Due to differences in geometry, the design provisions of ACI 349-80 for rectangular walls are not directly applicable to the hollow, cylindrical primary shield wall. To develop code margins and F_{SME} factors for shear on the primary shield wall, nominal ultimate shear stresses were compared to the maximum elastic shear stresses. The nominal ultimate shear stresses were derived from Equations 4-15 and 4-18 by dividing the nominal shear strengths by the effective wall depth d.

$$V_c = 2\sqrt{f'_c}\ h \qquad (4\text{-}19)$$

$$V_s = \frac{A_v f_y}{s_2} \qquad (4\text{-}20)$$

V_u = Nominal ultimate shear stress, lb/in

$$= \phi(V_c + V_s) \qquad (4\text{-}21)$$

Definition of the nominal ultimate shear stress using Equation 4-15 is expected to be conservative for low-rise walls such as the primary shield wall. For low-rise walls, shear strength is normally governed by Equation 4-16. Use of this equation would permit the prediction of a greater shear capacity. The shear stresses due to the applied seismic horizontal shear and torsion were determined from elastic theory.

$$v_{max\ (horizontal\ shear)} = \frac{VQ}{2I} \qquad (4\text{-}22)$$

$$v\ (torsion) = \frac{TRh}{J} \qquad (4\text{-}23)$$

V = Applied seismic horizontal shear force, lb

T = Applied seismic torsional moment, lb-in

I = Moment of inertia, in^4

Q = Statical moment of half of the cross-section about the neutral axis, in^3

J = Torsional moment of inertia, in^4

h = Wall thickness, in

R = Average wall radius, in

The shear capacity of the primary shield wall was evaluated at Elevation 603'-0" which is near the base and Elevation 626'-0" where several large pipe penetrations are located. For Elevation 603'-0", the membrane shear force per unit length of wall occurring at normal operating conditions was taken from the results for Element 111 of Bechtel's finite element model. This element is located at the northwest side of the primary shield wall. For Elevation 626'-0", the membrane shear force occurring at normal operating conditions was taken from the results for Element 339 which is also located at the northeast side of the wall. To account for the effects of the wall openings for the pipe penetrations at this elevation, the net cross-sectional area excluding the area of the openings was used to determine the tangential shear force due to the horizontal seismic shear.

The tangential shear forces due to the SME and the loads occurring at normal operating conditions are listed in Table II-4-5 along with the sums of these forces for the selected locations. Table II-4-5 also lists the calculated tangential shear capacities, code margins, and F_{SME} factors. The lowest code margin of 2.0 occurs at Elevation 626'-0" of the primary shield wall.

Forces in the primary shield wall must be transmitted to the base mat across the 0.25-inch thick continuous liner plate at the top of the base mat. The #18 vertical bars at the outside and inside faces of the primary shield wall are spliced across the liner by Cadweld connector sleeves welded to both sides of the liner. The plate at this splice detail is thickened to 0.75 inches. W8x35 structural steel sections 6.5 inches long are welded to both sides of the plate in between the reinforcement bars at the outside face of the primary shield wall. The webs of these members are oriented in the radial direction. A total of 100 of these W8x35 sections are provided.

Vertical compressive stresses in the concrete at the primary shield wall base mat interface are transmitted directly by bearing on opposite sides of the liner plate. Tensile stresses in the vertical reinforcement are transmitted across the interface by the Cadweld connectors. Since the Cadweld connectors typically have strength in excess of the bars they are connecting, their performance under the imposed forces was not investigated. Two separate mechanisms are available for transmitting the radial and tangential shears across the liner plate. One consists of the W8x35 sections performing as shear lugs. The other consists of the vertical reinforcement bars resisting the shear forces through shear friction. Design provisions for steel embedments of this type are contained in Appendix B of ACI 349-80. Section B.3.8 of ACI 349-80 specifically excludes the use of a combination of bearing and shear friction mechanisms for resisting shear forces. In accordance with this provision, only the shear capacity of the W8x35 shear lugs was accounted for. The radial shear transmitted from the primary shield wall to the base mat is resisted by the web of the section while the tangential shear is resisted by the flanges. Strength requirements for shear lugs are contained in Section B.6 of ACI 349-80. The design strength of steel embedments is specified to be based on a maximum steel stress of f_y where ϕ is 0.55 for shear on structural shapes and shear lugs. For the minimum specified yield strength for A36 steel of 36,000 psi, a maximum shear stress of 19,800 psi was permitted.

With this stress acting across the W8x35 flanges, a tangential shear strength at the primary shield wall-base mat interface of 157 k/ft was calculated.

Similar to the containment wall, horizontal shear forces acting on the primary shield wall primarily cause tangential shear stresses. A maximum tangential shear force due to the SME of 65 k/ft was calculated at the north and south sides of the wall. The tangential shear force due to loads occurring at normal operating conditions of 8 k/ft was taken from Element 48 of Bechtel's finite element model. For the net tangential shear force of 73 k/ft, a code margin of 2.2 was determined. The F_{SME} factor for this detail was found to be 2.3.

4.2.2 Secondary Shield Wall Capacities

The secondary shield walls are constructed of reinforced concrete and are arranged to form a structure approximately rectangular in plan. These walls are located within the reactor building between the primary shield wall and the containment wall. The walls are typically 4'-0" thick and are reinforced with four layers of reinforcement in the vertical and horizontal directions at each face together with horizontal ties.

The ability of the South and East secondary shield walls to resist vertical membrane forces and bending moments at the intersection of the walls and the base mat at Elevation 591'-6" was investigated. For the south wall, forces occurring at normal operating conditions at this elevation were taken from the results for Element 1 of Bechtel's finite element model. For the east wall, these forces were taken from the results for Element 10. Vertical membrane forces and moments per unit length of wall due to the SME and loads occurring at normal operating conditions are listed in Table II-4-6 for these locations.

Capacities for the South and East secondary shield walls were calculated in the same manner as those of the primary shield wall as described in Section 4.2.1. For the given applied vertical membrane

forces, corresponding moment capacities were determined. These moment capacities and their resulting code margins are listed in Table II-4-6. The lowest code margin of 4.5 was found to occur in the East wall. For the given applied moments, corresponding axial load capacities were determined. As noted in Section 4.2.1, two axial load capacities are possible for a given applied moment. Only the governing axial load capacities are listed in Table II-4-6. F_{SME} factors are also shown in Table II-4-6 for the South and East walls. For both of these walls, the governing F_{SME} factor was due to the SME causing a tensile vertical membrane force. As noted in Section 4.2.1, the calculated capacities are conservative and lead to a conservative code margins and F_{SME} factors.

Shear capacities of the South and East secondary shield walls at Elevation 591'-6" were also investigated. The East wall is separated into two lengths by a 12'-4" x 7'-0" opening towards the South end. Loads and capacities were developed for the 44 foot long portion north of this opening. The in-plane shear forces due to the SME and loads occurring at normal operating conditions were calculated as described in Section 3.3.3. These shear forces and the total forces are listed in Table II-4-7. The shear capacities for these walls were based on the ACI 349-80 design provisions given in Equations 4-15 and 4-18. The calculated shear capacities are listed in Table II-4-7 along with the resulting code margins and F_{SME} factors. The lowest code margin of 3.3 was found to occur in the East wall.

Forces in the secondary shield walls must be transmitted to the base mat across the liner plate at the top of the base mat. The liner plate is increased in thickness beneath the secondary shield walls. The vertical bars reinforcing the walls are spliced across the liner plate by Cadweld connector sleeves on both sides of the plate. In addition, 0.875-inch diameter by 3.5-inch long Nelson studs are welded to both sides of the plate in two rows along the lengths of the walls.

Vertical compressive stresses in the concrete at the secondary shield wall-base mat interfaces are transmitted directly by bearing on opposite sides of the liner plate. Tensile stresses in the vertical reinforcement bars are transmitted by the Cadweld connectors. Since the Cadweld connectors typically have greater strength than the bars they connect, their ability to resist forces was not evaluated. In-plane and transverse shears must be passed across the liner by shear friction developed by the vertical reinforcement bars and the Nelson studs. Design provisions for shear friction are contained in Section 11.7 and B.6 of ACI 349-80. Equation 11-26 of ACI 349-80 specifies the shear strength based on shear friction to be:

V_n = Nominal shear strength, lb

$$A_{vf}\, f_y\, \mu \qquad (4\text{-}24)$$

where

A_{vf} = Area of shear friction reinforcement, in^2

f_y = Minimum specified reinforcement yield strength, psi

μ = Coefficient of friction

The coefficient of friction μ for concrete placed against as rolled steel with the contact plane coincidental with the contact plane is specified to be 0.7 by Section B.6.2.2.2 of ACI 349-80. The total shear strength was taken to be the sum of the contributions from the reinforcement bars and the Nelson studs with a strength reduction factor ϕ of 0.85 used. Areas of the vertical reinforcement of the outside and inside faces of the secondary shield walls were included. Although the bars at the inside face may be stressed in tension due to bending moments, Reference 30 indicates that moments at the shear plane less than the ultimate flexural strength do not reduce the shear transfer strength. The minimum yield strength for the Nelson studs is specified to be 50 ksi in Reference 29. Available shear friction capacities were calculated to be 246 k/ft and 248 k/ft for the south and east secondary shield walls,

respectively. These capacities conservatively neglect the effects of the axial compressive forces at the interfaces. The development of shear capacities of horizontal wall construction joints in Reference 25 indicates that capacities are increased by the presence of these axial forces (see Section 4.1.1 also).

The vertical bars and Nelson studs at the interfaces must transfer transverse wall shears as well as in-plane wall shears. To decouple the effects of these forces, the available in-plane shear capacities were determined by conservatively deducting vectorially the maximum transverse shear from the net shear capacity similar to Equation 4-8. The transverse shears occur primarily due to normal operating conditions. Because these transverse shears were not readily available in the results of Bechtel's finite element analyses, they were estimated from the vertical moments available at the centroids of the bottom two rows of plate elements along the lengths of the walls. For each pair of elements aligned vertically, the transverse shear was calculated from the change in moments assuming the shear to be constant. In-plane shear capacities of 240 k/ft and 245 k/ft for the south and east walls were determined. Total interface in-plane shear capacities were then developed by factoring these values by the wall lengths. These total capacities, shear forces due to the SME and loads occurring at normal operating conditions, code margins, and F_{SME} factors are listed in Table II-4-8. The lowest code margin of 4.1 occurs at the interface between the east secondary shield wall and the base mat.

4.2.3 Refueling Canal Slab Capacity

The floor of the refueling canal is located along the East-West axis of the containment building to the east of the East secondary shield wall for the Unit 1 and opposite hand for Unit 2. The top of the slab is at Elevation 619'-6" and the total slab thickness is 4'-0". The slab is typically reinforced at both faces in both directions with vertical ties provided between the top and bottom longitudinal bars. Support for the slab is provided by the East secondary shield wall and by concrete columns at the Northeast and Southeast corners.

The wall at the East end of the refueling canal is discontinued at the slab with only the columns continuing down to the base mat. Horizontal seismic shear in this wall must be transmitted back into the secondary shield walls which are much stiffer than the columns. This force will be transferred by the refueling canal slab. Seismic forces acting on the slab were developed for the slab modeled as a cantilever loaded in-plane by the horizontal shear force from the East canal wall.

Capacities of the slab for in-plane shear and moment were determined, with the latter found to govern. In-plane stresses due to the seismic moment were calculated for the applied moments according to elementary beam theory. The effective cross-section was taken as the rectangular section of the slab only. This is conservative since the walls at the North and South ends of the refueling canal will actually behave as flanges which provide significant additional in-plane moment resistance.

Evaluation of a unit length of the slab subjected to membrane force and out-of-plane bending moment was conducted using the approach adopted for the primary shield wall. A membrane force of 16 k/ft in tension and a moment of 100 k-ft/ft acting on the slab due to loads occurring at normal operating conditions were taken from Element 909 of Bechtel's finite element model. The membrane force due to the SME at this location was calculated to be 89 k/ft. The net membrane force and moment were thus taken to be 105 k/ft in tension and 100 k-ft/ft for the worst case of the SME causing a tension force. For the given applied axial load, a moment capacity of 369 k-ft/ft was found with a corresponding code margin of 3.7. For the given applied moment, axial load capacities of 274 k/ft in tension and 1900 k/ft in compression were calculated. For the governing case of the SME causing a tension force, an F_{SME} factor of 2.9 was found. As noted in Section 4.2.1, these capacities are conservative and lead to a conservative code margin and F_{SME} factor.

4.3 EFFECTS OF REINFORCEMENT BAR CUTTING

The calculated capacities reported were based on information available from the structural drawings for the selected elements. Available non-conformance reports noting deviations from the construction specifications were reviewed to verify that there were no gross deviations that would significantly influence the capacity of the selected structural elements. The calculated capacities do not include the effects of any minor deviations. These capacities also do not address the reduction in strength due to reinforcement cutting permitted by Reference 31 since the exact location and number of reinforcement bars cut within this allowance was unavailable. Per Section 2.1 of Appendix E of Reference 31, one bar could be cut each way, each face, with the radial distance to the next cut bar on the same face, in the same direction, no less than five feet. Per Section 2.2 of Appendix E of Reference 31, two bars could be cut each way, each face, with the radial distance to the next cut bar on the same face, in the same direction, no less than 10 feet. Additional limitations are noted in Section 7.2 of Volume I.

To determine the effect of the reinforcement cutting allowance and non-conformances on the shear capacity of the walls, the shear strength of the East secondary shield wall was recalculated. The effect of reinforcement cutting is expected to be dependent on the crack pattern that leads to failure of the wall. If a crack crosses a horizontal bar where it has been cut or where it does not have sufficient development length from the cut to develop its yield strength, then the effectiveness of that bar may be significantly reduced. As an approximation, a crack was assumed to form a 45 degree angle from horizontal through the story height of the wall noted above. This angle is approximately consistent with the crack angle assumed in the derivation of the shear strength provided by web reinforcement of concrete beams. For the worst case of horizontal bars cut at both faces every five feet along the assumed crack, the reinforcement area effective in resisting shear was modified

and the total wall shear strength recalculated. Using the revised shear strength, a code margin of 2.7 was determined for this wall. This value compares to a code margin without reinforcement cutting of 3.3.

To determine the effect of the reinforcement cutting allowance and the non-conformances of the vertical axial load and moment capacity of the walls, the capacity for the East secondary shield wall was treated similarly. It was assumed that vertical bars at each face were cut every five feet along a horizontal plane. Using the effective reinforcement area, the moment capacity was recalculated. A code margin of 3.7 corresponds to this revised capacity. This value compares to a code margin of 4.5 without reinforcement cutting.

The shear capacity at the East secondary shield wall base mat was also recalculated to account for the reinforcement cutting. The same cutting pattern used for the vertical axial load-moment interaction capacity was assumed to occur close enough to the base of the wall to reduce the shear friction capacity. Based on the revised capacity, a code margin for shear at the interface of 3.1 was determined. This value compares to a code margin of 4.1 without reinforcement cutting.

The code margins against shear, axial load-moment interaction, and shear friction for the walls were still found to be substantially greater than unity when the reinforcement cutting allowance and non-conformances were considered for the selected examples. It can be concluded that the cutting allowance and non-conformances do not adversely affect the results of this study for the elements of the internal structures. Significant cutting of reinforcement is not expected for the containment structure so the effects of allowable cutting were not addressed.

Table II-4-1

Containment Wall Meridional Membrane Forces and Bending Moments

Wall Section No.(1)	Approximate Elevation	SME	$D + F + L + T_o$ (Winter)		$D + F + L + T_o$ (Summer)		$D + F + L + P + T_A$ (Winter)		$D + F + L + P + T_A$ (Summer)	
		P_m (k/ft)	P_m (k/ft)	M_m (k-ft/ft)	P_m (k/ft)	M_m (k-ft/ft)	P_m (k/ft)	M_m (k-ft/ft)	P_m (k/ft)	M_m (k-ft/ft)
11	594'-11"	± 135	-463	-437	-458	-645	-189	-341	-190	-402
10	605'-10"	± 125	-467	-28	-467	-163	-182	-388	-182	-425
9	650'-0"	± 85	-445	-385	-445	-101	-160	-340	-160	-275

Notes: (1) See Figure II-4-3 For Location Of Wall Sections

$D + F + L + T_o$ - Normal Operating Conditions

$D + F + L + P + T_A$ - Accident Conditions

P_m - Meridional Membrane Force, Positive In Tension

M_m - Meridional Bending Moment, Positive When Causing Tension On Inside Face

Table II-4-2

Code Margins and F_{SME} Factors For Containment Wall
Meridional Membrane Force and Bending Moment

Wall Section No.[1]	Allowable Concrete Stress (psi)	Allowable Reinforcement Stress (psi)	Load Combination[2]	Net Applied Forces		Maximum Concrete Stress (psi)	Maximum Reinforcement Stress (psi)	Code Margin[4]	F_{SME}
				P_m (k/ft)	M_m (k-ft/ft)				
11	5100	54,000	1	-55	-402	1990	21,100	2.6[3]	3.8[3]
			2	-325	-402	2040	5,200	2.5	Large
			3	-323	-645	3120	18,300	1.6	4.6[3]
			4	-593	-645	3200	15,600	1.6	Large
10	5100	54,000	1	-57	-425	2380	32,700	1.7[3]	2.4[3]
			2	-307	-425	2250	9,000	2.3	Large
			3	-342	-163	1140	-5,600	4.5	6.0[3]
			4	-592	-163	1610	-8,600	3.2	Large
9	4500	54,000	1	-75	-340	2340	36,300	1.5[3]	2.0[3]
			2	-245	-340	2050	9,800	2.2	Large
			3	-360	-385	2220	5,300	2.0	5.0[3]
			4	-530	-385	2330	200	1.9	Large

Notes: (1) See Figure II-4-3 for Location of Wall Sections

(2) Load Combination 1 - $D + F + L + P + T_A + SME$
2 - $D + F + L + P + T_A - SME$
3 - $D + F + L + T_o + SME$
4 - $D + F + L + T_o - SME$

(3) Governed by Reinforcement Stress. All Other Code Margins and F_{SME} Factors Governed by Concrete Stress

(4) Code Margins at Sections 10 & 11 Governed by Summer Thermal Conditions While Code Margins at Section 9 Governed by Winter Conditions

Table II-4-3

Code Margins and F_{SME} Factors For Containment Wall
Tangential Shear Limited by the Principal Tensile Stress

Wall Section No.(1)	V_t (k/ft)	P_m (k/ft)	P_h (k/ft)	$V_{t,all}$ (k/ft)	Code Margin	F_{SME}
11	57	-54	-300	310	5.4	2.3
10	57	-57	-227	236	5.0	2.3
9	52	-75	-95	241	4.6	2.8
8	47	-84	-92	244	5.2	3.4
7	38	-93	-80	242	6.4	4.5

Note: (1) See Figure II-4-3 for location of wall sections

(2) All sections are governed by load combination D + F + L + P + T_A + SME. Sections 7 and 11 are governed by winter thermal conditions. All other sections are governed by summer thermal conditions.

(3) V_t = Applied tangential shear

$V_{t,all}$ = Allowable tangential shear

P_m = Meridional membrane force

P_h = Hoop membrane force

Table II-4-4

Code Margins and F_{SME} Factors for Containment Wall Tangential Shear Limited by Shear-Friction

Wall Section No. (1)	V_t (k/ft)	A_{sm} (in^2/ft)	P_m (k/ft)	V_r (k/ft)	$V_{t,all}$ (k/ft)	Code Margin	F_{SME}
11 (2)	57	9.12	-323	160	343(3)	5.3	4.7 (3.6)
10 (2)	57	7.12	-342	19	343(3)	6.0	4.7 (3.2)
9	52	2.34	-75	1	183	3.5	2.1
8	47	2.34	-85	1	191	4.1	2.5
7	38	2.34	-93	1	199	5.2	3.4

Notes:

(1) See Figure II-4-3 for location of wall sections

(2) The code margins for these sections are governed by $D + F + L + T_o$ + SME due to the shear at normal operating conditions. However, the F_{SME} factors that govern at these sections, shown in parentheses, are governed by accident conditions. Code margins and F_{SME} factors at the other sections are governed by accident conditions.

(3) The shear friction capacity is limited by ϕ 800 bt.

Table II-4-5

Code Margins and F_{SME} Factors For Shear On The Primary Shield Wall

Elevation	V_u (k/ft)	V_{SME} (k/ft)	V_{NOL} (k/ft)	V_{NET} (k/ft)	Code Margin	F_{SME}
603'-0"	476	46	39	85	5.6	Large
626'-0"	254	74	55	129	2.0	2.7

Notes: (1) V_u = Ultimate Shear Strength

V_{SME} = Shear Due to the SME

V_{NOL} = Shear Due to Loads at Normal Operating Conditions

V_{NET} = Net Shear

$= V_{SME} + V_{NOL}$

Table II-4-6

Code Margins and F_{SME} Factors For Axial Load and Bending Moment

On The Secondary Shield Walls

Wall	SME	Normal Operating Loads		Net Applied Forces		M_u (k-ft/ft)	Code Margin	P_u (k/ft)	F_{SME}
	P (k/ft)	P (k/ft)	M (k-ft/ft)	P (k/ft)	M (k-ft/ft)				
South	+78	-217	128	-139	128	851	6.6	+306	6.7
East	+78	-89	162	-11	162	727	4.5	+323	5.3

Notes: (1) P = Applied Axial Load, positive in tension

M = Applied Bending Moment

M_u = Ultimate Moment Capacity Given Net Applied Axial Load

P_u = Ultimate Axial Load Capacity Given Net Applied Moment

Table II-4-7

Code Margins and F_{SME} Factors For Shear On The Secondary Shield Walls

Wall	V_u (k)	V_{SME} (k)	V_{NOL} (k)	V_{NET} (k)	Code Margin	F_{SME}
South	7700	1075	980	2050	3.8	6.3
East	8450	970	1620	2590	3.3	5.2

Notes: (1) V_u = Ultimate Shear Strength

V_{SME} = Shear Due to SME

V_{NOL} = Shear Due to Loads at Normal Operating Conditions

V_{NET} = Net Shear

$= V_{SME} + V_{NOL}$

Table II-4-8

Code Margins and F_{SME} Factors For Shear at the Interfaces Between the Secondary Shield Walls and the Base Mat

Wall	V_u (k)	V_{SME} (k)	V_{NOL} (k)	V_{NET} (k)	Code Margin	F_{SME}
South	8970	1070	977	2050	4.4	7.4
East	10700	970	1620	2590	4.1	Large

Notes: (1) V_u = Ultimate shear strength

V_{SME} = Shear due to SME

V_{NOL} = Shear due to loads at normal operating conditions

V_{NET} = Net shear

= $V_{SME} + V_{NOL}$

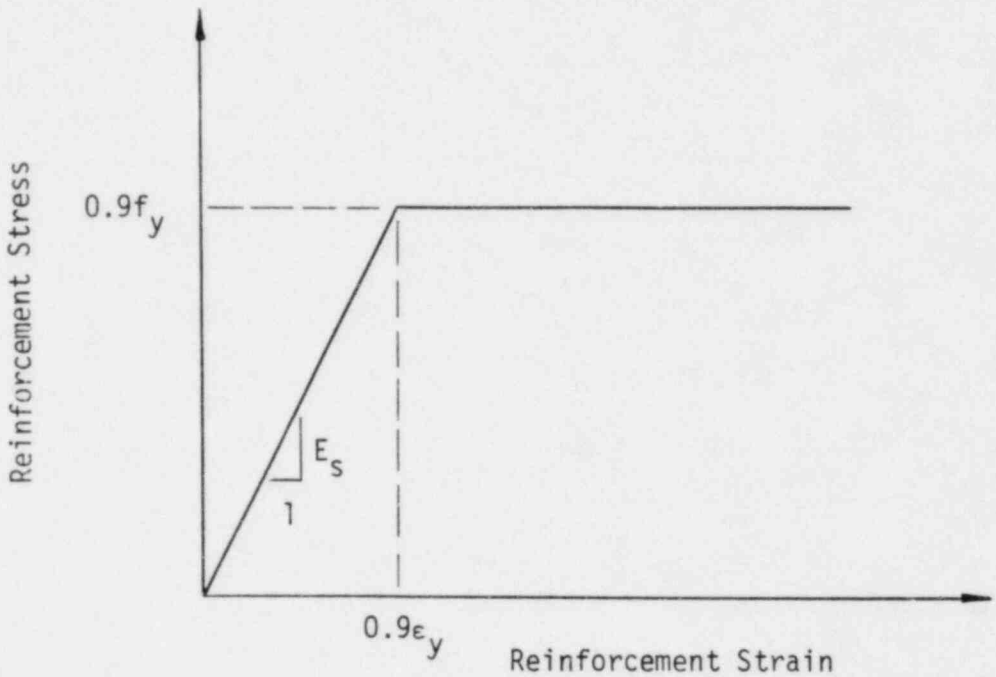

f_y = Minimum specified yield strength, psi

$\varepsilon_y = \dfrac{f_y}{E_s}$

E_s = Modulus of elasticity

= 29,000,000 psi

FIGURE II-4-1. REINFORCEMENT STRESS-STRAIN RELATIONSHIP

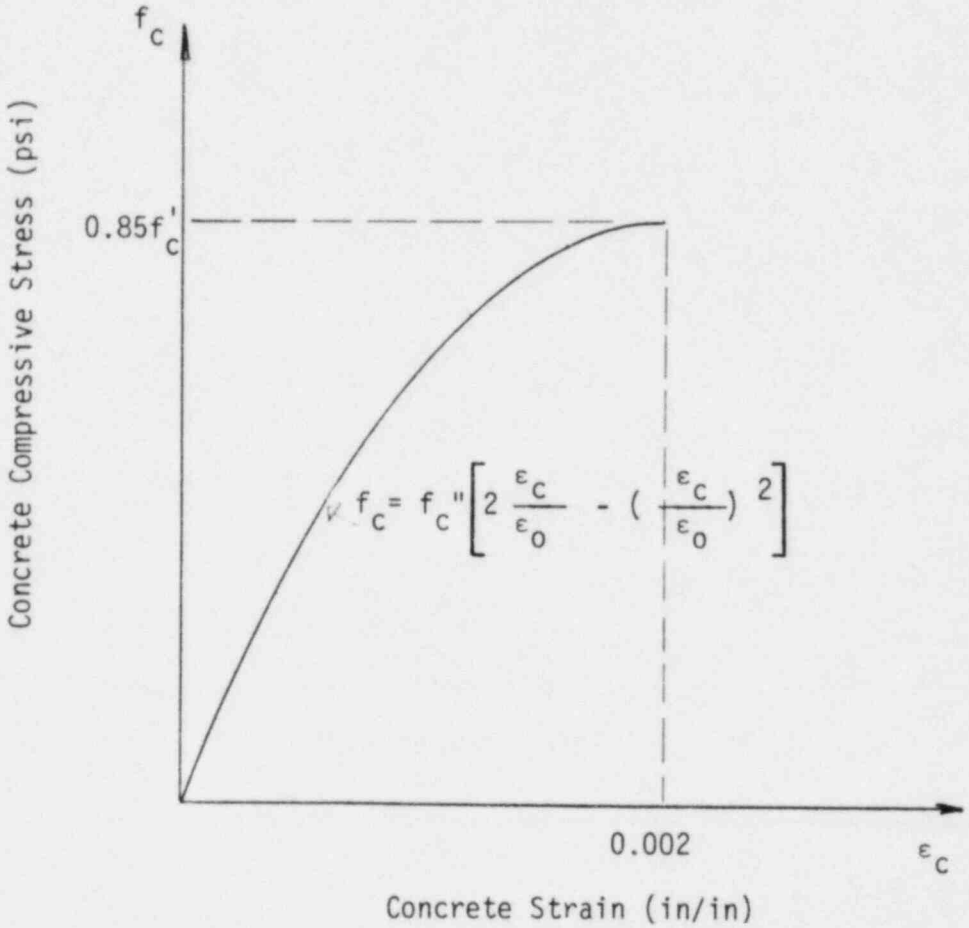

Note: See text for definition of terms.

FIGURE II-4-2. CONCRETE COMPRESSIVE STRESS-STRAIN RELATIONSHIP (FROM REFERENCE 25)

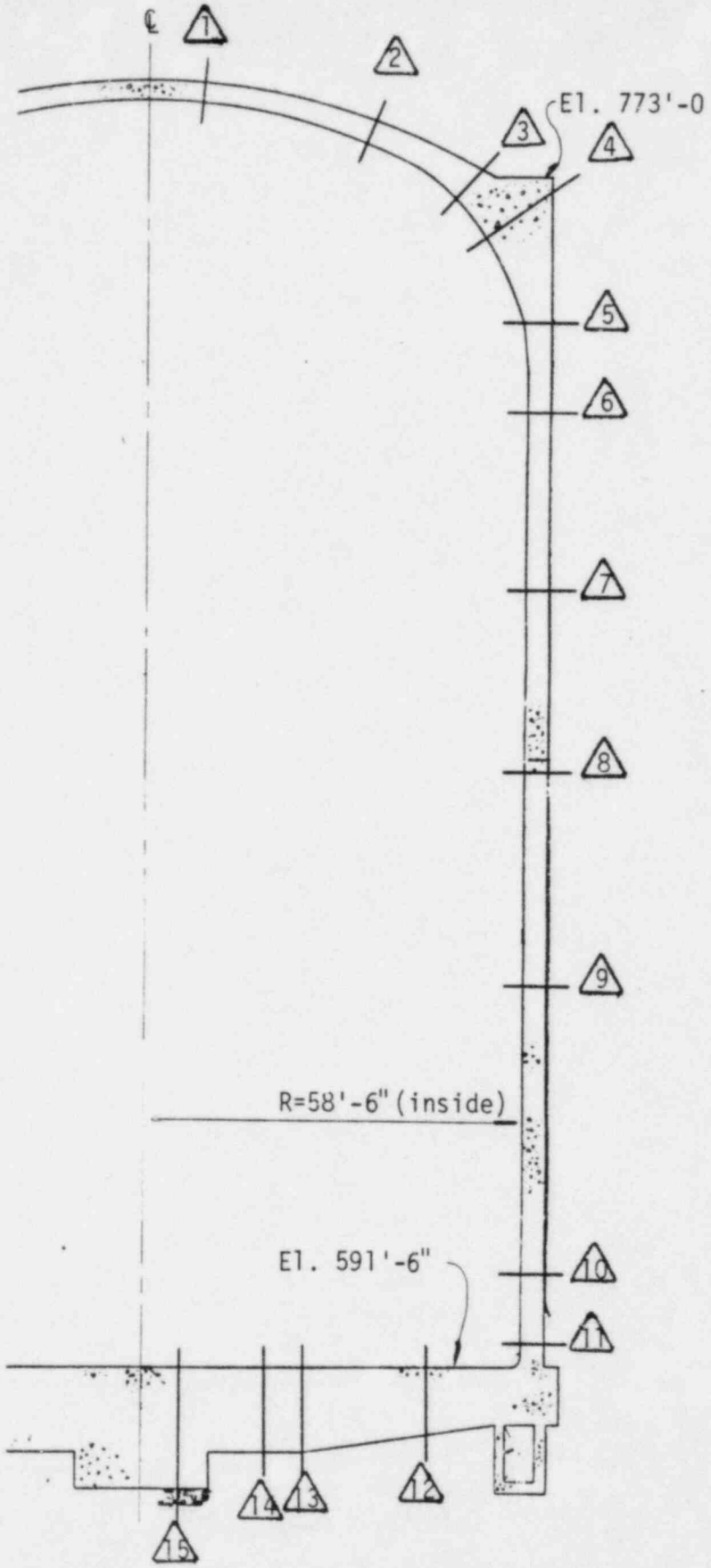

FIGURE II-4-3. LOCATION OF CONTAINMENT SECTIONS IDENTIFIED IN THE FSAR

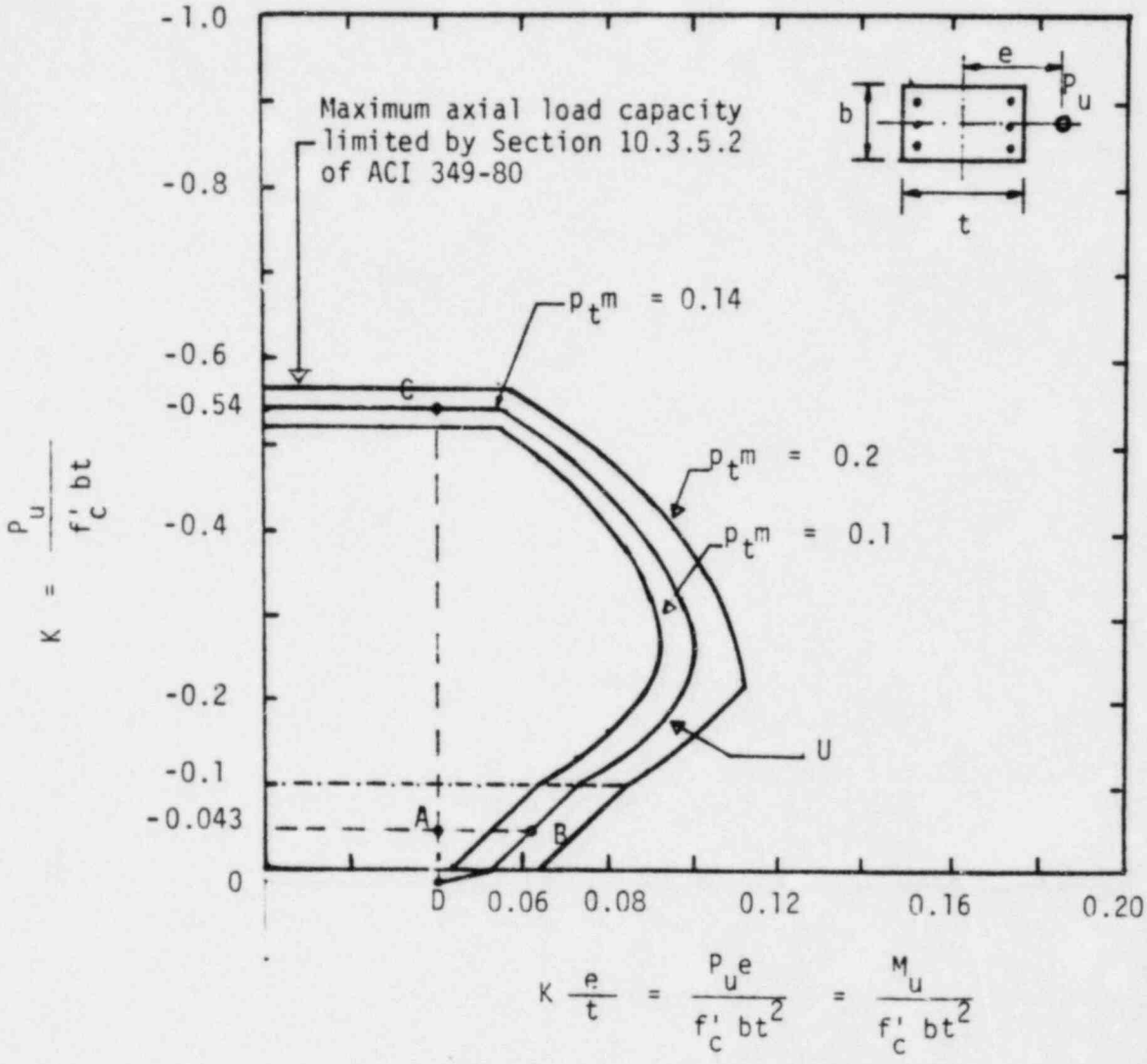

Note: P_u = Ultimate axial load capacity, positive in tension

M_u = Ultimate moment capacity

A_s = Total reinforcement area

$p_t = \frac{A_s}{bt}$

$m = \frac{f_y}{0.85\, f'_c}$

FIGURE II-4-4. AXIAL LOAD -BENDING INTERACTION CURVES FOR THE PRIMARY SHIELD WALL (FROM REFERENCE 28)

Rev. 1

5. INPUT TO EQUIPMENT

Seismic input to equipment for the SME was specified by in-structure response spectra. These spectra were generated by time history analysis using the coupled equations of motion of the structure as discussed in Section 8 of Volume I of this report. The time history input used was an artificial earthquake whose response spectra essentially envelop the SME ground response spectra at the original ground location. The development of the artificial earthquake is discussed in Section 2 of Volume I of this report. The spectra developed for the reactor building considered the effects of multidirection excitation for the range of soil characteristics previously discussed. Torsional response of the structure was not calculated since the structure is essentially symmetric.

In-structure response spectra were developed for all locations of critical equipment within the containment structure and on the reinforced concrete reactor internal support structure. Spectra were generated for the lower bound, intermediate, and upper bound soil conditions. These spectra were smoothed and the peaks broadened $\pm$ 10 percent as discussed in Section 8 of Volume I. Final spectra were developed from an envelope of the three soil conditions. Enveloped in-structure response spectra for the N-S, E-W, and vertical directions for equipment damping ratios of 2, 3, 4, and 7 percent of critical are shown in Figures II-5-1 through II-5-5.

The vertical spectra as shown are applicable for piping and equipment located adjacent to major walls or on rigid slabs. Amplification of the vertical floor spectra due to floor slab flexibility was not considered for this structure. Much of the equipment is mounted on the base slab which rests on the soil and is not expected to be affected by slab amplification. Other equipment mounted on grating or steel framing had the flexibility of the support structure included in their design as discussed in Appendix A of Volume I of this report.

Damping ratios of 2 through 7 percent of critical are considered appropriate for the response of piping and equipment for the SME. In some cases, this is higher than the damping assumed for design. Comparisons of the SME in-structure spectra with corresponding design spectra throughout the reactor building are presented in Volume VI of this report.

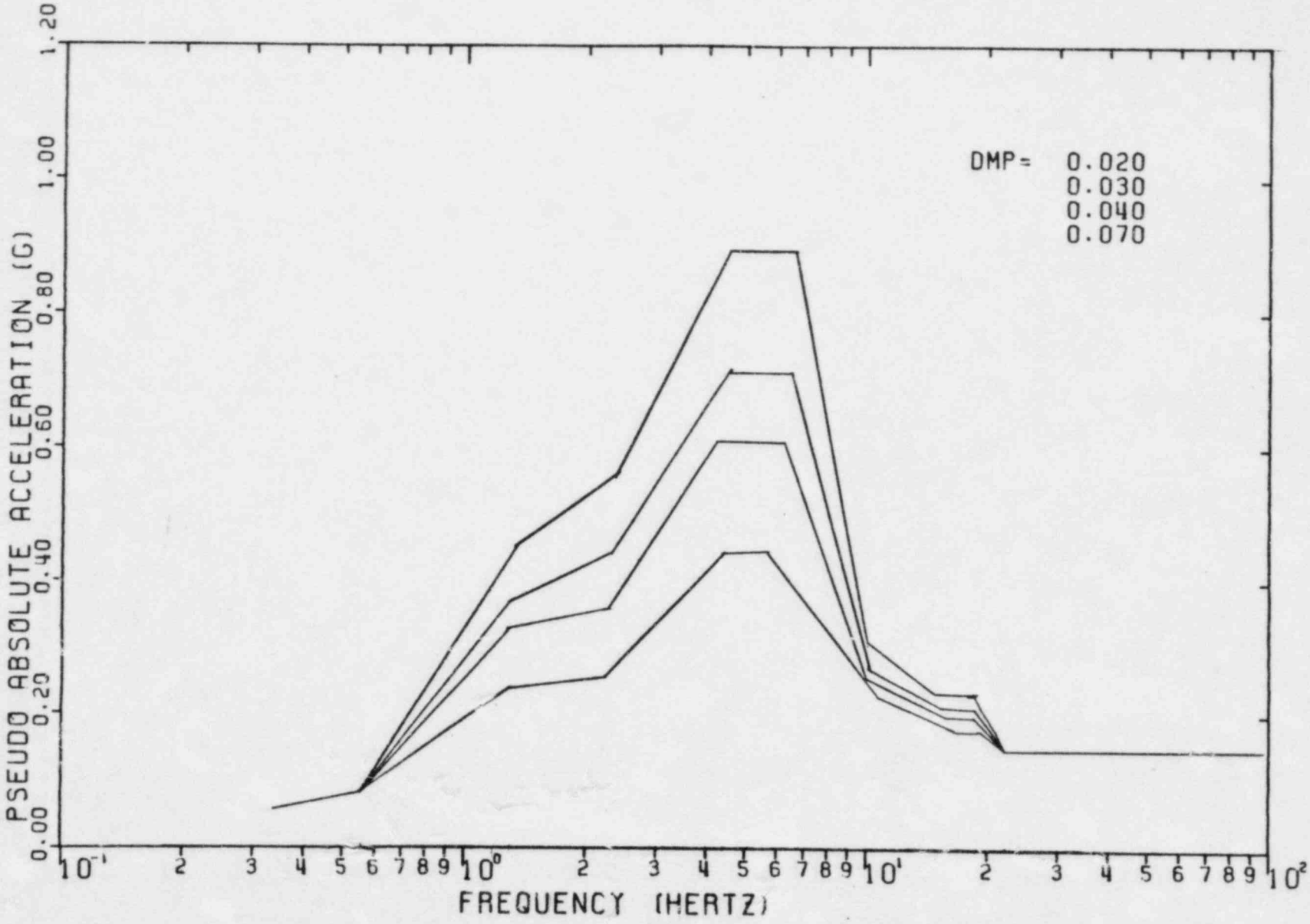

FIGURE II-5-1. ENVELOPED SRSS COMBINED RESPONSE SPECTRA, REACTOR BUILDING INTERNAL STRUCTURE, ELEVATION 603'-0", NORTH-SOUTH DIRECTION

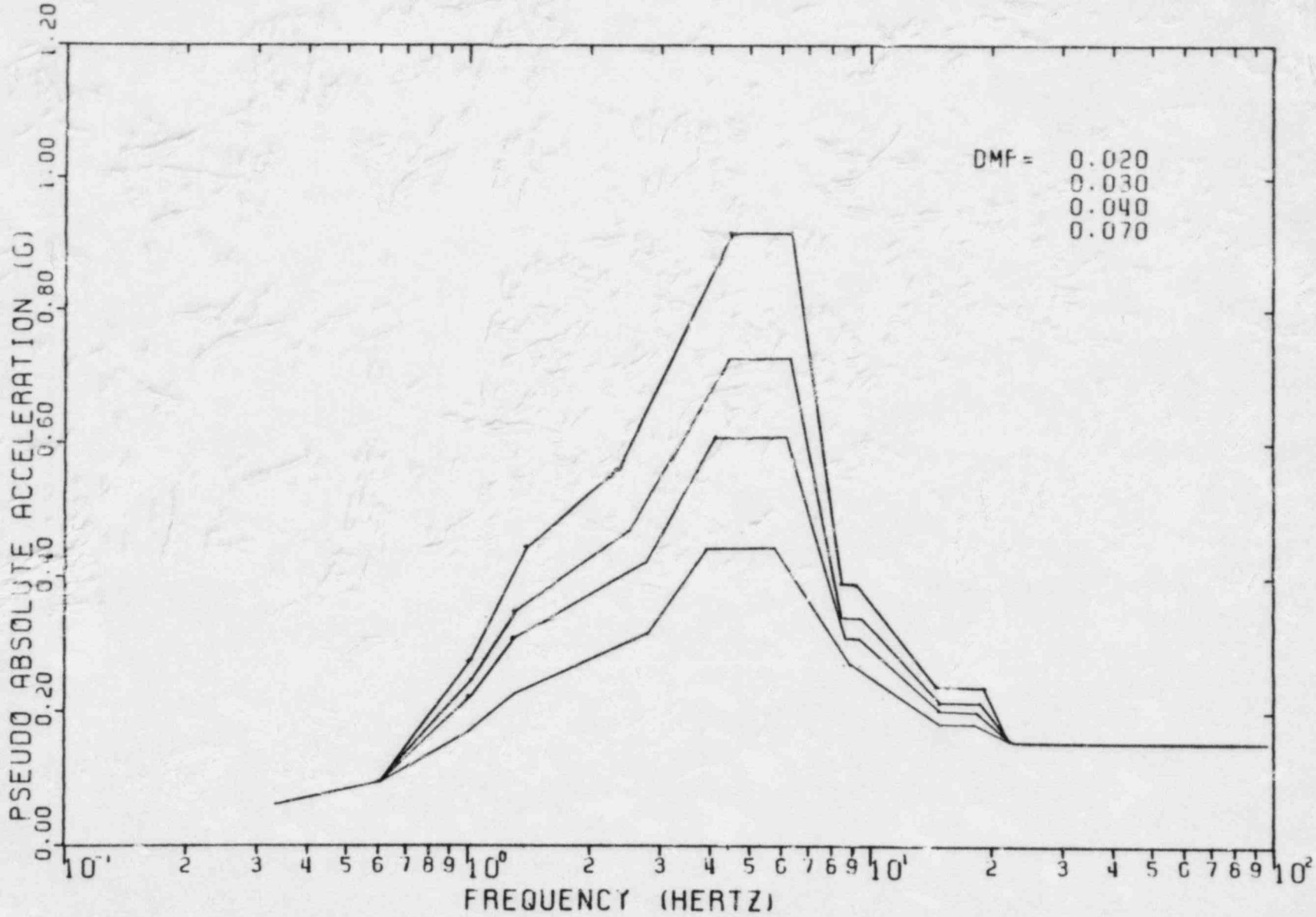

FIGURE II-5-2. ENVELOPED SRSS COMBINED RESPONSE SPECTRA, REACTOR BUILDING INTERNAL STRUCTURE, ELEVATION 603'-0", EAST-WEST DIRECTION

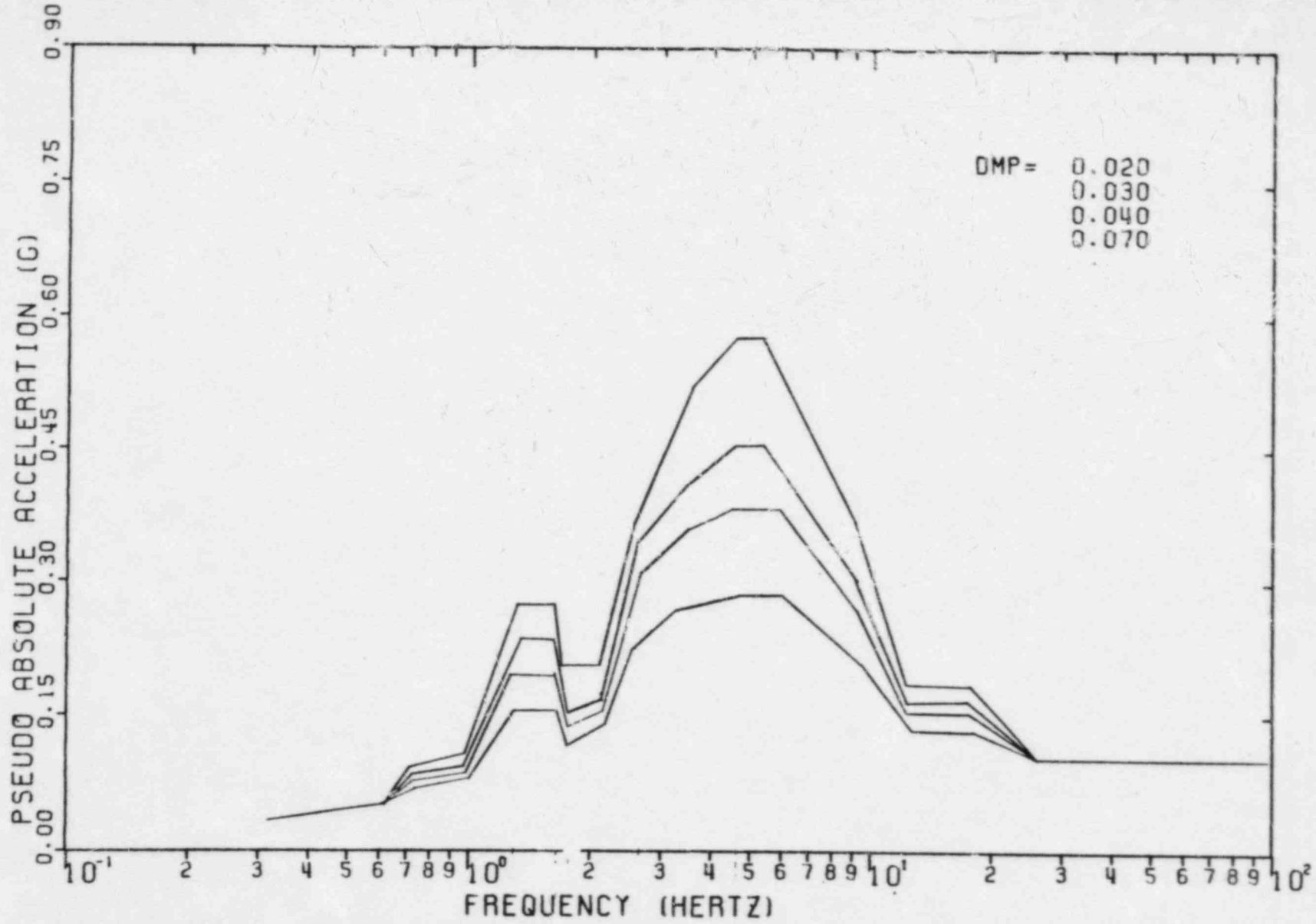

FIGURE II-5-3. ENVELOPED SRSS COMBINED RESPONSE SPECTRA, REACTOR BUILDING INTERNAL STRUCTURE, ELEVATION 603'-0", VERTICAL DIRECTION

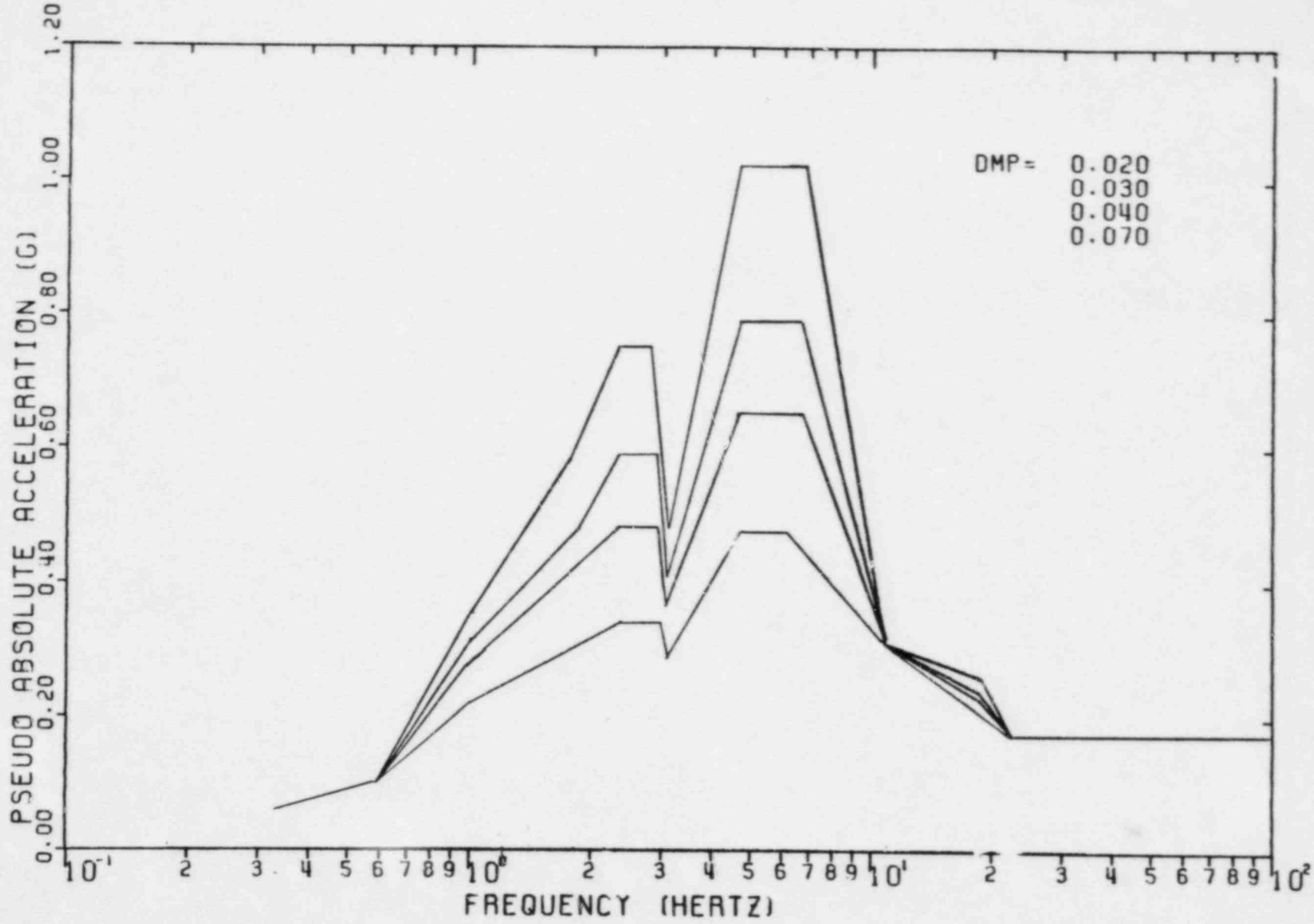

FIGURE II-5-4. ENVELOPED SRSS COMBINED RESPONSE SPECTRA REACTOR BUILDING, INTERNAL STRUCTURE, ELEVATION 626'-0" NORTH-SOUTH DIRECTION

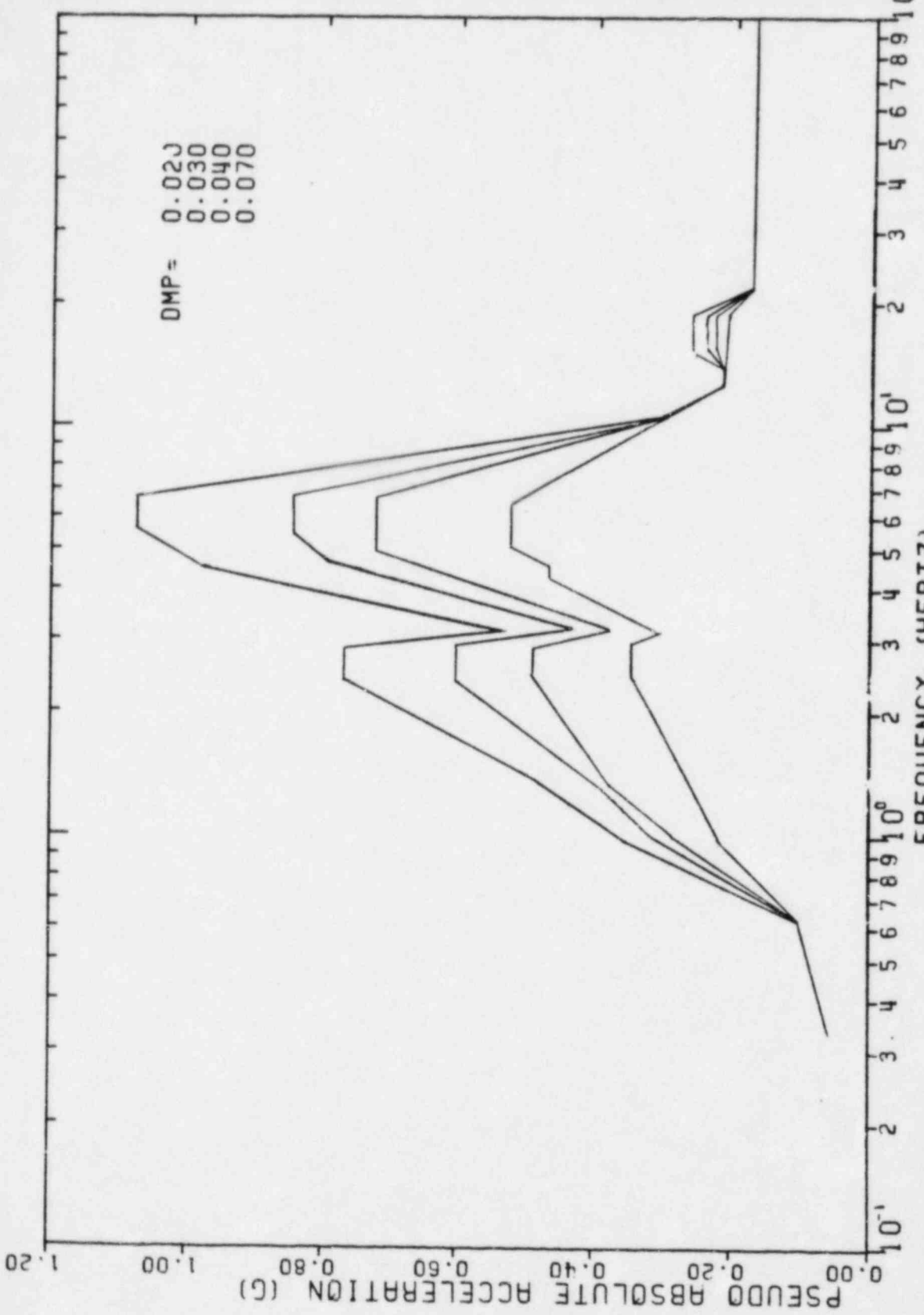

FIGURE II-5-5. ENVELOPED SRSS COMBINED RESPONSE SPECTRA REACTOR BUILDING, INTERNAL STRUCTURE, ELEVATION 626'-0" EAST-WEST DIRECTION

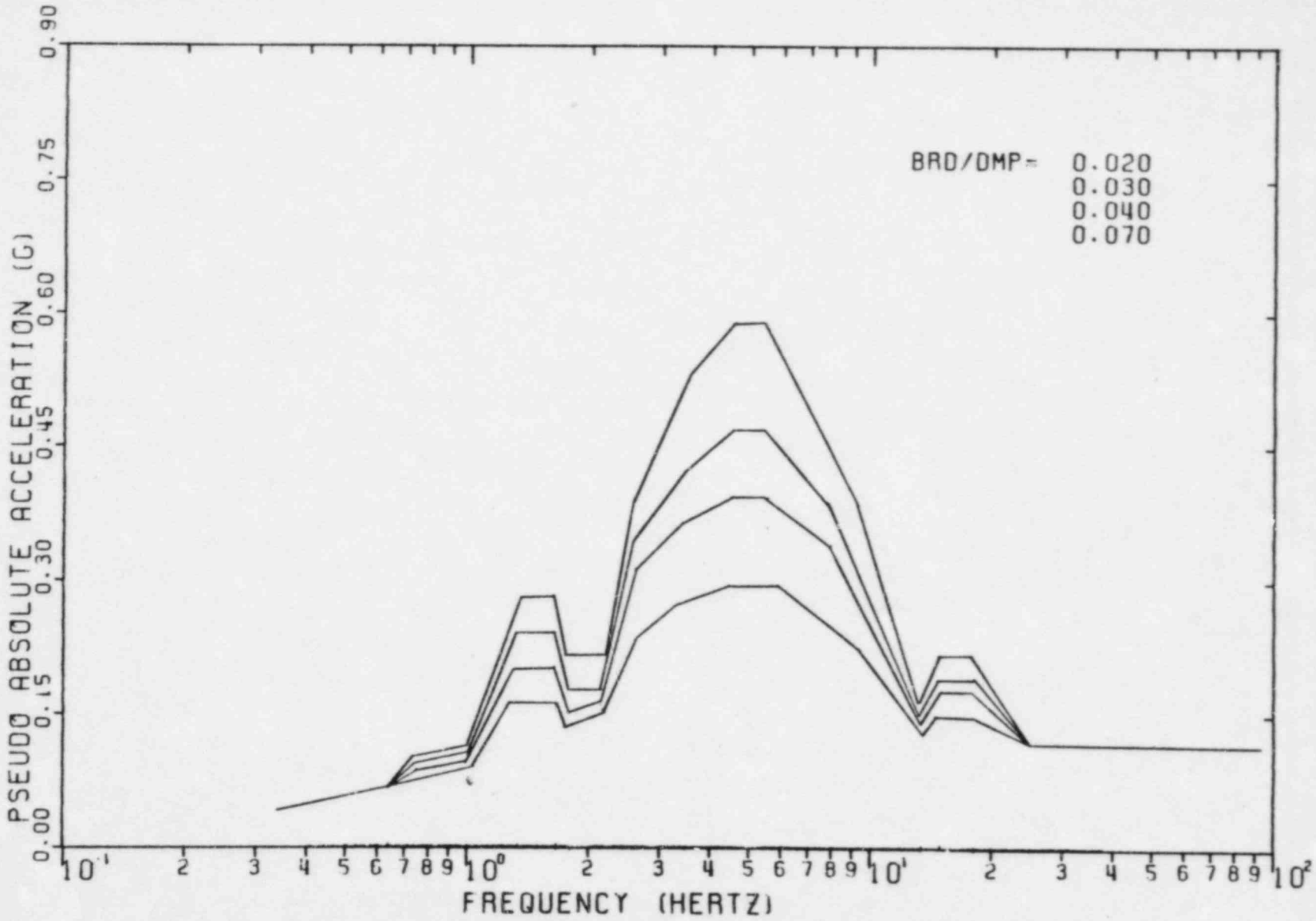

FIGURE II-5-6. ENVELOPED SRSS COMBINED RESPONSE SPECTRA, REACTOR BUILDING, INTERNAL STRUCTURE, ELEVATION 626'-0", VERTICAL DIRECTION

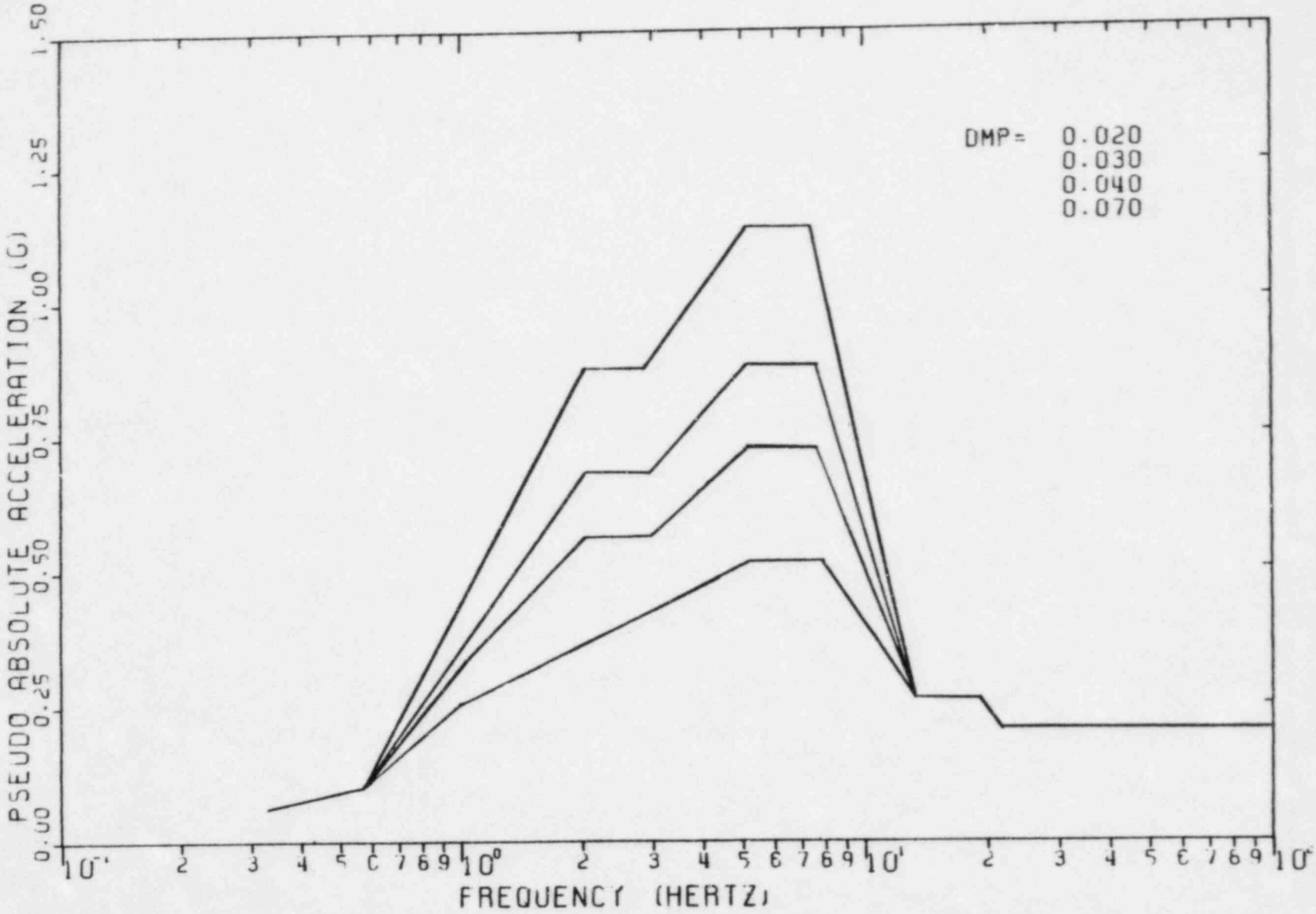

FIGURE II-5-7. ENVELOPED SRSS COMBINED RESPONSE SPECTRA, REACTOR BUILDING, INTERNAL STRUCTURE, ELEVATION 640'-0", NORTH-SOUTH DIRECTION

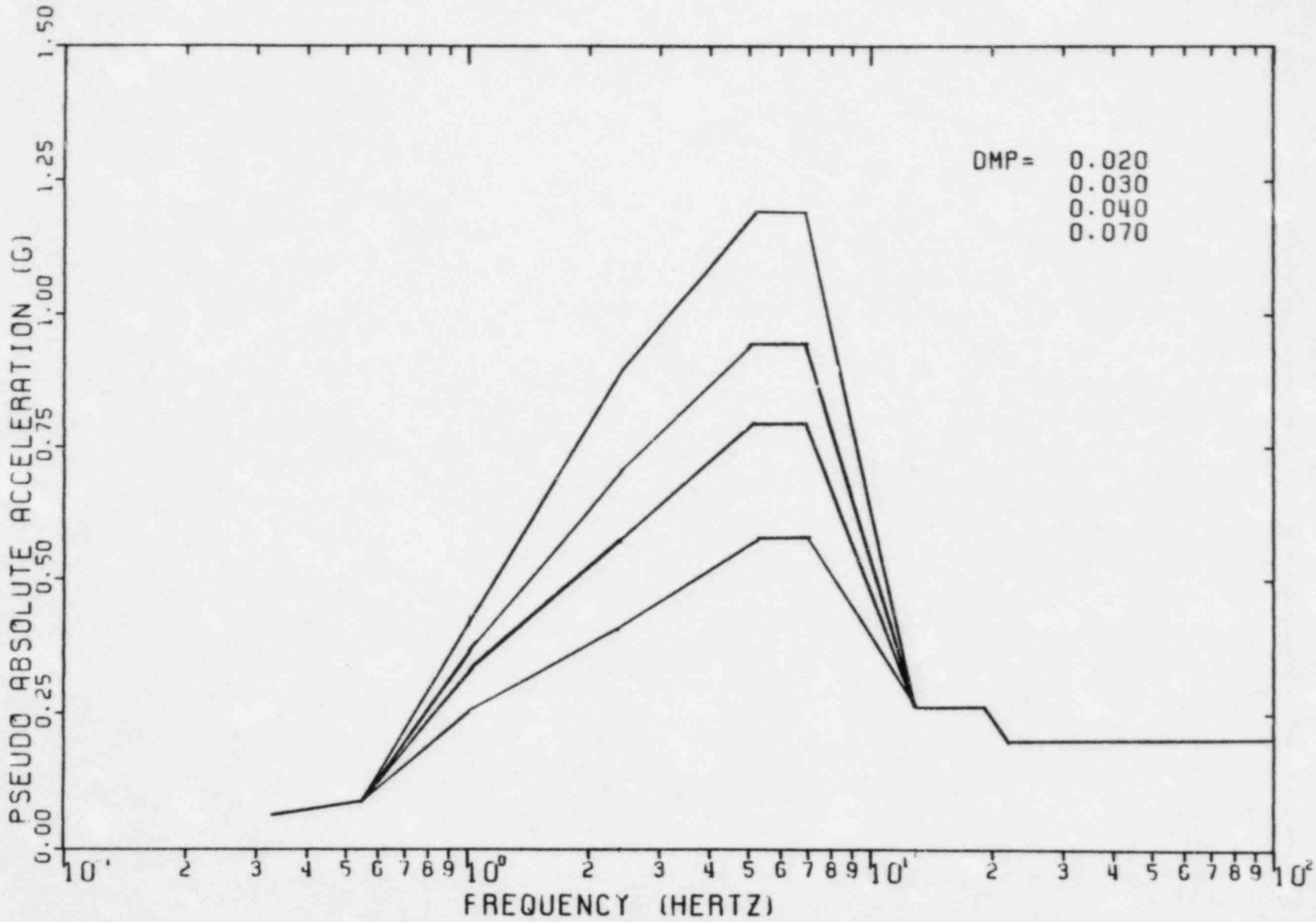

FIGURE II-5-8. ENVELOPED SRSS COMBINED RESPONSE SPECTRA, REACTOR BUILDING INTERNAL STRUCTURE, ELEVATION 640'-0", EAST-WEST DIRECTION

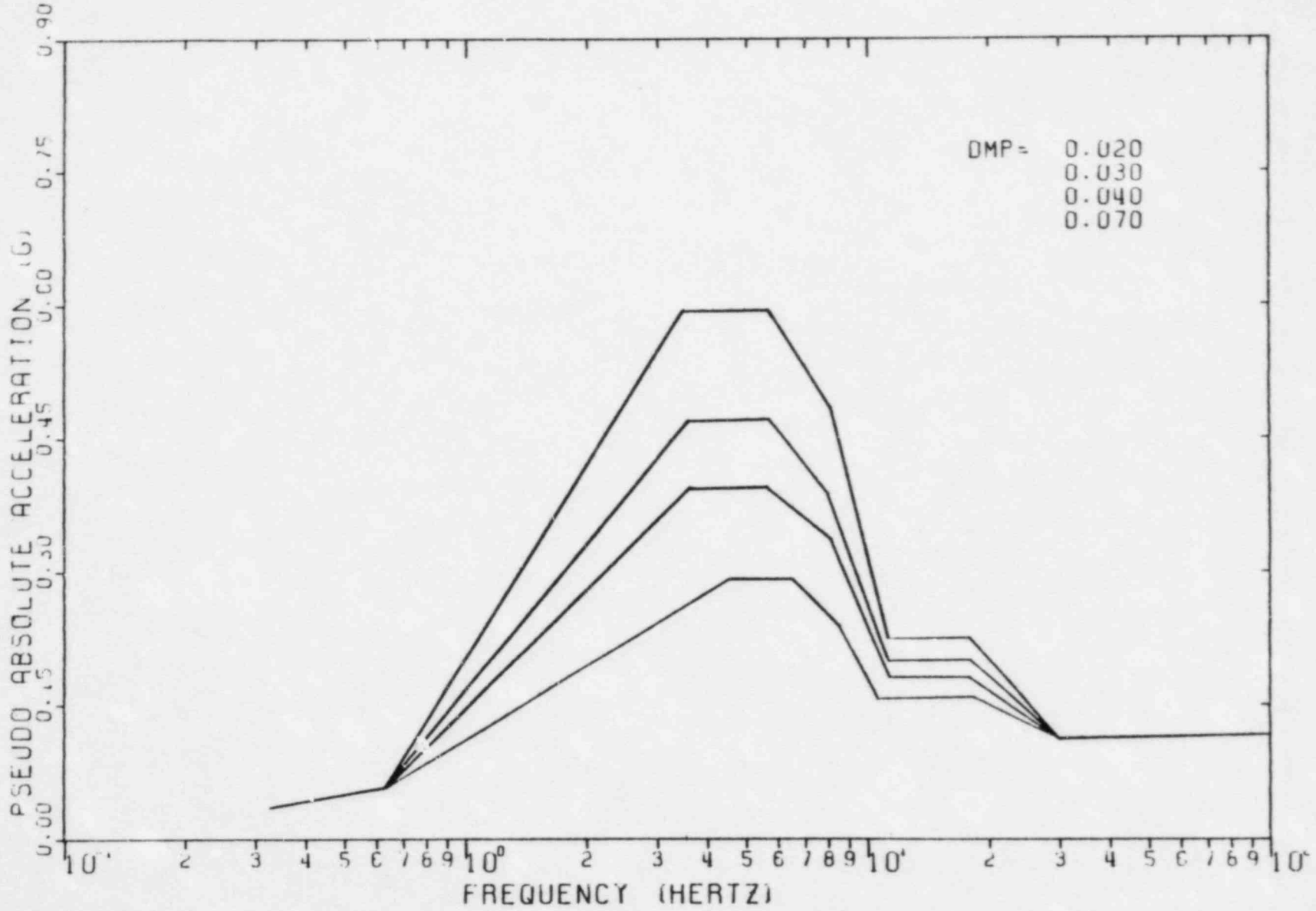

FIGURE II-5-9. ENVELOPED SRSS COMBINED RESPONSE SPECTRA, REACTOR BUILDING INTERNAL STRUCTURE, ELEVATION 640'-0", VERTICAL DIRECTION

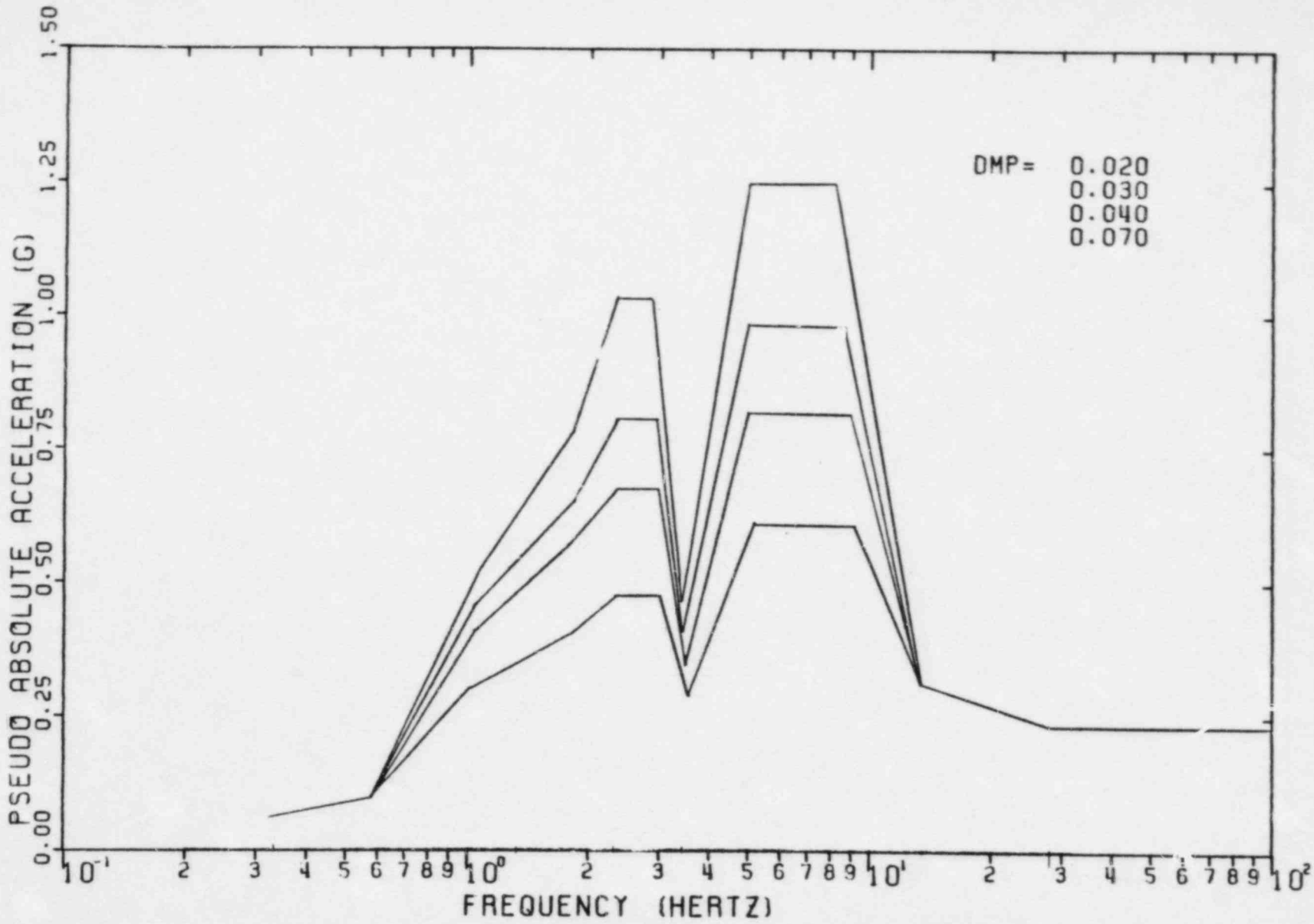

FIGURE II-5-10. ENVELOPED SRSS COMBINED RESPONSE SPECTRA, REACTOR BUILDING, INTERNAL STRUCTURE, ELEVATION 659'-0", NORTH-SOUGH DIRECTION

FIGURE II-5-11. ENVELOPED SRSS COMBINED RESPONSE SPECTRA REACTOR BUILDING, INTERNAL STRUCTURE, ELEVATION 659'-0", EAST-WEST DIRECTION

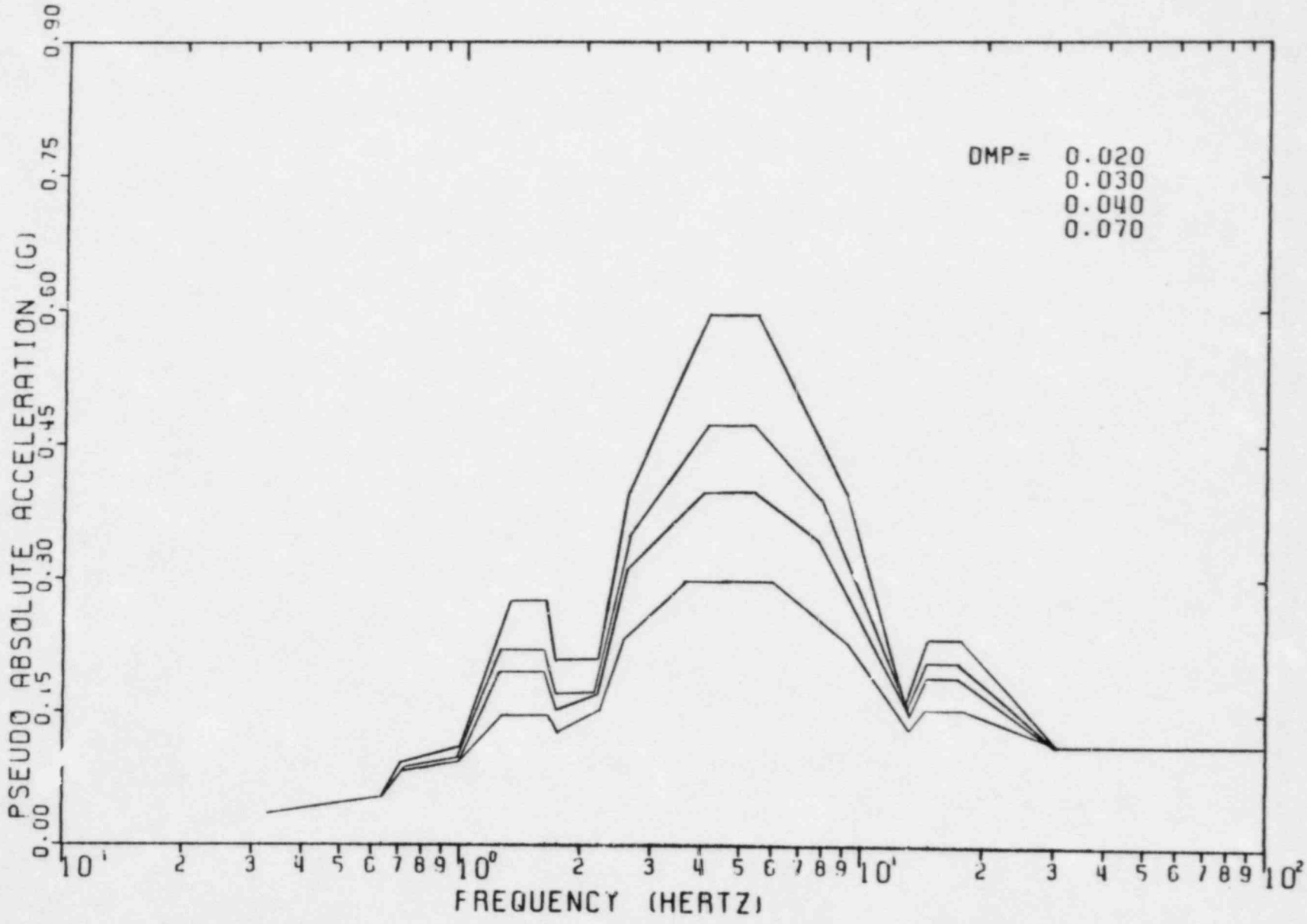

FIGURE II-5-12. ENVELOPED SRSS COMBINED RESPONSE SPECTRA, REACTOR BUILDING, INTERNAL STRUCTURE, ELEVATION 659'-0", VERTICAL DIRECTION

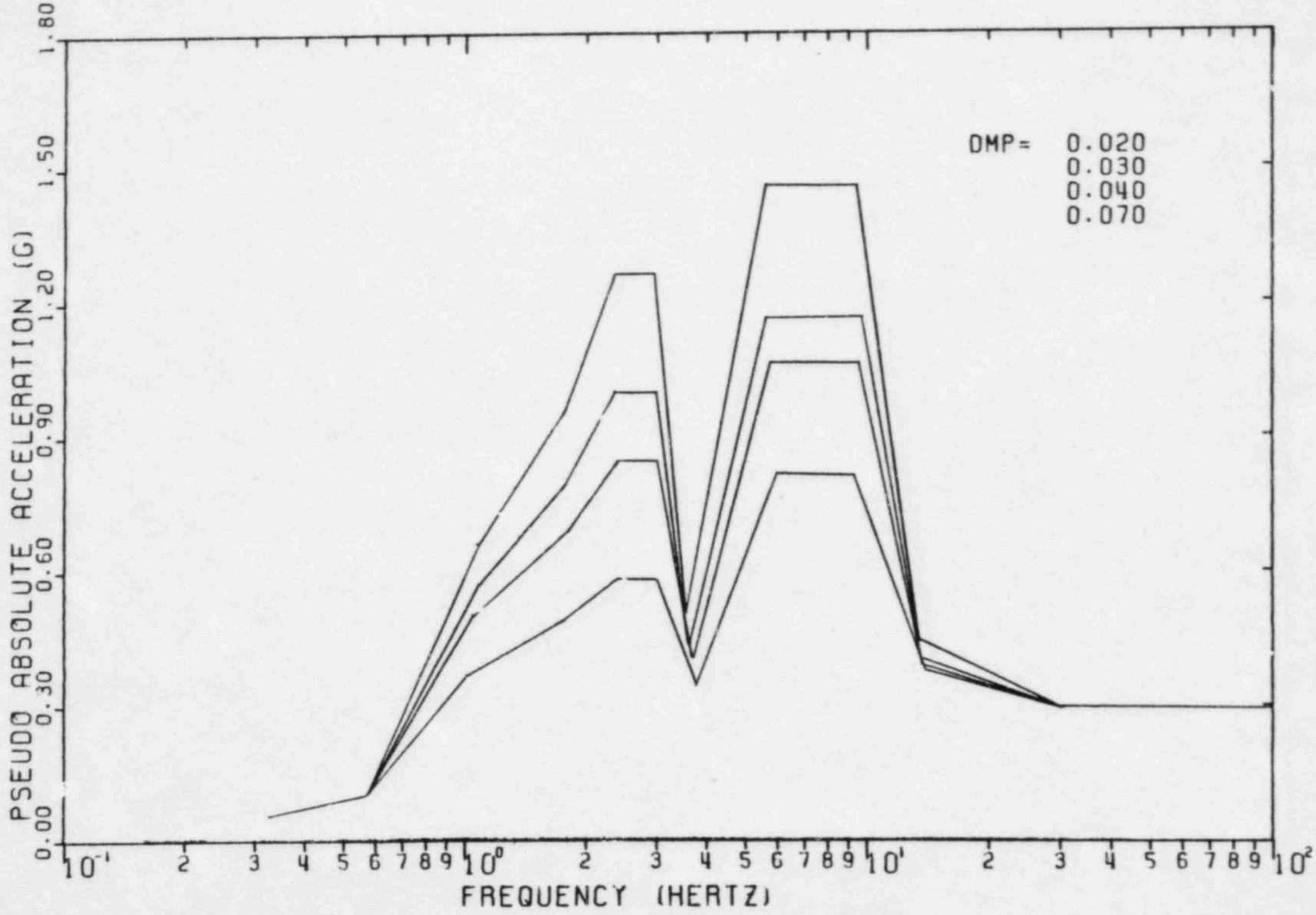

FIGURE II-5-13. ENVELOPED SRSS COMBINED RESPONSE SPECTRA, REACTOR BUILDING, INTERNAL STRUCTURE, ELEVATION 685'-0", NORTH-SOUTH DIRECTION

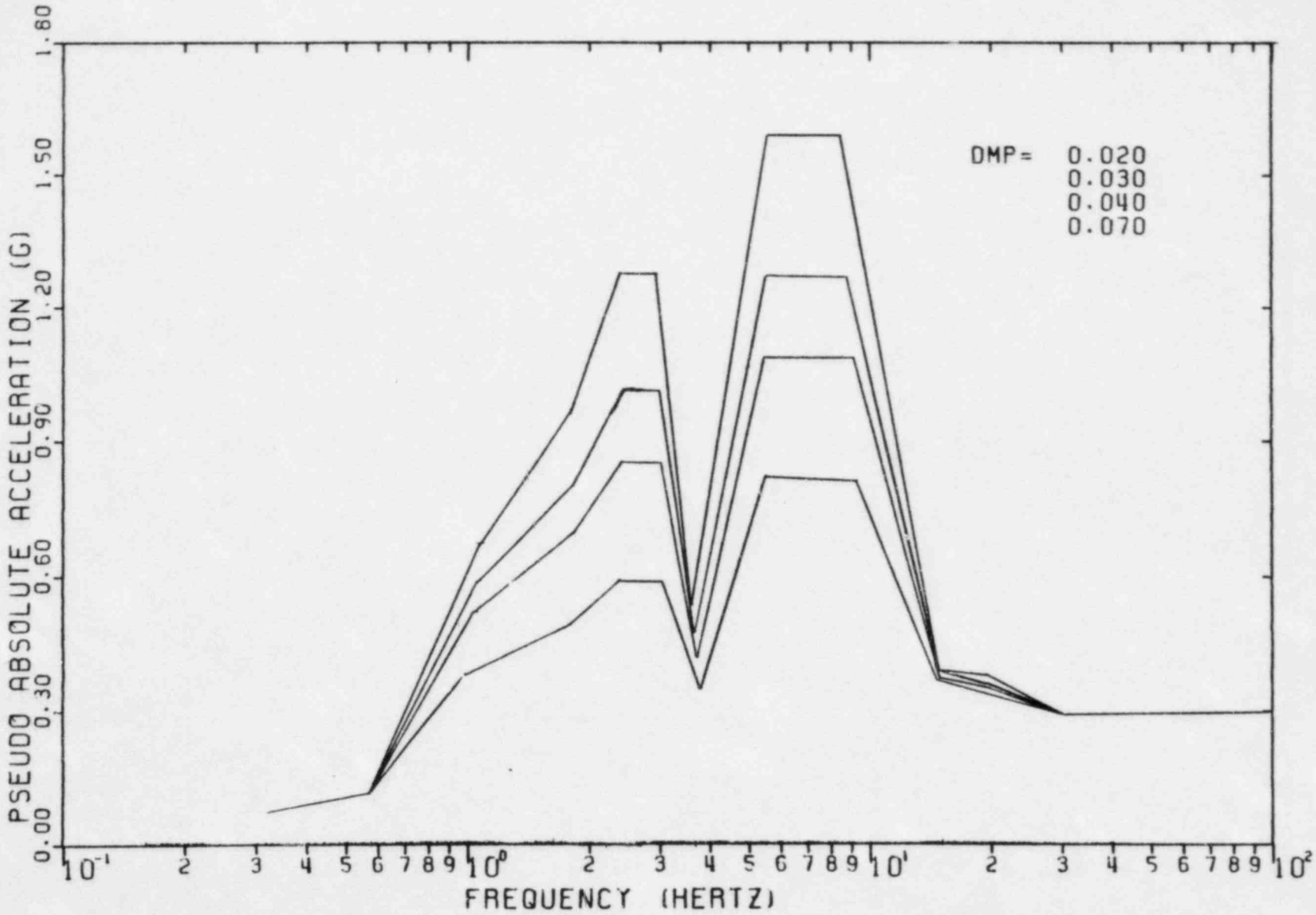

FIGURE II-5-14. ENVELOPED SRSS COMBINED RESPONSE SPECTRA, REACTOR BUILDING, INTERNAL STRUCTURE, ELEVATION 685'-0", EAST-WEST DIRECTION

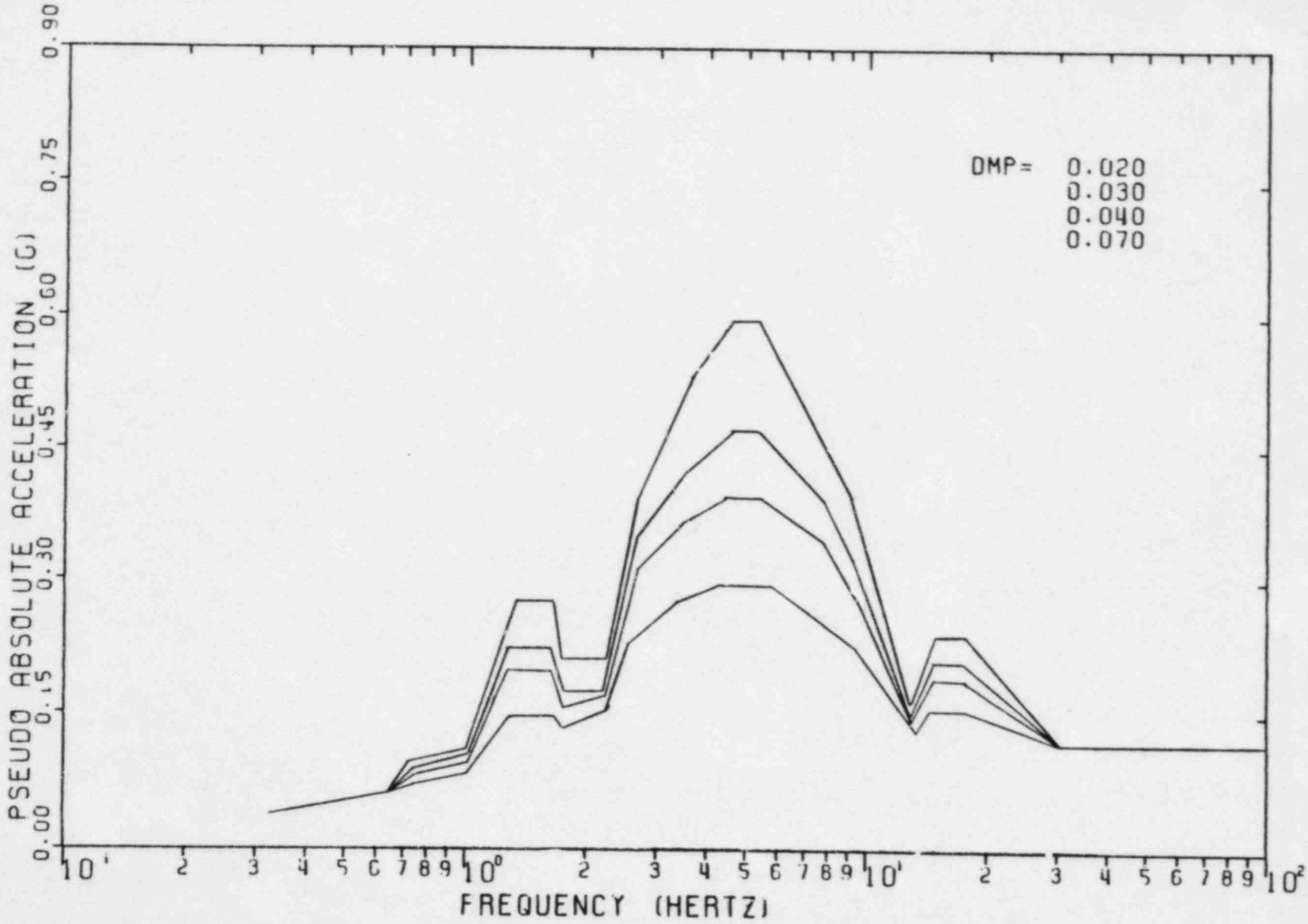

FIGURE II-5-15. ENVELOPED SRSS COMBINED RESPONSE SPECTRA, REACTOR BUILDING, INTERNAL STRUCTURE, ELEVATION 685'-0", VERTICAL DIRECTION

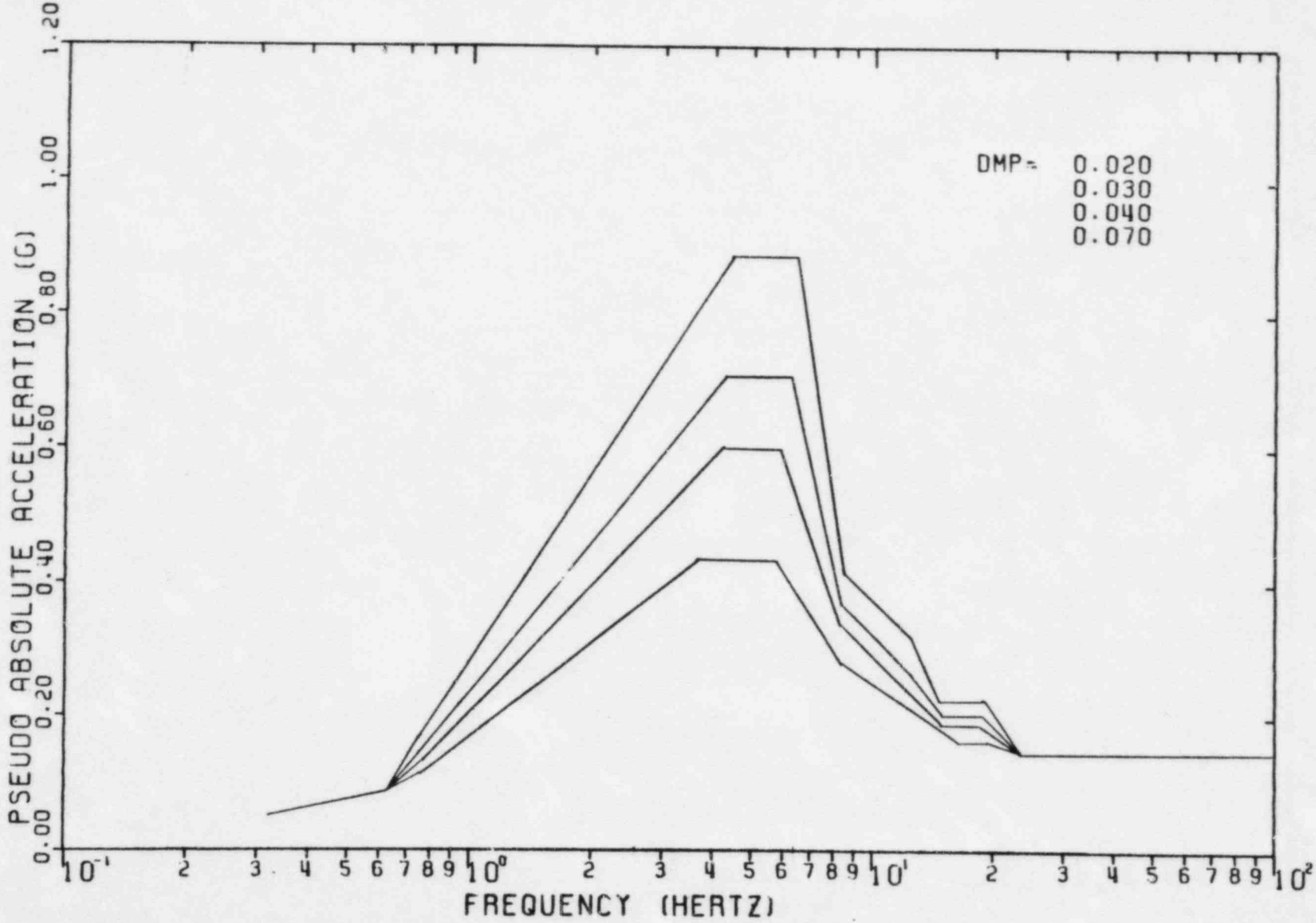

FIGURE II-5-16. ENVELOPED SRSS COMBINED RESPONSE SPECTRA, REACTOR BUILDING, CONTAINMENT, ELEVATION 591'-6", NORTH-SOUTH DIRECTION

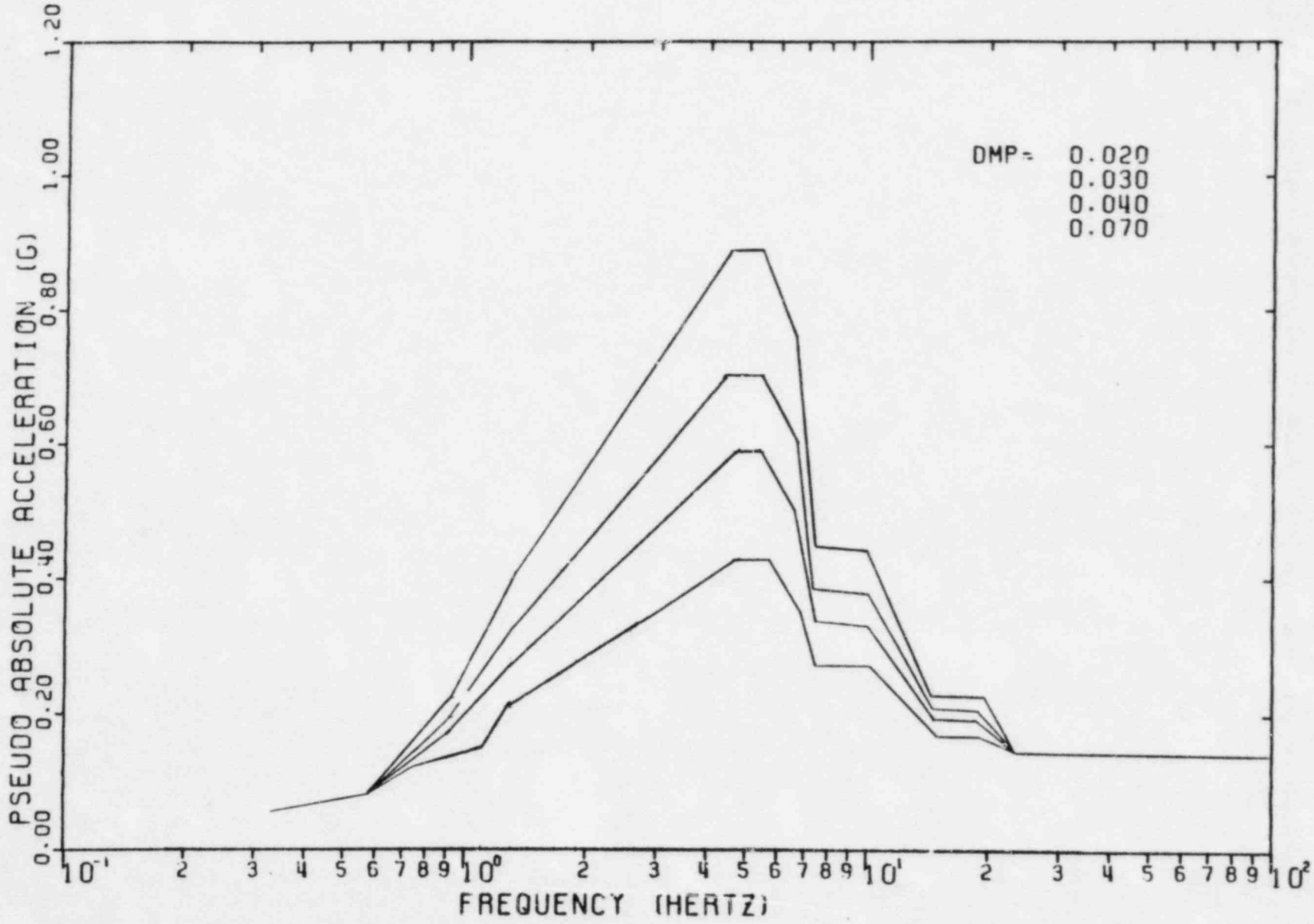

FIGURE II-5-17. ENVELOPED SRSS COMBINED RESPONSE SPECTRA, REACTOR BUILDING, CONTAINMENT, ELEVATION 591'-6", EAST-WEST DIRECTION

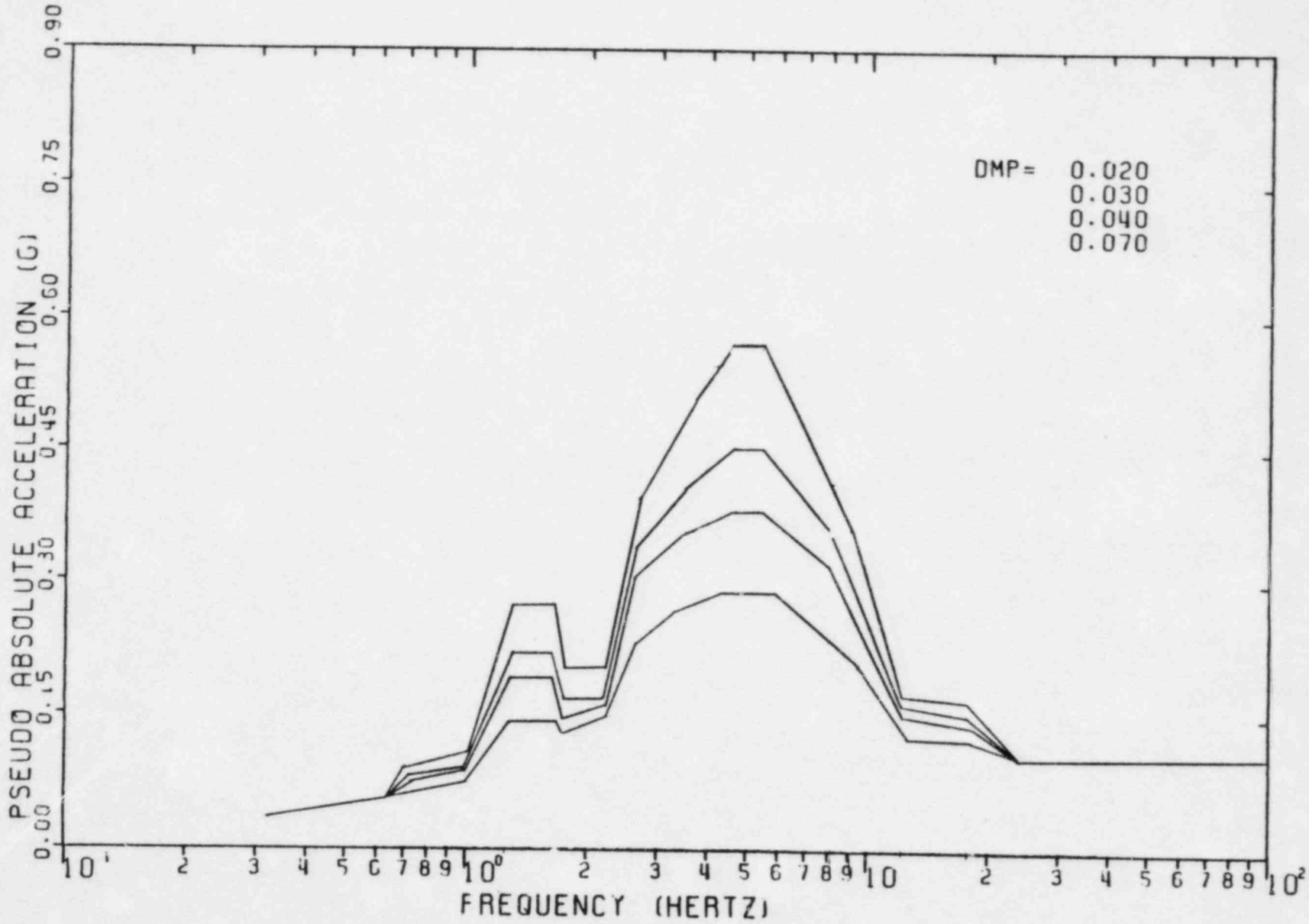

FIGURE II-5-18. ENVELOPED SRSS COMBINED RESPONSE SPECTRA, REACTOR BUILDING, CONTAINMENT, ELEVATION 591'-6", VERTICAL DIRECTION

FIGURE II-5-19. ENVELOPED SRSS COMBINED RESPONSE SPECTRA, REACTOR BUILDING, CONTAINMENT, ELEVATION 622'-0", NORTH-SOUTH DIRECTION

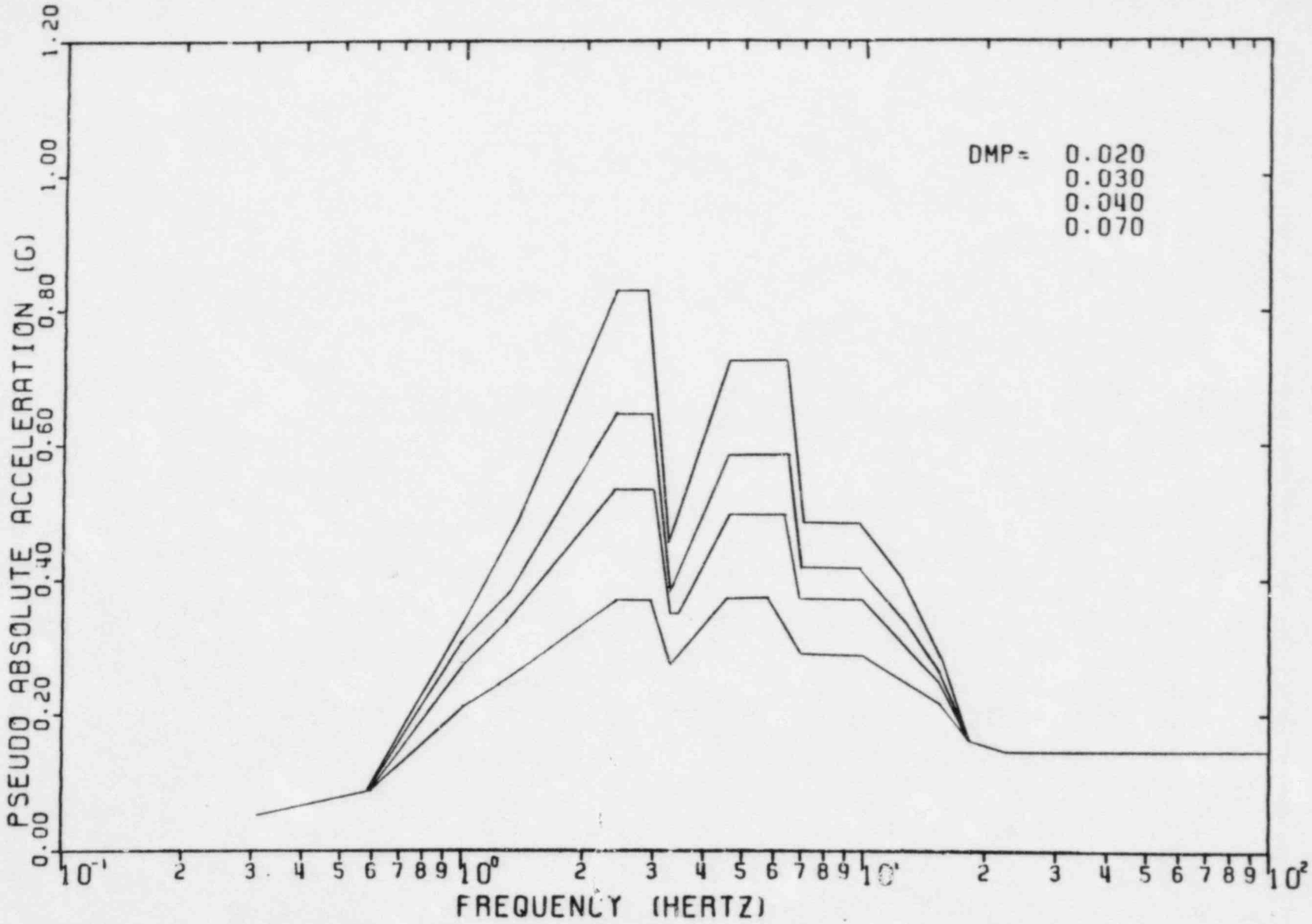

FIGURE II-5-20. ENVELOPED SRSS COMBINED RESPONSE SPECTRA, REACTOR BUILDING, CONTAINMENT, ELEVATION 622'-0", EAST-WEST DIRECTION

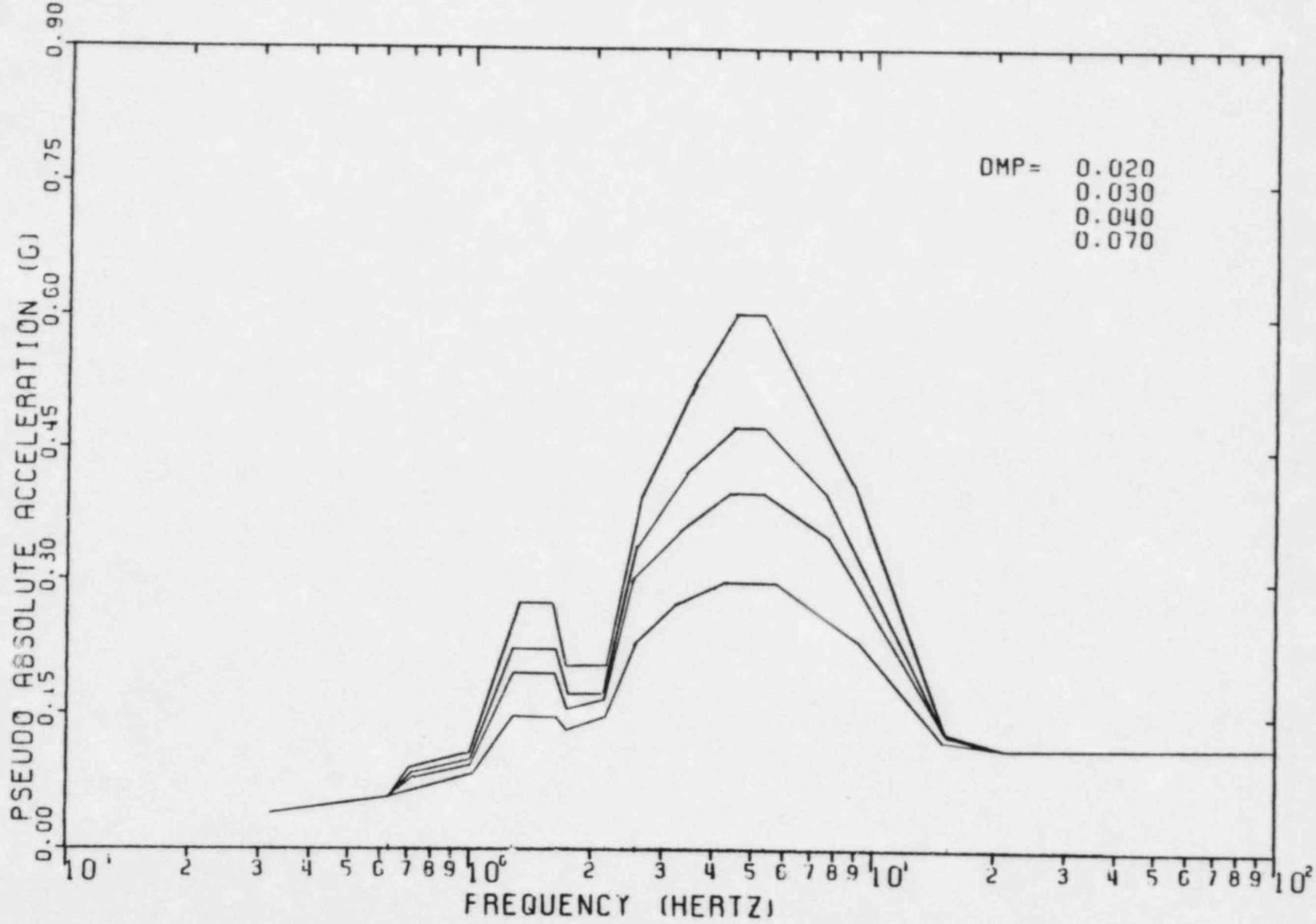

FIGURE II-5-21. ENVELOPED SRSS COMBINED RESPONSE SPECTRA, REACTOR BUILDING, CONTAINMENT, ELEVATION 622'-0", VERTICAL DIRECTION

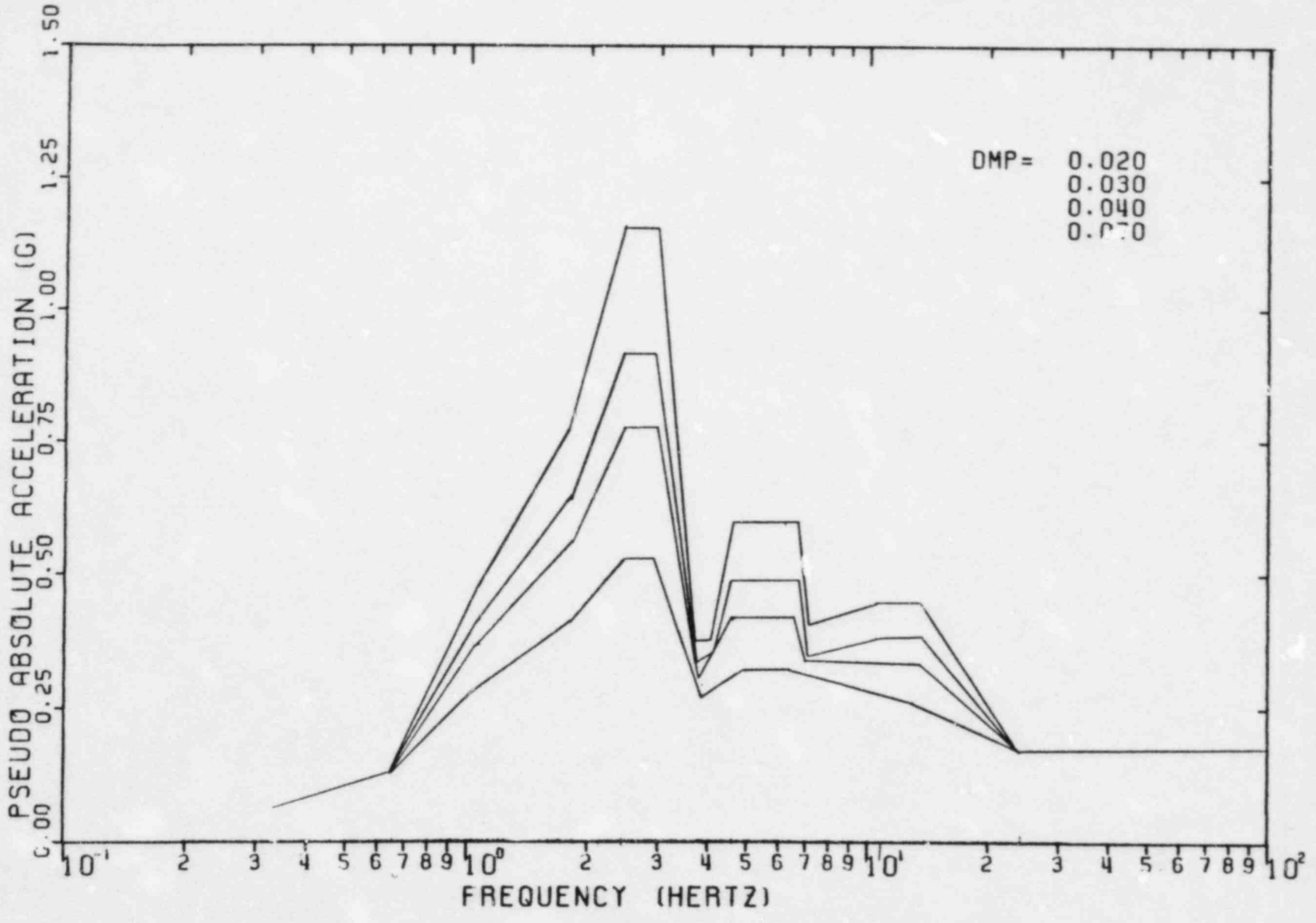

FIGURE II-5-22. ENVELOPED SRSS COMBINED RESPONSE SPECTRA, REACTOR BUILDING, CONTAINMENT, ELEVATION 646'-0", NORTH-SOUTH DIRECTION

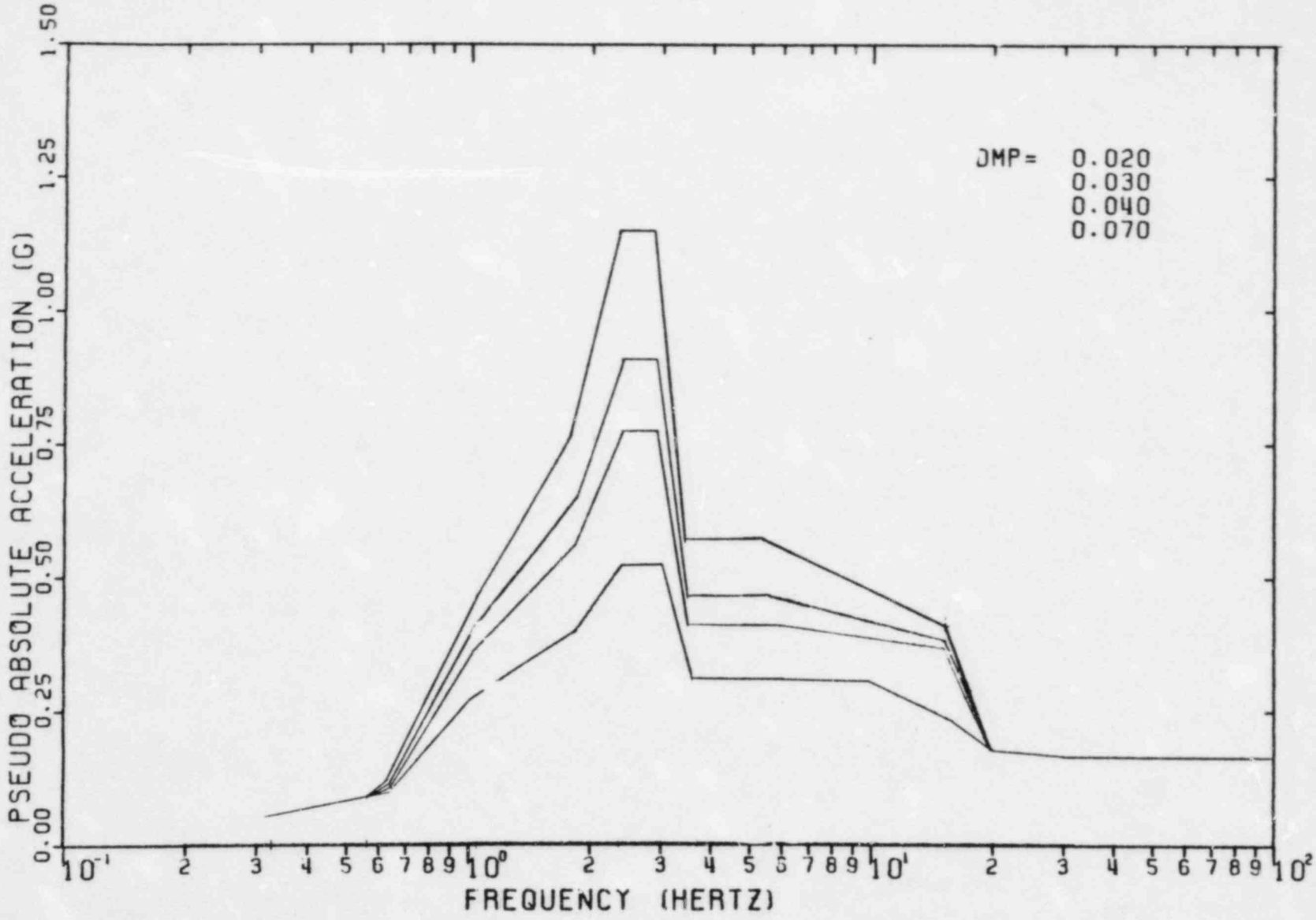

FIGURE II-5-23. ENVELOPED SRSS COMBINED RESPONSE SPECTRA, REACTOR BUILDING, CONTAINMENT, ELEVATION 646'-0",EAST-WEST DIRECTION

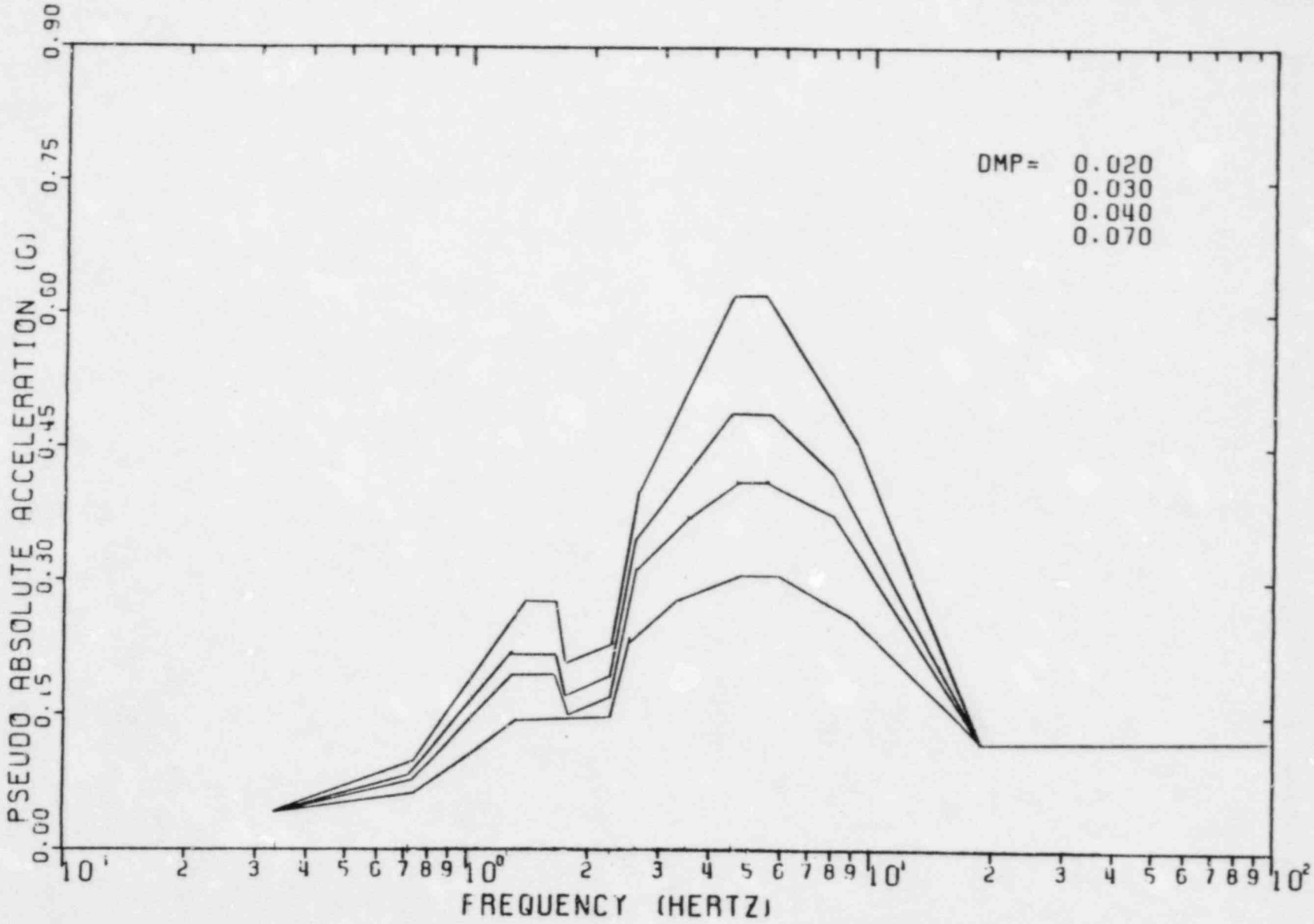

FIGURE II-5-24. ENVELOPED SRSS COMBINED RESPONSE SPECTRA, REACTOR BUILDING, CONTAINMENT, ELEVATION 646'-0",VERTICAL DIRECTION

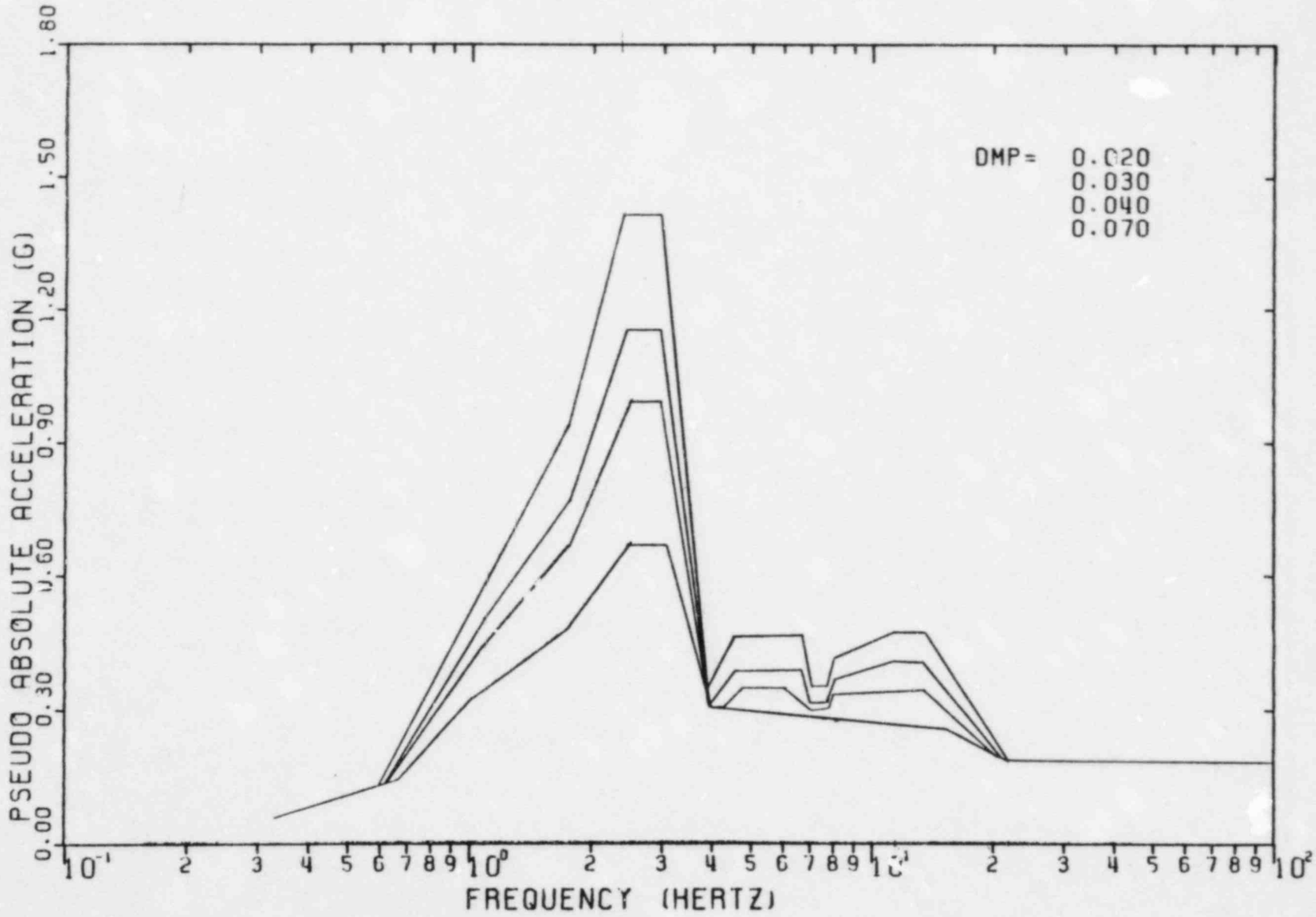

FIGURE II-5-25. ENVELOPED SRSS COMBINED RESPONSE SPECTRA, REACTOR BUILDING, CONTAINMENT, ELEVATION 664'-0" NORTH-SOUTH DIRECTION

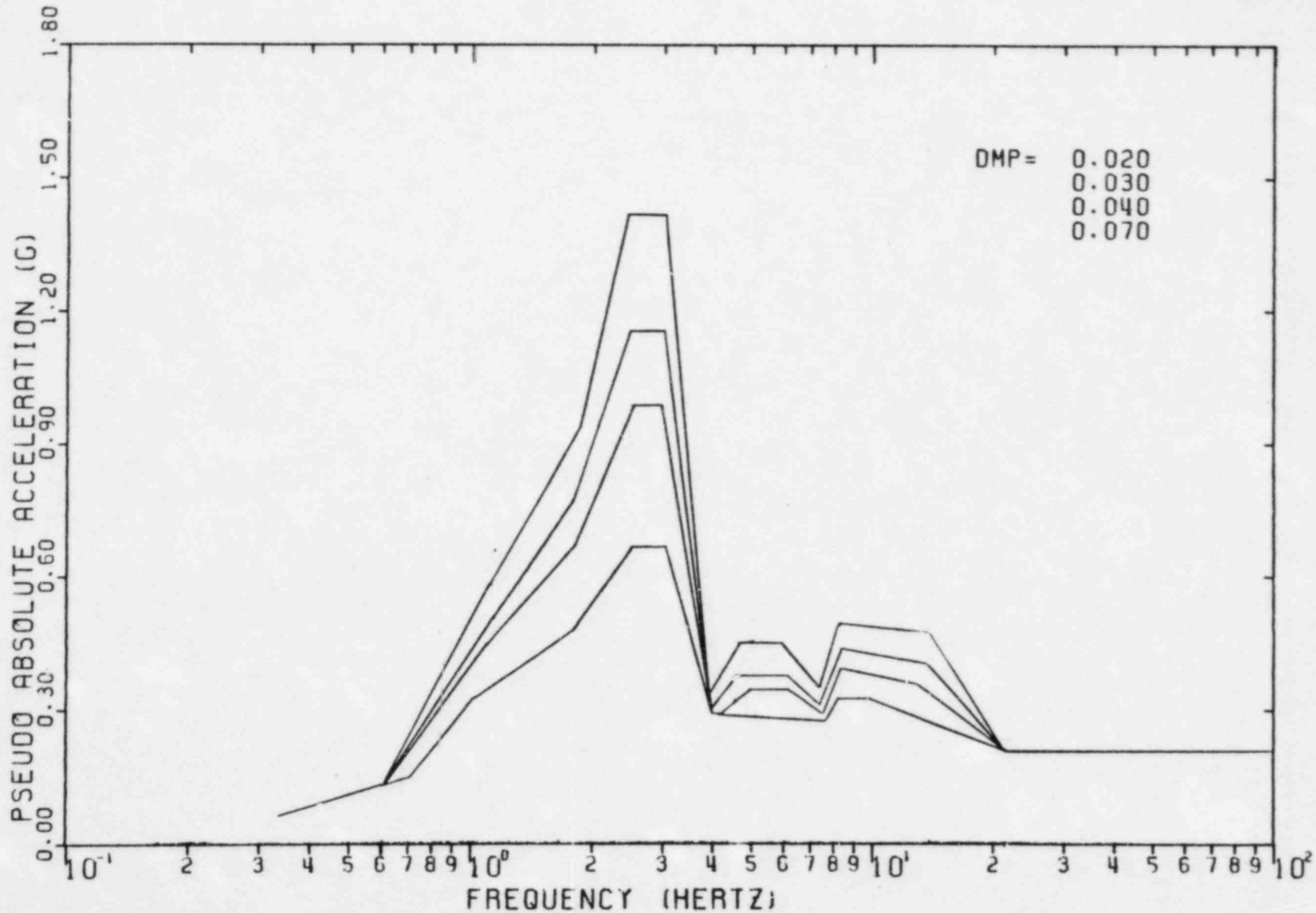

FIGURE II-5-26. ENVELOPED SRSS COMBINED RESPONSE SPECTRA, REACTOR BUILDING, CONTAINMENT, ELEVATION 664'-0" EAST-WEST DIRECTION

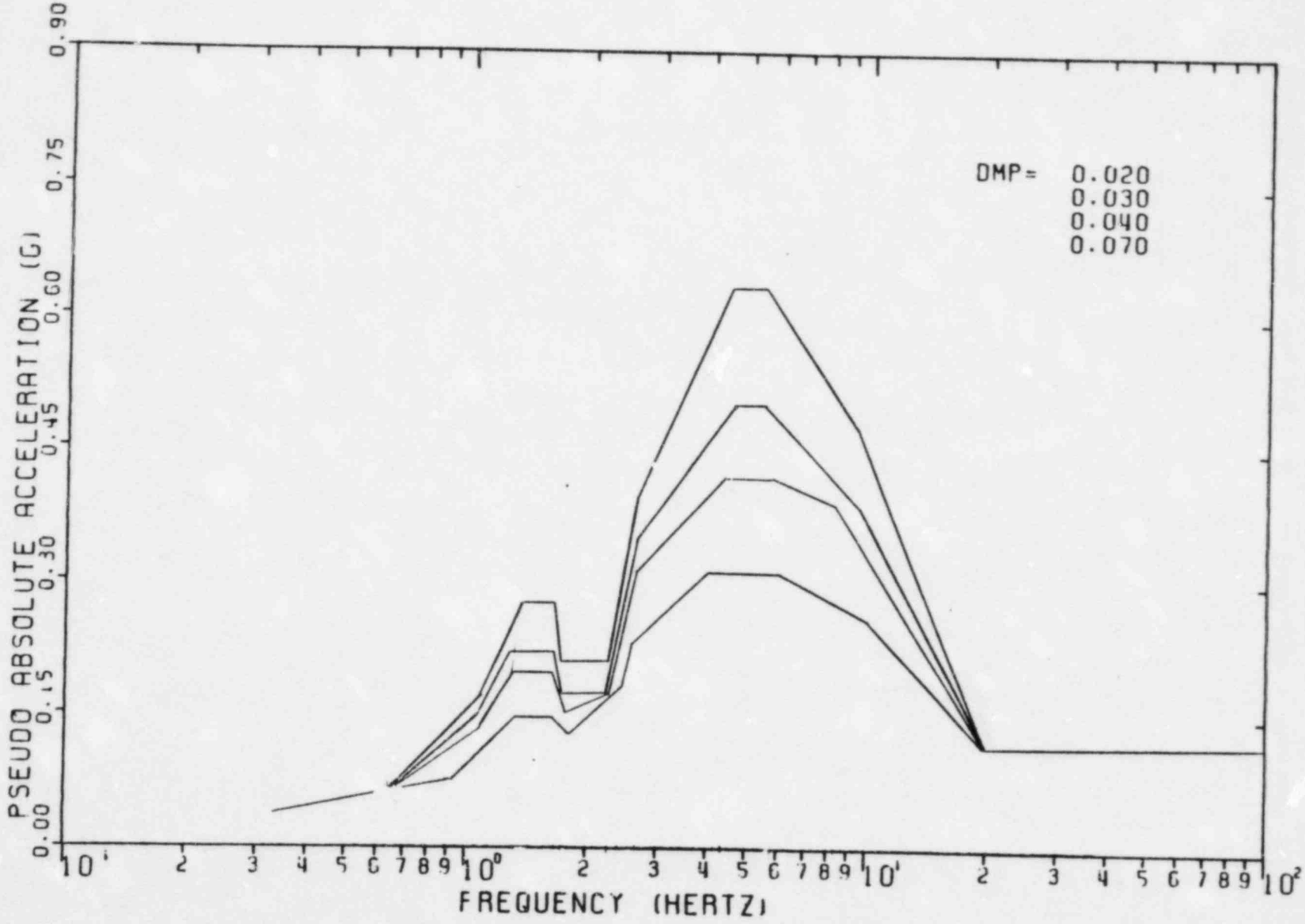

FIGURE II-5-27. ENVELOPED SRSS COMBINED RESPONSE SPECTRA, REACTOR BUILDING, CONTAINMENT, ELEVATION 664'-0" VERTICAL DIRECTION

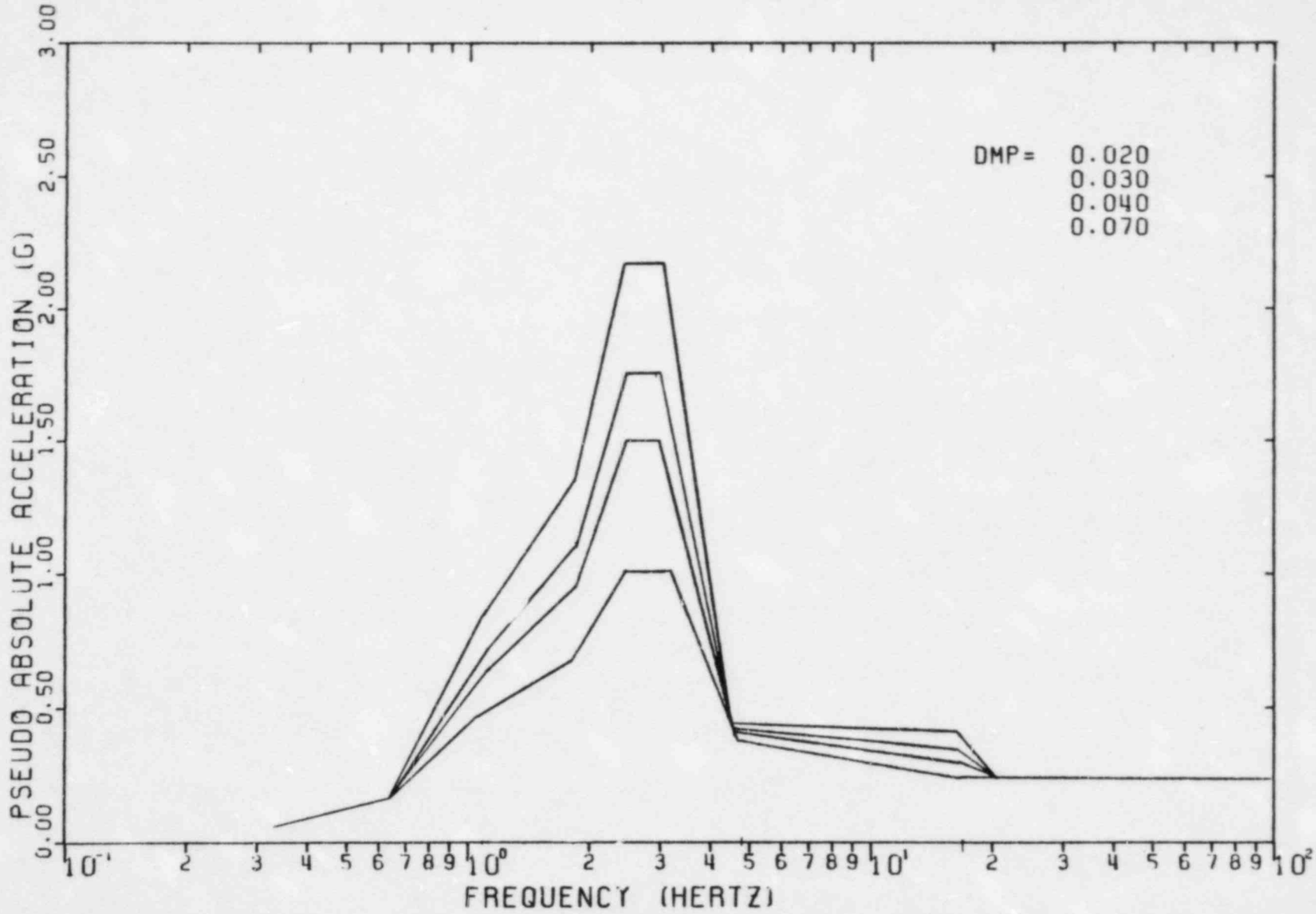

FIGURE II-5-28. ENVELOPED SRSS COMBINED RESPONSE SPECTRA, REACTOR BUILDING, CONTAINMENT, ELEVATION 707'-0", NORTH-SOUTH DIRECTION

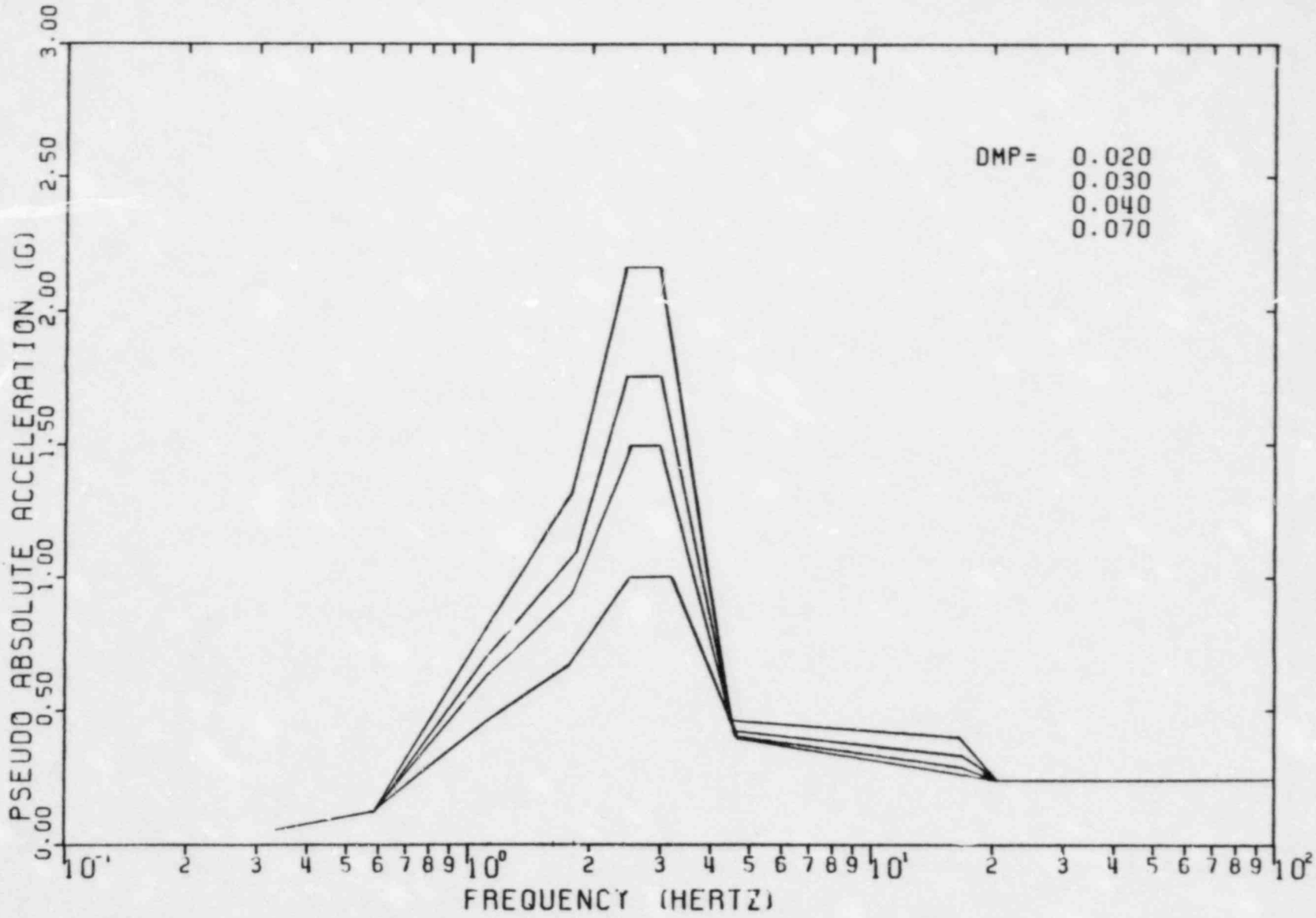

FIGURE II-5-29. ENVELOPED SRSS COMBINED RESPONSE SPECTRA, REACTOR BUILDING, CONTAINMENT, ELEVATION 707'-0", EAST-WEST DIRECTION

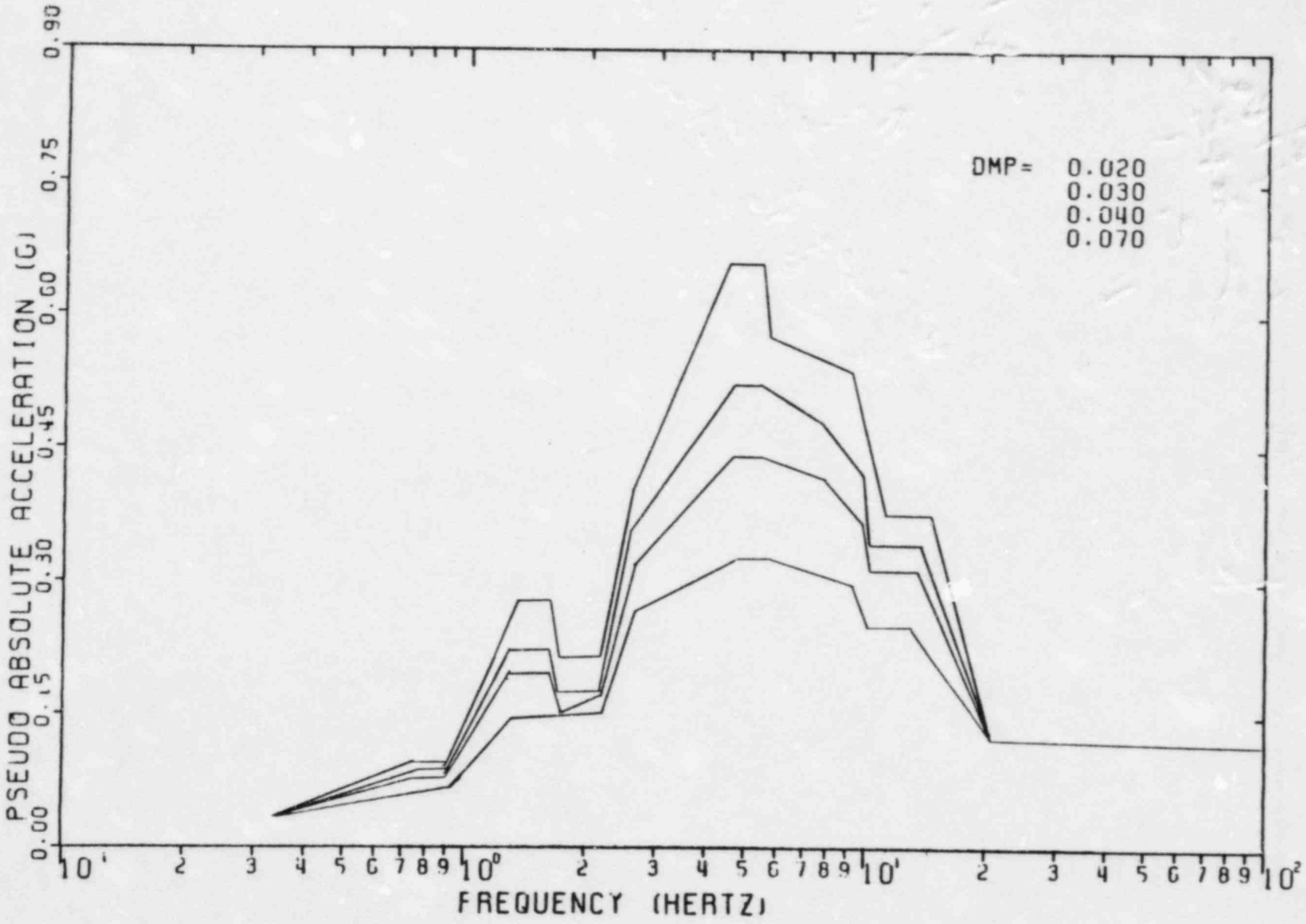

FIGURE II-5-30. ENVELOPED SRSS COMBINED RESPONSE SPECTRA, REACTOR BUILDING, CONTAINMENT, ELEVATION 707'-0", VERTICAL DIRECTION

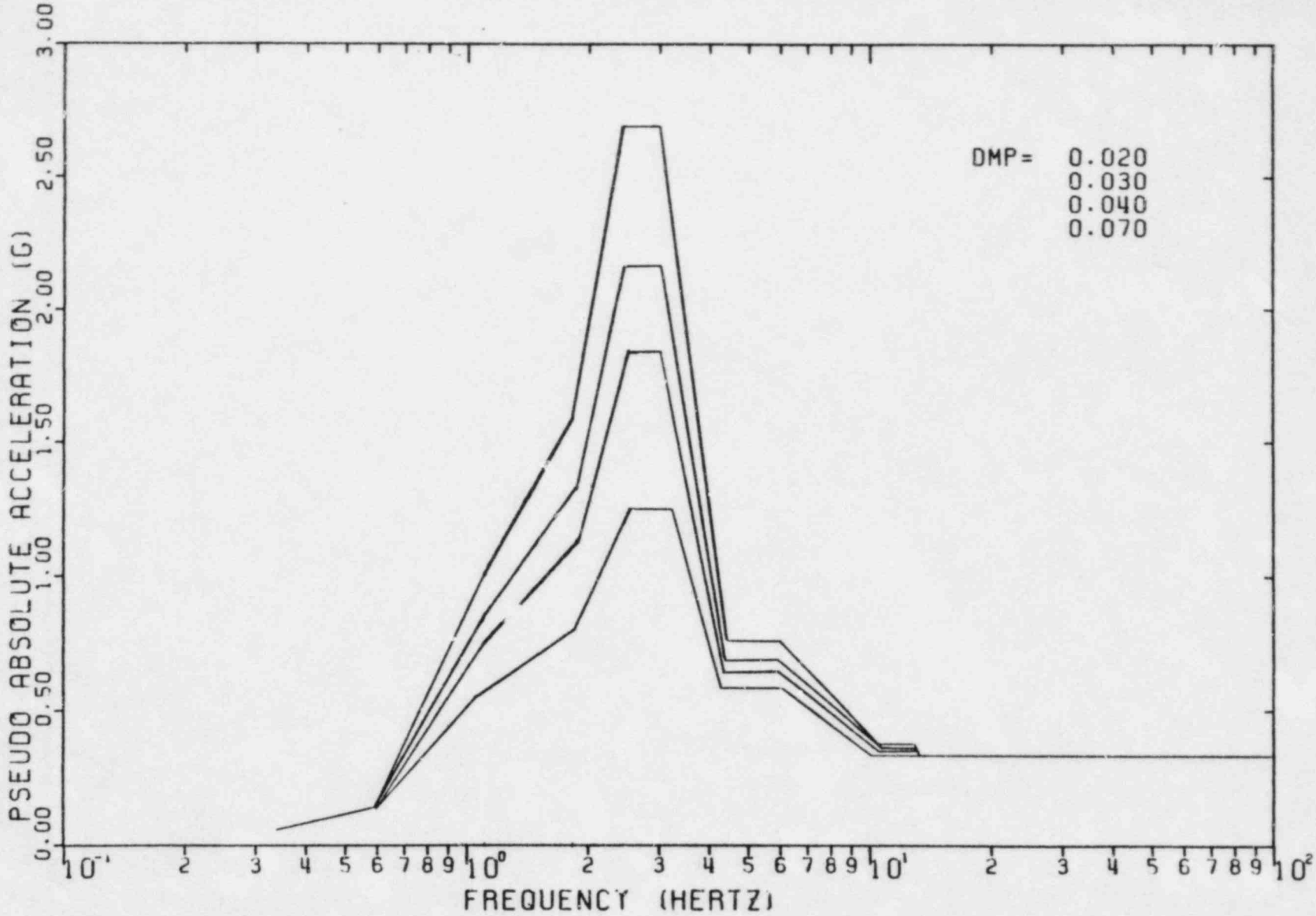

FIGURE II-5-31. ENVELOPED SRSS COMBINED RESPONSE SPECTRA, REACTOR BUILDING, CONTAINMENT, ELEVATION 736'-8", NORTH-SOUTH DIRECTION

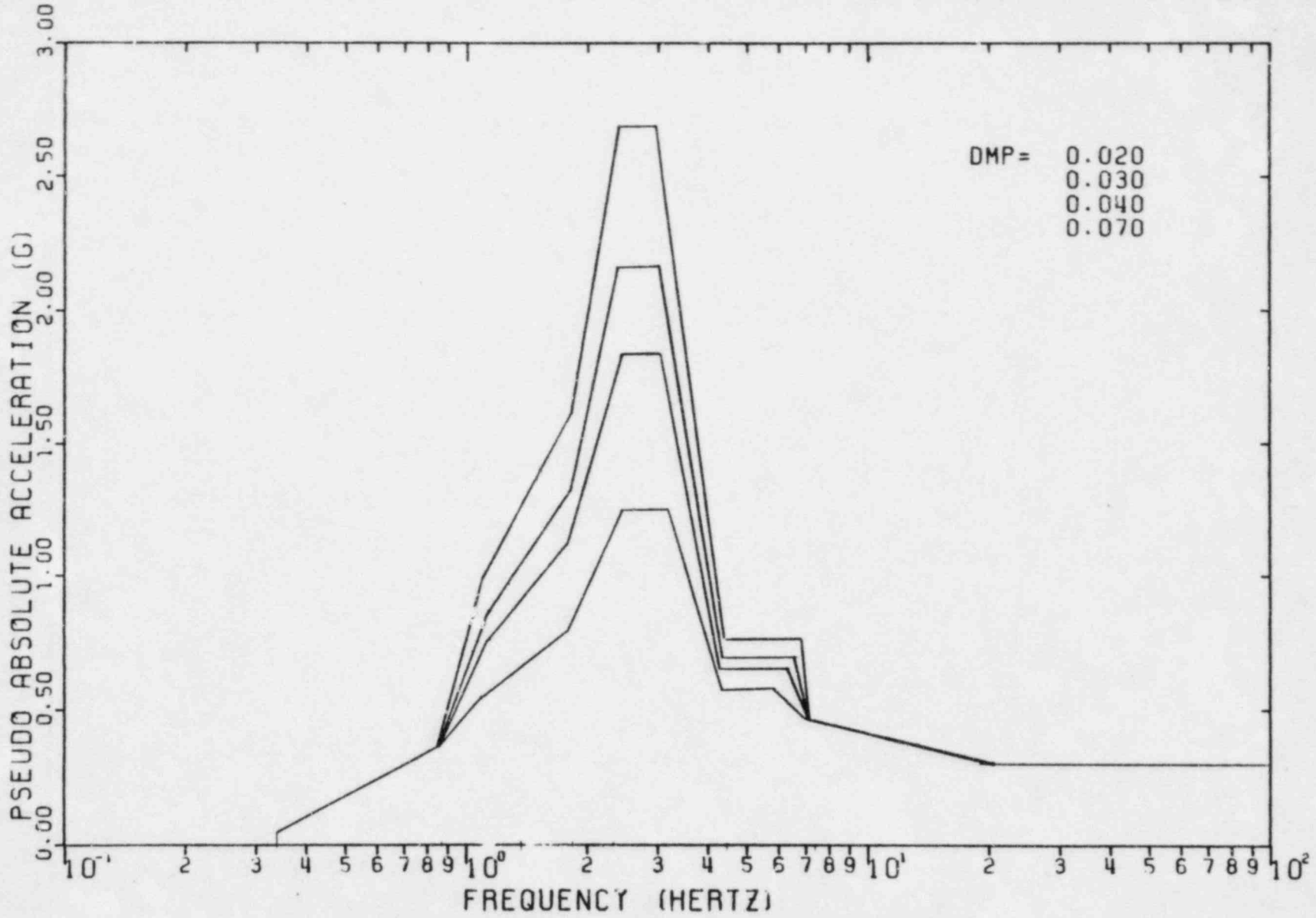

FIGURE II-5-32. ENVELOPED SRSS COMBINED RESPONSE SPECTRA, REACTOR BUILDING, CONTAINMENT, ELEVATION 736'-8", EAST-WEST DIRECTION

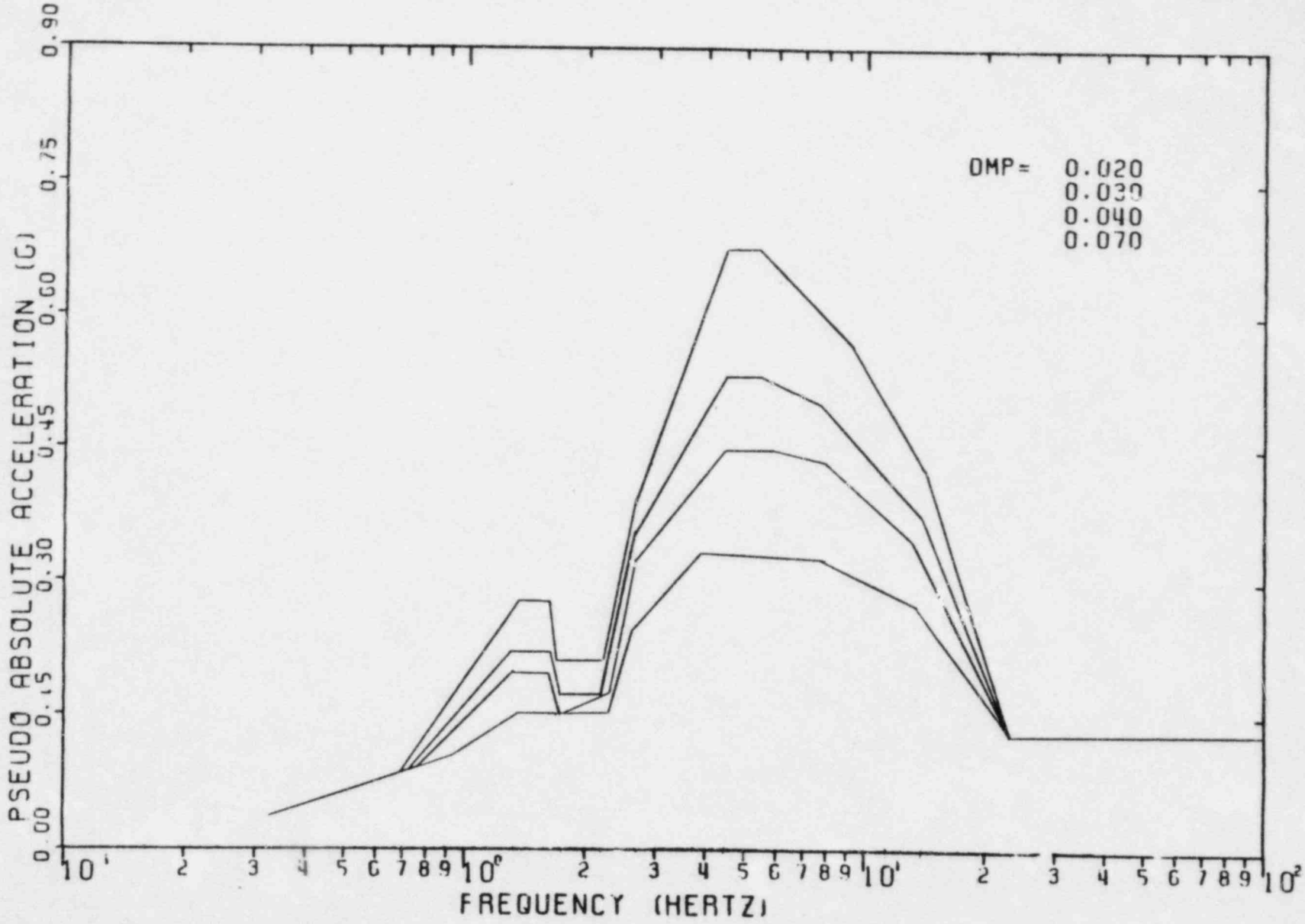

FIGURE II-5-33. ENVELOPED SRSS COMBINED RESPONSE SPECTRA, REACTOR BUILDING, CONTAINMENT, ELEVATION 736'-8", VERTICAL DIRECTION

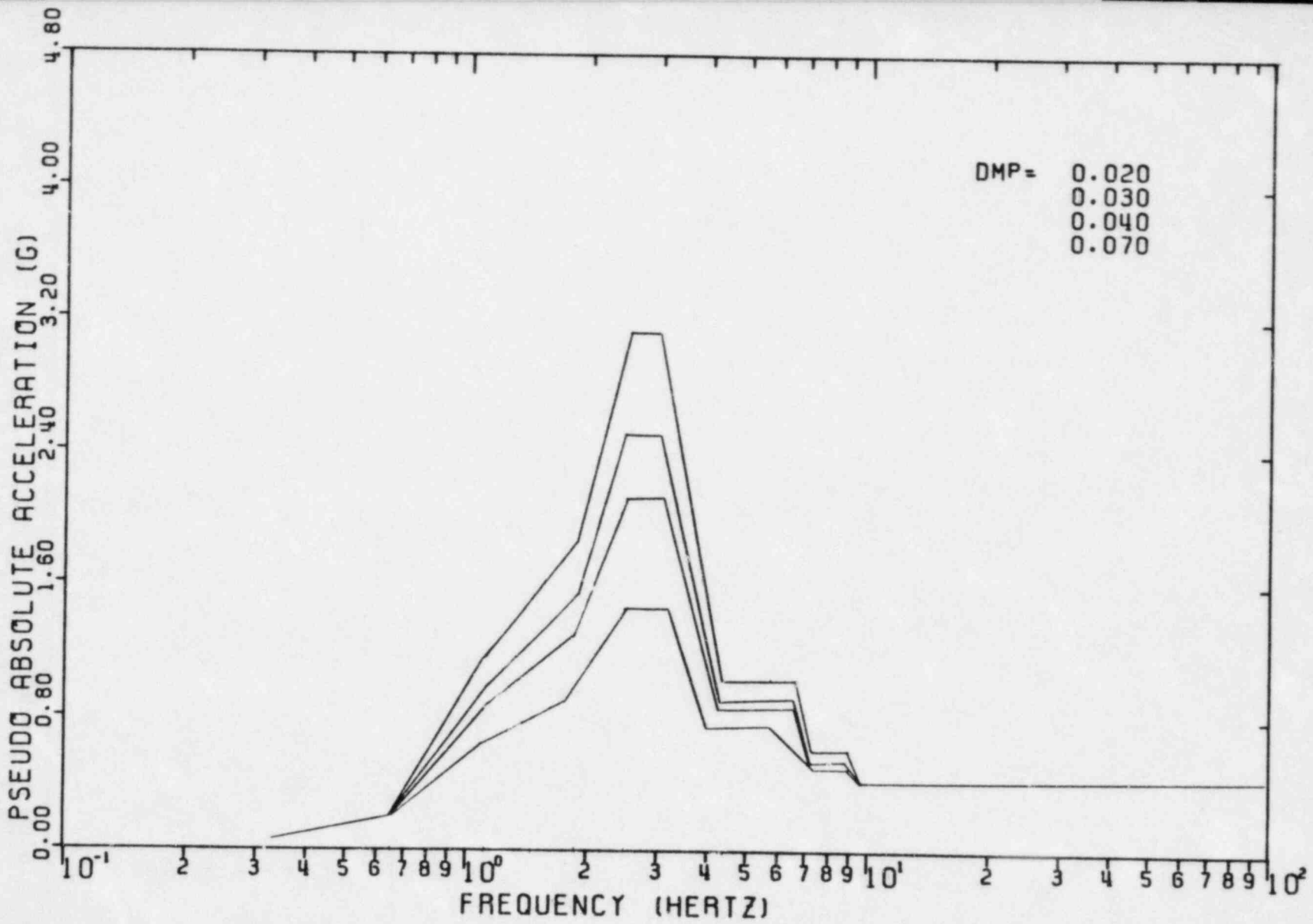

FIGURE II-5-34. ENVELOPED SRSS COMBINED RESPONSE SPECTRA, REACTOR BUILDING, CONTAINMENT, ELEVATION 764'-6", NORTH-SOUTH DIRECTION

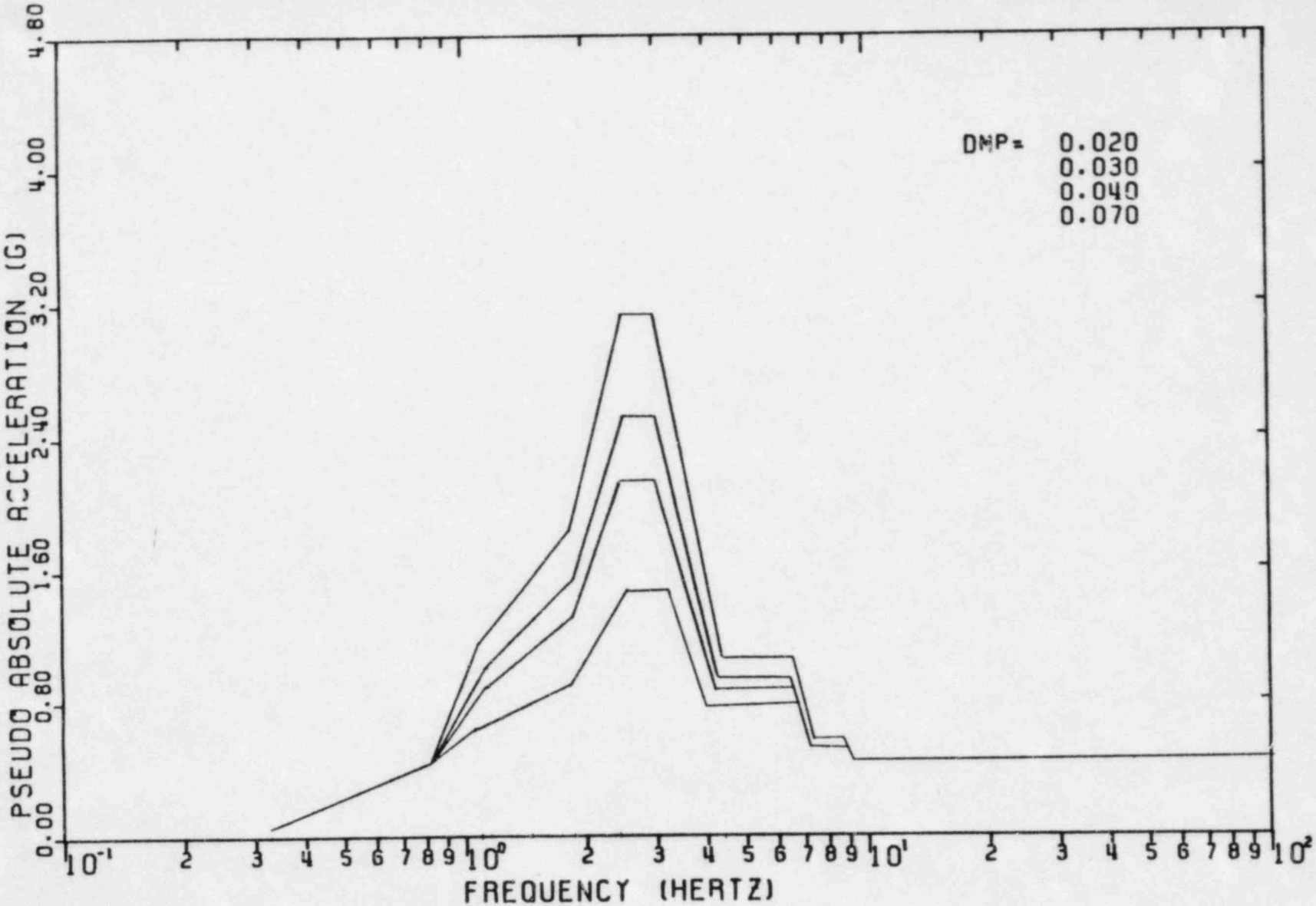

FIGURE II-5-35. ENVELOPED SRSS COMBINED RESPONSE SPECTRA, REACTOR BUILDING, CONTAINMENT, ELEVATION 764'-6", EAST-WEST DIRECTION

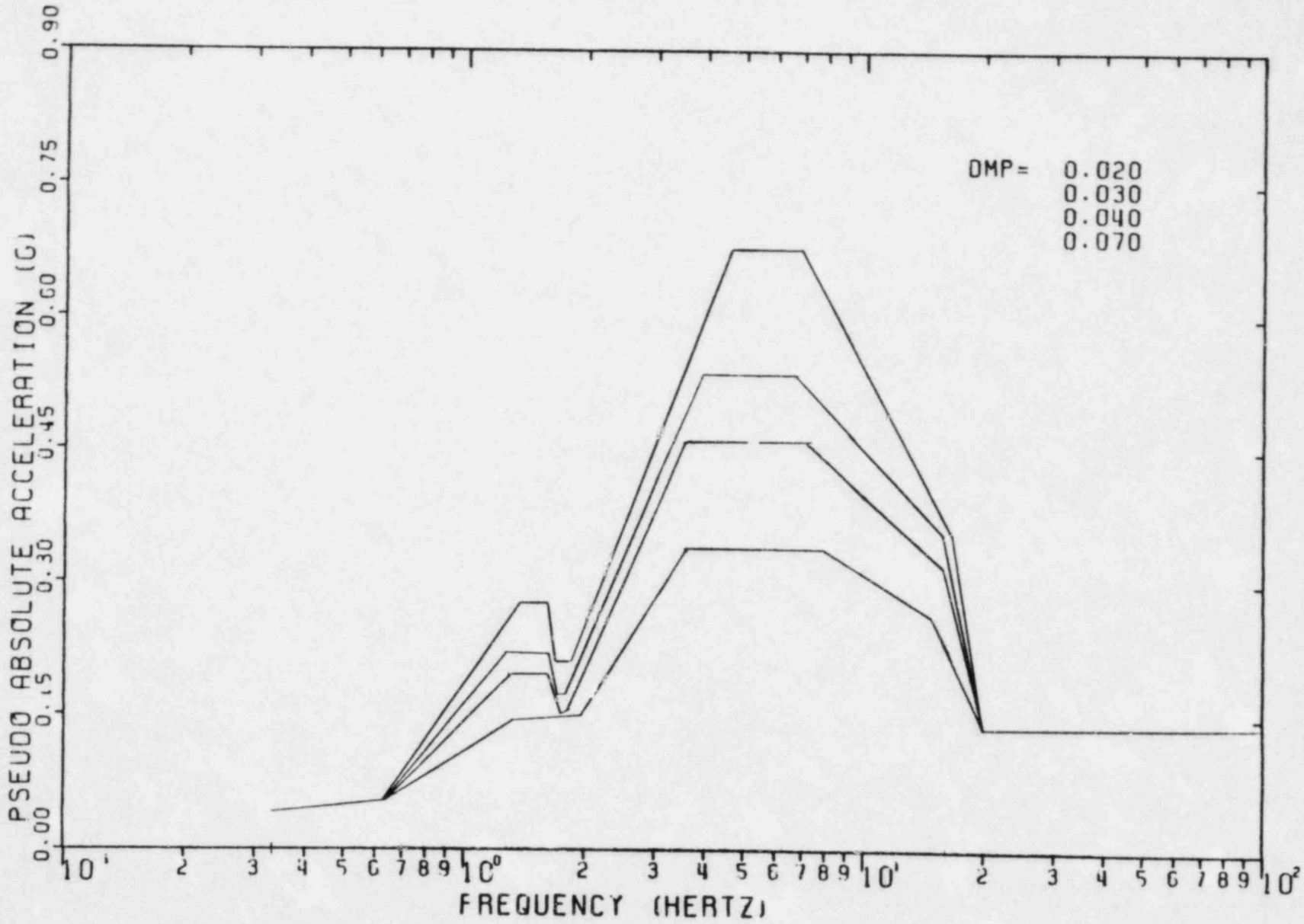

FIGURE II-5-36. ENVELOPED SRSS COMBINED RESPONSE SPECTRA, REACTOR BUILDING, CONTAINMENT, ELEVATION 764'-6", VERTICAL DIRECTION

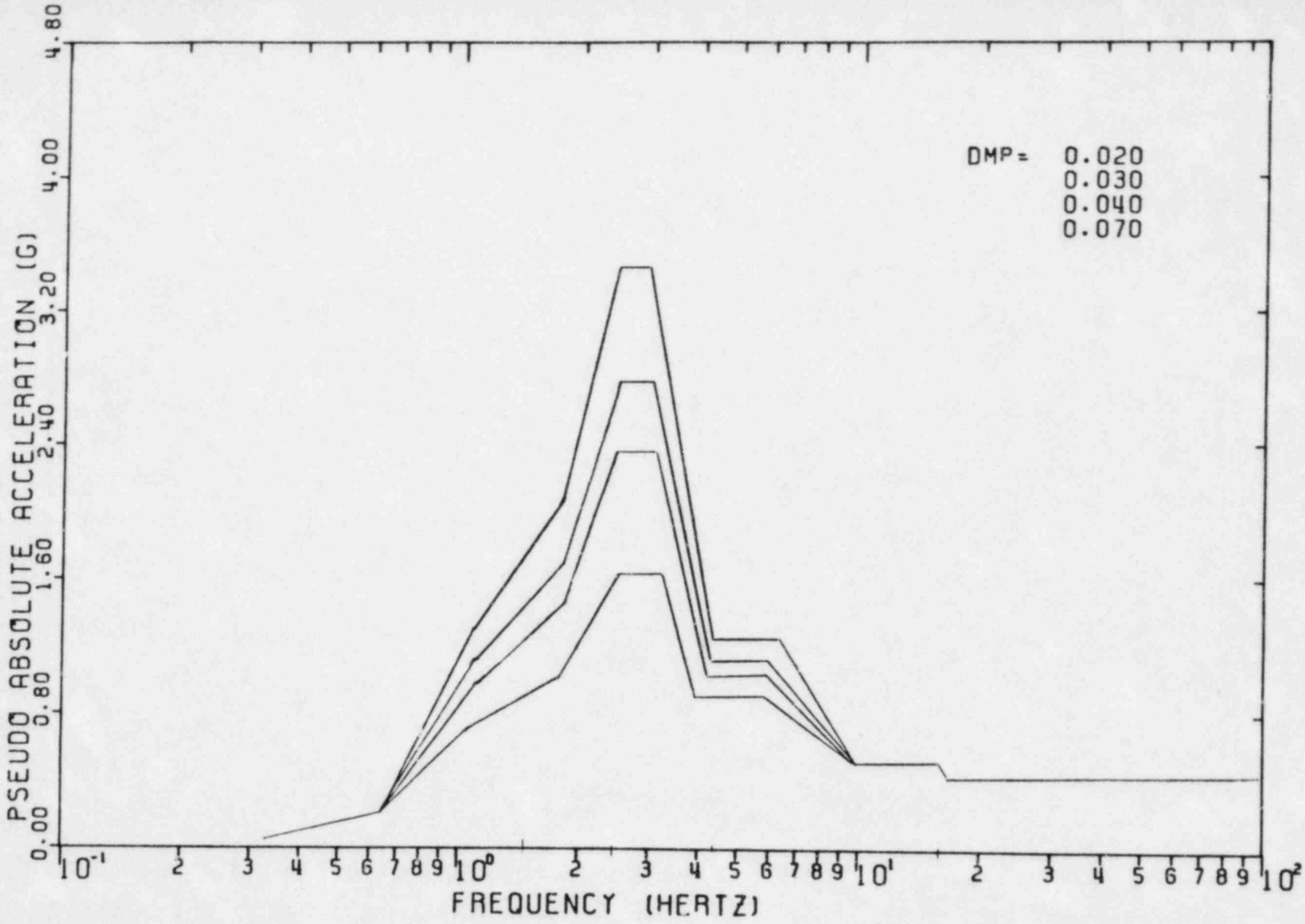

FIGURE II-5-37. ENVELOPED SRSS COMBINED RESPONSE SPECTRA REACTOR BUILDING, CONTAINMENT, ELEVATION 786'-0" NORTH-SOUTH DIRECTION

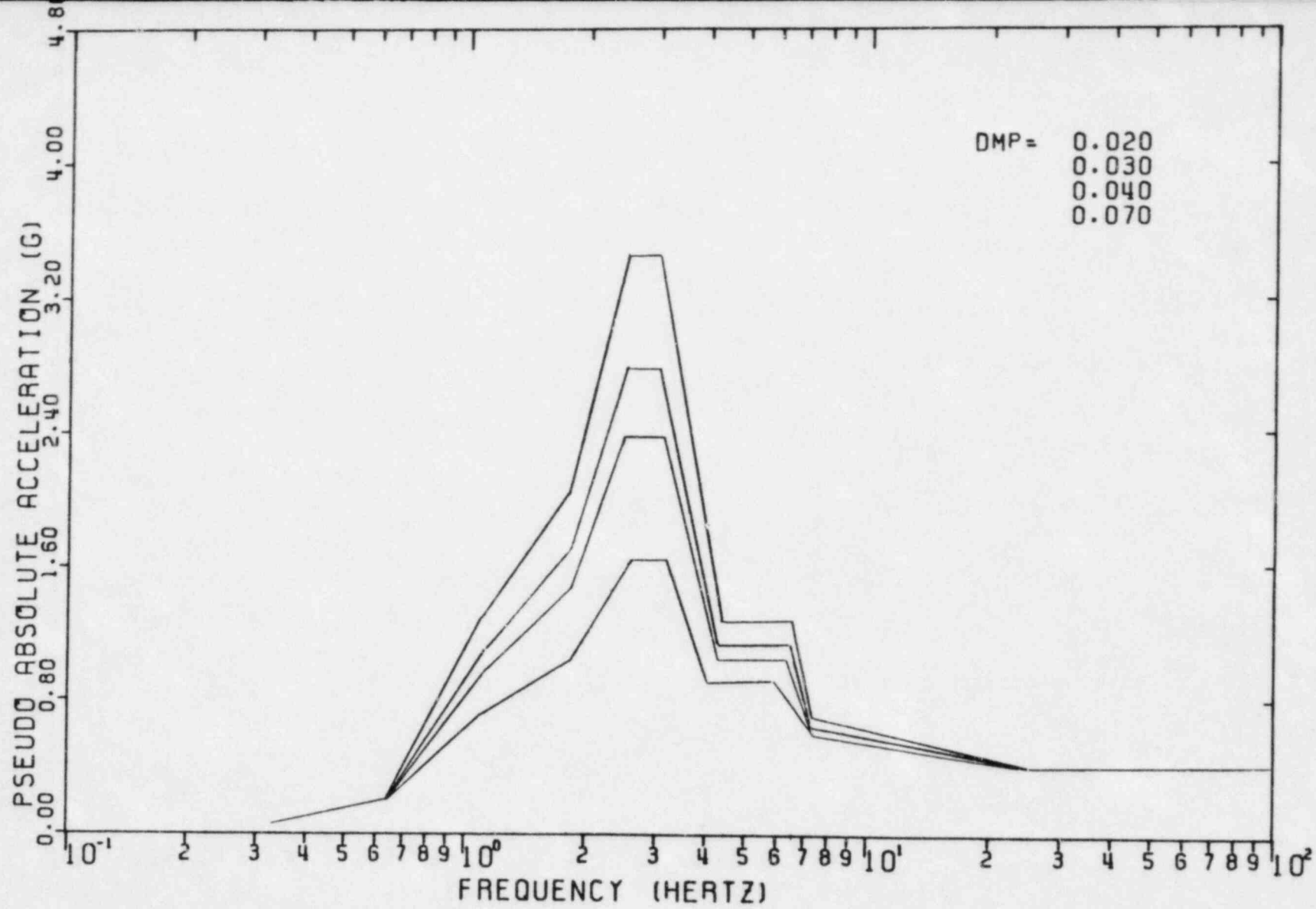

FIGURE II-5-38. ENVELOPED SRSS COMBINED RESPONSE SPECTRA, REACTOR BUILDING, CONTAINMENT, ELEVATION 786'-0", EAST-WEST DIRECTION

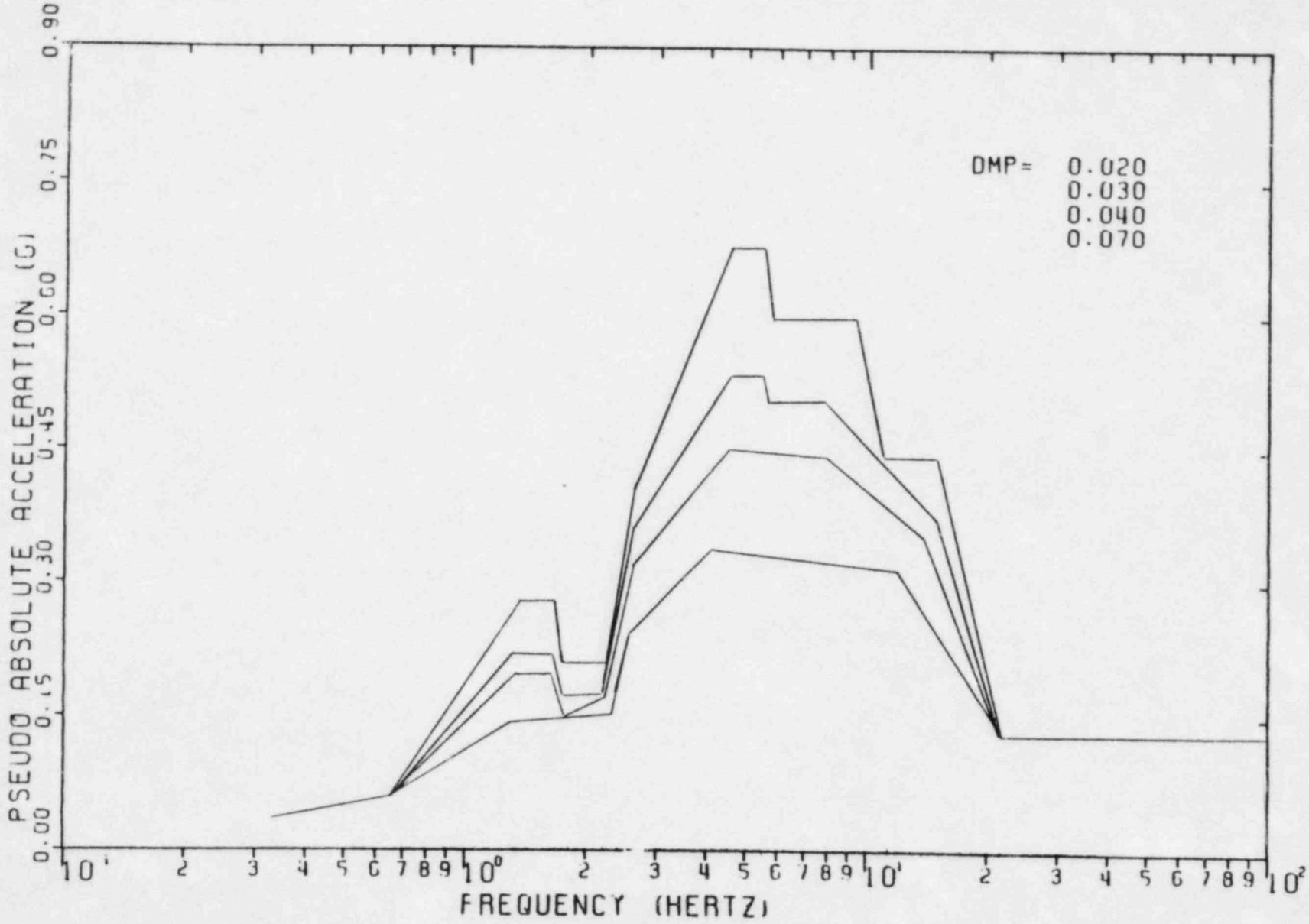

FIGURE II-5-39. ENVELOPED SRSS COMBINED RESPONSE SPECTRA, REACTOR BUILDING, CONTAINMENT, ELEVATION 786'-0", VERTICAL DIRECTION

6. SUMMARY

As part of the Seismic Margin Earthquake (SME) evaluation conducted for Midland, the ability of the reactor building structure to withstand seismic excitation was investigated. The evaluation was conducted using new seismic response loads developed for the SME together with design dead, live, and accident loads. The seismic loads were developed using a site specific earthquake for Midland as well as new soil-structure interaction parameters which reflect the site layering characteristics. Margins against code allowable values were calculated for selected elements throughout the structure.

The seismic excitation of the structure was specified in terms of site specific response spectra developed for the original ground location. These spectra have a peak ground acceleration of approximately 0.13g. The vertical component was specified as 2/3 of horizontal.

6.1 SOIL-STRUCTURE INTERACTION

Three soil profiles representing soft site, stiff site, and intermediate soil conditions were used in the analysis. Layered site analyses were used to develop the soil impedance functions for the structure using the actual foundation plan. Effective shear moduli (G_{eff}) were calculated based on elastic half-space formulae by maintaining the same stiffness values as those obtained for the layered site analyses for each of the three soil profiles. In order to account for uncertainties in the soil data, global stiffness and damping parameters were developed based on a lower bound of 0.6 G_{eff} for the soft soil profile and 1.3 G_{eff} for the stiff soil profile. These parameters were then adjusted to account for embedment effects which was not included in the layered site analyses. Damping values were conservatively limited

1

to 75 percent of theoretical elastic half-space values for vertical translation, to 50 percent of theoretical for horizontal translation, and to 25 percent of theoretical for rocking degrees-of-freedom.

Dynamic models of the reactor building in the North-South, East-West, and vertical directions were used to develop seismic respose loads in the structure. Because the structure is essentially symmetric, torsional building response due to structural eccentricities was not considered in the dynamic models. As part of the SME evaluation, these models were reviewed for the general methodology used in their development and for adequacy to characterize the seismic response of the structure. The detailed calculations used in the model development were not checked as part of the SME program.

Composite modal damping ratios were computed for the combined soil-structure model by matching structural response determined by directly integrating the coupled equations of motion to the response calculated by modal analysis techniques at several locations in the structure. Structural damping of five percent of critical was used for the prestressed concrete containment shell. The reinforced concrete internal structure was considered to be damped at seven percent of critical while the reactor vessel and steam generator were considered to be damped at two percent of critical.

Structural loads were determined using response spectrum modal analysis. Modal responses were combined on an SRSS basis except for closely space modes which were combined by the absolute sum. The responses to three directions of input motion were calculated independently.

6.2 SME STRUCTURAL LOADS

The upper bound soil condition resulted in maximum structural loads. The code margin evaluation was based on the maximum load condition in all instances. When compared with seismic design loads, the maximum SME loads were generally lower throughout the containment shell and

dome. However, in the reinforced concrete internal support structure, the SME maximum lateral shear and overturning moments exceeded the design loads in all members.

Overall seismic loads determined by the structure response spectrum analyses were distributed to the resisting structural elements by methods appropriate to the load-resisting system being evaluated. For a circular cylinder such as the containment wall, the elastic seismic stress distributions are predicted with sufficient accuracy by elementary beam theory. The seismic overturning moments and vertical axial forces result primarily in membrane meridional stresses while the horizontal seismic shears result primarily in tangential shear stresses. Seismic forces in the dome are expected to occur mainly from vertical response. The fundamental frequency of the dome was estimated using approximate closed-form solutions. Dome forces due to inertial loading were then determined from available classical solutions.

The base mat is loaded transversely by reactions from the containment wall and the internal structures as well as by corresponding soil bearing pressures. Soil pressures were approximated as being uniformly distributed due to the seismic vertical forces and linearly varying due to the overturning moments. Base mat forces due to seismic loads from the containment wall were calculated from available classical solutions for circular plates. Forces due to loads from the internal structures were based on the classical solutions for circular plates loaded through a central, rigid portion.

Seismic forces on the elements of the containment structure due to the SME were combined with forces due to loads occurring at normal operating or accident conditions. The forces occurring at normal operating and accident conditions were based on analytical results reported in the FSAR. Accident conditions used in the SME evaluation correspond to the full design basis accident and pressure loads for a large LOCA.

The internal structures form an open, hollow section generally lacking the horizontal diaphragms of a conventional building structure that would distribute the seismic loads to the vertical load-resisting elements. As with the containment wall, the elastic seismic stress distributions are predicted with sufficient accuracy by elementary beam theory. Vertical membrane stresses in the walls due to seismic overturning moments and vertical axial force were based on the dynamic model beam element stiffness properties. The overall seismic horizontal shears were distributed to the individual walls in proportion to their contributions to the dynamic model shear areas. Forces and stresses in the internal structures at normal operating conditions were based on the available results from Bechtel's static finite element analyses.

6.3 SME CODE MARGINS

The capacities evaluation of the containment structure was conducted following the provisions of the ASME Code. Stresses in the concrete and reinforcement due to applied membrane forces and moments were determined using assumptions on cross-sectional behavior meeting the ASME Code requirements. These requirements pertain to the satisfaction of equilibrium and strain compatibility and acceptable material stress-strain behavior. Allowable material stresses permitted in this evaluation were those specified in the ASME Code. All code margins computed for the SME evaluation were found to be greater than unity. | 1

The lowest code margin for the reactor building structure was found to be associated with the vertical tendons in the containment structure cylindrical wall. The effective stress in the prestress tendons after losses have occurred was found to give a code margin of 1.16 prior to the application of loading, where the applied loading includes the full design pressure and thermal effects as well as the SME loads. Including the calculated stress due to the applied load results in a code margin of 1.12 for the tendons. For this detail, the earthquake does not develop the controlling loads. The SME would have to be increased | 1 | 1

be increased by a factor of 23 before the code capacity is reached, and failure would not be expected until a significantly greater level of earthquake-induced loads are present. 1

The lowest code margins for membrane force and moment occurring in the containment wall, dome, and base mat were found to be 1.5, 1.6, and 1.8, respectively. Containment capacities due to other applied loadings, such as tangential shear on the wall and transverse shear on the base mat, were investigated using design provisions contained in the Standard Review Plan and ACI 349-80. Code margins associated with these capacities were found to be greater than those reported above. A summary of the code margins and corresponding F_{SME} factors for the controlling elements of the reactor building is shown in Table 6-1.

Capacities for the selected elements of the internal structures were developed in accordance with the ultimate strength design provisions contained in ACI 349-80. These members were checked for their ability to resist in-plane shear and combined axial load and moment. In addition, the ability of the details at the primary and secondary shield wall interfaces with the base mat liner plate to transmit shear was investigated. The lowest code margin for the internal structures was found to be 1.6. The SME would have to be increased by a factor of 2.3 before the code capacity of any element would be exceeded. To account for the effects of reinforcement cutting allowance and available non-conformance reports indicating deviations from the construction specifications, the east secondary shield wall was re-evaluated assuming the worst case possible due to these field conditions. Code margins for in-plane shear, axial load-moment interaction, and shear transfer to the base mat of 2.7, 3.7, and 3.1 were determined.

Code margins for the selected structural elements were all conservatively based on minimum specified material strengths and maximum seismic load cases. No reductions in loads to account for inelastic energy dissipation were used for the reactor building. All code margins

were determined to be greater than unity. Before the code capacity is reached for any reactor building element investigated, the SME would have to be increased by a factor of 2.0. This factor corresponds to the stress occurring in the meridional wall reinforcement at one of the cross-sections evaluated. It can, therefore, be concluded that the reactor building has more than sufficient structural capacity to resist the SME based on code criteria and significantly higher capacity before failure is expected. 1

TABLE II-6-1

SME CODE MARGIN AND F_{SME} SUMMARY

Structure	Location	Controlling Capacity	Code Margin	F_{SME}
Containment Structure	Wall	Tendon stress	1.12	Large
	Wall at EL. 650'-0"	Meridional membrane force and moment	1.5	2.0
	Dome near apex	Meridional membrane force and moment	1.6	Large
	Wall at EL. 650'-0"	Construction joint tangential shear	3.5	2.1
Base Slab	Radius = 44'	Radial membrane force and moment	1.8	2.5
	Radius = 44'	Transverse shear	3.5	Large
Concrete Internal Structures	Primary shield wall at EL. 603'-0"	Axial load and moment	1.6	7.6
	Primary shield wall at EL. 626'-0"	Tangential shear	2.0	2.7
	Primary shield wall-base mat interface	Tangential shear	2.2	2.3
	East secondary shield wall at EL. 591'-6"	In-plane shear	3.3	5.2
	East secondary shield wall-base mat interface	In-plane shear	4.1	Large
	East secondary shield wall at EL. 591'-6"	Axial load and moment	4.5	5.3

1

REFERENCES

1. Final Safety Analysis Report (FSAR), Midland Plant - Units 1 and 2, Consumers Power Company.

2. TID-7024, Nuclear Reactors and Earthquakes, Lockheed Aircraft Corporation and Holmes and Narver, Inc., August, 1963.

3. Site Specific Response Spectra, Midland Plant - Units 1 and 2, Part I, Response Spectra - Safe Shutdown Earthquake, Original Ground Surface, Weston Geophysical Corp., prepared for Consumers Power Company, February, 1981.

4. Site Specific Response Spectra, Midland Plant - Units 1 and 2, Part II, Response Spectra - Applicable for the Top of Fill Material at the Plant Site, Weston Geophysical Corp., prepared for Consumers Power Company, April, 1981.

5. Draft, Site Specific Response Spectra, Midland Plant - Units 1 and 2, Part III, Seismic Hazard Analysis, Weston Geophysical Corp., prepared for Consumers Power Company, Revision 1, May, 1982.

6. Wesley, D. A., Campbell, R. D., Kennedy, R. P., Kincaid, R. H., and P. S. Hashimoto, "Seismic Margin Review, Midland Energy Center Project, Volume I, Methodology and Criteria", February, 1983, SMA 13701.05R003 (Volume I).

7. Letter correspondence dated February 23, 1982 from E. M. Hughes (Bechtel) to R. P. Kennedy (SMA) Subject: "Seismic Model properties for the Reactor Building Midland Units 1 and 2."

8. Wong, H. L. and J. E. Luco, "Soil-Structure Interaction: A Linear Continuum Mechanics Approach (CLASSI), Report, CE, Department of Civil Engineering, University of Southern California, Los Angeles, California, 1980.

9. Wesley, D. A., Kennedy, R. P., Kincaid, R. H., Hashimoto, P. S., Thrasher R. D., and W. H. Tong, "Seismic Margin Review, Volume III, Auxiliary Building", February, 1983, SMA 13701.05R003 (Volume III).

10. Woodward-McNeill and Associates, "Development of Soil-Structure Interaction Parameters Proposed Units 2 and 3, San Onofre Nuclear Generating Station", San Onofre, California, January 1974.

11. Richart, F. E., Hall, Jr. R. and R. A. Woods, Vibrations of Soils and Foundations, Prentice-Hall, Inc., New Jersey, 1970.

REFERENCES (Continued)

12. Kausel, E., and R. Ushijima, "Vertical and Torsional Stiffness of Cylindrical Footings", Massachusetts Institute of Technology, Research Report R79-6, February, 1979.

13. Veletsos, A. S., and Y. T. Wei, "Lateral and Rocking Vibration of Footings", Journal of the Soil Mechanics and Foundations Division, Proceedings of ASCE, EM5, pp 1381-1395, October, 1971.

14. Luco, J. E., and R. A. Westmann, "Dynamic Response of Circular Footings", Journal of the Engineering Mechanics Division, Proceedings of ASCE, EM5, pp 1381-1395, October 1971.

15. Johnson, J. J., "SOILST - A Computer Program for Soil-Structure Interaction Analyses", General Atomic Company, GA-A15067, April, 1979.

16. Blevins, R. D., Formulas for Natural Frequency and Mode Shape, Van Nostrand Reinhold Company, 1979.

17. Roark, R. J. and W. C. Young, Formulas for Stress and Strain, Fifth edition, McGraw-Hill Book Company, 1975.

18. Kraus, H., Thin Elastic Shells, John Wiley and Sons, Inc., 1967.

19. Timoshenko, S. and S. Woinowsky-Krieger, Theory of Plates and Shells, Second edition, McGraw-Hill Book Company, 1959.

20. Letter correspondence from E. M. Hughes to R. P. Kennedy, April 12, 1982, Subject: Midland Plant Units 1 and 2, Consumers Power Company, Bechtel Job 7220, Seismic Margin Analysis.

21. Letter correspondence from E. M. Hughes to R. P. Kennedy, April 20, 1982, Subject: Midland Plant Units 1 and 2, Consumers Power Company, Bechtel Job 7220, Seismic Margin Analysis.

22. ASME Boiler and Pressure Vessel Code, Section III, Division 2, "Code for Concrete Reactor Vessels and Containments", American Society of Mechanical Engineers, 1980.

23. ACI 349-80, "Code Requirements for Nuclear Safety Related Concrete Structures", American Concrete Institute, 1980.

24. Structural Analysis and Design of Nuclear Plant Facilities, American Society of Civil Engineers, 1980.

REFERENCES (Continued)

25. Park, R. and T. Paulay, Reinforced Concrete Structures, John Wiley and Sons, 1975.

26. ACI 318-63, "Building Code Requirements for Reinforced Concrete", American Concrete Institute, 1963.

27. Cardenas, A. E., et. al., "Design Provisions for Shear Walls", ACI Journal, March, 1973.

28. "Ultimate Strength Design Handbook", Volume 2, American Concrete Institute, Publication SP-17A, 1975.

29. "Stud Welding Data for Architects and Engineers", TRW Nelson Division.

30. Mattock, A. H. et. al , "Shear Transfer in Reinforced Concrete with Moment or Tension Acting Across the Shear Plane", PCI Journal, July/August, 1975.

31. Bechtel Associates Professional Corporation, "Technical Specifications for Forming, Placing, Finishing and Curing of Concrete for the Consumers Power Company Midland Plant - Midland, Michigan", Spec. 7220-C-231Q, Revision 21, September 28, 1981.

32. Letter correspondence from J. P. Kindinger to H. F. Perla, August 17, 1981.

33. Lin, T. Y., Design of Prestressed Concrete Structures, Second Edition, John Wiley and Sons, Inc., 1963.

1